FRET-based cGMP Imaging in the Nervous System

Dissertation

der Mathematisch-Naturwissenschaftlichen Fakultät

der Eberhard Karls Universität Tübingen

zur Erlangung des Grades eines

Doktors der Naturwissenschaften

(Dr. rer. nat.)

vorgelegt von

Stefanie Peters

aus Nauen

Tübingen

2023

Gedruckt mit Genehmigung der Mathematisch-Naturwissenschaftlichen Fakultät der Eberhard Karls Universität Tübingen.

Tag der mündlichen Qualifikation:	09.01.2024
Dekan:	Prof. Dr. Thilo Stehle
1. Berichterstatter:	Prof. Dr. Robert Feil
2. Berichterstatter:	Prof. Dr. Peter Ruth

EIGENSTÄNDIGKEITSERKLÄRUNG

Ich erkläre hiermit, dass ich die zur Promotion eingereichte Arbeit mit dem Titel „FRET-based cGMP imaging in the nervous system“ selbstständig verfasst, nur die angegebenen Quellen und Hilfsmittel benutzt und wörtlich oder inhaltlich übernommene Stellen als solche gekennzeichnet habe. Ich erkläre, dass die Richtlinien zur Sicherung guter wissenschaftlicher Praxis der Universität Tübingen (Beschluss des Senats vom 25.05.2000) beachtet wurden. Ich versichere Eides statt, dass die falsche Abgabe einer Versicherung an Eides statt mit Freiheitsstrafe bis zu drei Jahren oder mit Geldstrafe bestraft wird.

Nauen, 2023

ZUSAMMENFASSUNG

Beeinträchtigungen innerhalb der cGMP-Signalkaskade im Gehirn können zu verschiedenen neurologischen Krankheiten führen. Dazu zählen beispielsweise Fehlbildungen bei der Ausbildung von Axonen, die für die Weiterleitung von Informationen im Nervensystem essentiell sind. Bisherige Untersuchungen zeigten, dass der Verzweigungsprozess der Hinterwurzelganglien im Rückenmark von Mäusen, abhängig von einer cGMP-Signalkaskade ist, die das C-Typ natriuretische Peptid (CNP), die partikuläre Guanylatzyklase (pGC oder GC-B) und die cGMP-abhängige Proteinkinase Typ I (cGKI) einschließt. Jedoch sind die Phosphodiesterasen (PDEs), welche cGMP in den Neuronen der Spinalganglien abbauen, sowie weitere Signalpartner der beschriebenen Kaskade noch nicht näher untersucht. In dieser Arbeit wurde daher die Fluoreszenz-Resonanzenergietransfer (FRET) Mikroskopie genutzt. Hierzu wurden u.a. transgene Mäuse genutzt, die den cGMP-FRET Sensor cGi500 oder mcGi500 in allen oder in spezifischen Geweben exprimieren. So wurde herausgefunden, dass die PDE2A verantwortlich ist für den Abbau von intrazellulärem cGMP in den Neuronen embryonaler Spinalganglien in der Maus. Darüber hinaus wurde durch Echtzeit-Mikroskopie festgestellt, dass es in den Somata bzw. Wachstumskegeln der Spinalganglien, Wechselwirkungen zwischen der CNP/GC-B/cGKI-Signalkaskade und Acetylcholin- bzw. ATP-induziertem Ca^{2+} gibt. Ein weiteres, gut geeignetes Model zur Untersuchung der Entwicklung von Nervenzellen, ist der Hühnerembryo. Hier wurde der CMV-cGi500 Vektor in das Neuralrohr des Hühnerembryos eingebracht und durch Elektroporation wurden die Neuralleistenzellen transfiziert. Diese differenzieren sich während der Embryonalentwicklung zu den sensorischen Neuronen der Spinalganglien, welche dann den cGi500-FRET Sensor exprimieren. Somit konnten Echtzeit-cGMP-Messungen *in ovo* durchgeführt werden. Diese Echtzeit-Messungen sowie Immunfärbungen zeigten, dass in den Neuronen der Spinalganglien von Hühnerembryonen sowohl die NO/cGMP/cGKI- als auch die CNP/cGMP/cGKI-Signalkaskade präsent sind. Somit könnte cGMP ebenfalls eine bedeutende Rolle bei der Verzweigung der Axone der Spinalganglienneurone im Hühnerembryo spielen.

Die NO-abhängigen Guanylatzyklasen, von denen zwei Isoformen (NO-GC1 und NO-GC2) bekannt sind, stellen für die Medikamentenforschung wichtige molekulare Zielstrukturen dar. In der Vergangenheit wurden bereits einige medikamentenähnliche Moleküle entwickelt, welche synergistisch mit NO die NO-GCs aktivieren und so für einen erhöhten cGMP-Spiegel in der Zelle sorgen. Die Wirkung dieser Moleküle in verschiedenen Bereichen des Gehirns, ist jedoch noch nicht ausreichend verstanden. Daher wurde in dieser Arbeit die Wirkung zweier

strukturell unterschiedlicher NO-GC-Stimulatoren – Bay 41-2272 und IWP-051 – im Hippocampus, Cerebellum und Striatum von Mäusen untersucht. Echtzeit-cGMP-Messungen von akuten Hirnschnitten transgener Mäuse ergaben, dass der NO-GC-Stimulator Bay 41-2272 in allen zuvor genannten Hirnbereichen eine Erhöhung der DEA/NO-induzierten cGMP-Level bewirkt. IWP-051 hingegen erhöhte die cGMP-Level ausschließlich in Cerebellum und Striatum, aber nicht in der CA1 Region des Hippocampus oder in primären Hippocampusneuronen. *In-situ* Hybridisierungsdaten ergaben, dass im Cerebellum und Striatum die mRNAs beider NO-GC-Isoformen exprimiert werden, während in der CA1 Region des Hippocampus nur NO-GC2 exprimiert wird. Diese Ergebnisse deuteten auf eine Isoform-spezifische Funktion des IWP-051 hin. Deshalb wurden die Echtzeit-cGMP Messungen jeweils mit NO-GC1- bzw. NO-GC2 Knockout Mäusen durchgeführt. Es wurde gezeigt, dass IWP-051 die DEA/NO-induzierten cGMP-Level im Striatum der NO-GC1 Knockout Mäuse nicht erhöhen konnte, jedoch in den NO-GC2 Knockout Mäusen, was die Vermutung einer Isoform-spezifischen Wirkung des IWP-051 auf die NO-GC1 verstärkt. Zusammengefasst konnte hier gezeigt werden, dass bereits entwickelte medikamentenähnliche Moleküle, wie Bay 41-2272 und IWP-051 die cGMP-Konzentration in bestimmten Hirnbereichen erhöhen und ihre Wirkung deshalb auch unbedingt in Hinblick auf Krankheiten des Nervensystems untersucht werden sollte.

ABSTRACT

Impaired cyclic 3' 5' guanosine monophosphate (cGMP) signaling has been linked to several neurological disorders, including inaccurate axon formation and pathfinding. It is well known that a cGMP signaling cascade, comprising the C-type natriuretic peptide (CNP), its guanylyl cyclase GC-B and cGMP-dependent protein kinase I (cGKI) is necessary for correct axon bifurcation of dorsal root ganglion neurons (DRGs) in mouse spinal cord. However, the identity of phosphodiesterases (PDEs) that degrade cGMP in DRGs as well as further signaling partners are not well understood. Here, we used Fluorescence resonance energy transfer (FRET)-based cGMP imaging to study cGMP signaling in the nervous system. Therefore, transgenic mice expressing the cGMP sensors cGi500 or mcGi500 globally or in specific tissues were used. We identified PDE2A to be the major enzyme responsible for the degradation of CNP-induced cGMP in DRG neurons. Real-time imaging of DRG somata and growth cones revealed a crosstalk between the CNP/cGMP/cGKI signaling cascade and acetylcholine- or ATP-induced Ca^{2+}. Another appropriate model to investigate neuronal development is the chicken embryo. Transfection of the CMV-cGi500 plasmid into neural crest cells that migrate and became DRG neurons made it possible to perform *in ovo* real-time cGMP imaging. Imaging experiments and immunostainings revealed a NO/cGMP/cGKI and CNP/cGMP/cGKI pathway in DRGs of chick embryos indicating a relevance of cGMP for DRG axon bifurcation.

The NO-dependent soluble guanylyl cyclases, of which two isoforms (NO-GC1 and NO-GC2) are known, are promising drug targets to increase cGMP in the brain. Drug-like small molecules were identified to work synergistically with NO. However, the effects of NO stimulators in the brain are poorly investigated. In this study, we analyzed the impact of two structurally different NO-GC stimulators, IWP-051 and Bay 41-2272, on cGMP signaling in the murine cerebellum, striatum, and hippocampus. FRET-based cGMP imaging revealed that Bay 41-2272 increased DEA/NO-induced cGMP in all three brain regions. Interestingly, IWP-051 potentiated DEA/NO-induced cGMP only in cerebellum and striatum but not in the hippocampal CA1 area or primary hippocampal neurons. *In-situ* hybridization indicated that in murine cerebellum and striatum mRNAs of both NO-GC isoforms are expressed, while in the hippocampal CA1 area only NO-GC2 is expressed. These results suggest an isoform-specific effect of IWP-051 on NO-GC1. Indeed, real-time cGMP imaging of acute brain slices revealed that IWP-051 did not potentiate DEA/NO-induced cGMP in striatum of NO-GC1 knockout mice, while in the striatum of NO-GC2 knockout mice it did. This study showed that NO-GC stimulators enhance cGMP in the brain and should be further investigated for the treatment of brain diseases.

TABLE OF CONTENTS

LIST OF ABBREVIATIONS

ACh	Acetylcholine
ADP	Adenosine diphosphate
ANP	Atrial natriuretic peptide
Ara-C	Cytosine-β-D-arabinofuranoside hydrochloride
ATP	adenosine triphosphate
BNP	Brain natriuretic peptide
BSA	Bovine serum albumin
CA1 – 3	Cornu Ammonis 1 – 3
Ca^{2+}	Calcium
CAG	CMV immediate early enhancer, chicken β-actin and rabbit β-globin
cAMP	Cyclic 3’ 5’ adenosine monophosphate
CF	Climbing fibre
CFP	Cyan fluorescent protein
cGi	cGMP indicator
cGK	cGMP-dependent protein kinase
cGMP	Cyclic 3’ 5’ guanosine monophosphate
CGNs	Cerebellar granule neurons
CICR	Ca^{2+}-induced Ca^{2+} release
CNGs	Cyclic nucleotide-gated channels
CNP	C-type natriuretic peptide
CO_2	Carbon dioxide
Cre	Cyclisation/recombination site-specific recombinase
DCN	Deep cerebellar nuclei
DEA/NO	2-(N,N-diethylamino)-diazenolate-2-oxide diethylammonium salt
DG	Dentate gyrus
DMEM	Dulbecco’s modified Eagle medium
DMSO	Dimethyl sulfoxide
DNA	Deoxyribonucleic acid
dNTP	Deoxynucleotide triphosphate

DREZ	Dorsal root entry zone
DRG	Dorsal root ganglion
EDTA	Ethylenediaminetetraacetic acid
EHNA	Erythro-9-(2-hydroxy-3-nonyl)-adenine
EPSC	Excitatory postsynaptic current
EtOH	Ethanol
FBS	Fetal bovine serum
FCS	Fetal calf serum
FRET	Fluorescence resonance energy transfer
GABA	Gamma-aminobutyric acid
GC-A	Particulate guanylyl cyclase A
GC-B	Particulate guanylyl cyclase B
GC-C	Particulate guanylyl cyclase C
GCL	Granule cell layer
GFP	Green fluorescent protein
GTP	Guanosine triphosphate
HBSS	Hank's balanced salt solution
H_2O	Water
HCNs	Hyperpolarization-activated cyclic nucleotide-gated channels
HNs	Hippocampal neurons
IBMX	3-Isobutyl-1-methylxanthine
IICR	Inositol-1,4,5-triphosphate ($InsP_3$)-induced Ca^{2+} release
$InsP_3$	Inositol-1,4,5-triphosphate
$InsP_3R$	Inositol-1,4,5-triphosphate receptor
K^+	Kalium
loxP	Locus of X-over in P1
LTD	Long-term depression
LTP	Long-term potentiation
mAChR	Muscarinic acetylcholine receptor
mcGi	Membrane-targeted cGMP indicator
MEM	Minimum essential medium

ML	Molecular layer
MSN	Medium-sized spiny neuron
Na^+	Natrium
nAChR	Nicotinic acetylcholine receptor
Nes	Nestin
NGF	Nerve growth factor
NDS	Normal donkey serum
NMDA	*N*-methyl-D-aspartic acid
NO	Nitric oxide
NO-GC	Soluble guanylyl cyclase
NOS	Nitric oxide synthase
ODQ	1H-[1,2,4]oxadiazolo[4,3-a]quinoxalin-1-one
PBS	Phosphate buffered saline
PC	Purkinje cell
PCL	Purkinje cell layer
PCR	Polymerase chain reaction
PDL	Poly-D-lysine hydrobromide
Pen/Strep	Penicillin/Streptomycin
PDE	Phosphodiesterase
PF	Parallel fibre
PFA	Paraformaldehyde
pGC	Particulate guanylyl cyclase
RNA	Ribonucleic acid
ROI	Region of interest
ROSA	Reverse orientation splice acceptor
RT	Room temperature
RyR	Ryanodine receptors
Sema3a	Semaphorin 3a
Tris	Tris(hydroxymethyl)aminomethane
YFP	Yellow fluorescent protein

1 INTRODUCTION

1.1 cGMP signaling

The second messenger cyclic 3',5' guanosine monophosphate (cGMP) is involved in various physiological processes like cellular growth and contractility, cardiovascular homeostasis, inflammation, sensory transduction and neuronal plasticity and learning.[1,2] cGMP is generated from guanosine triphosphate (GTP) by either nitric oxide (NO)-activated soluble guanylyl cyclases (NO-GCs, also termed sGCs) or by membrane-bound (particulate) guanylyl cyclases (pGCs) that are activated by peptide hormones like the natriuretic peptides, guanylin/uroguanylin or enterotoxins.[3,4] NO is generated from L-arginine and oxygen by nitric oxide synthases (NOS). There are at least three isoforms of NOS which are derived from distinct genes: NOS-1, also termed as neuronal NOS (nNOS), is especially expressed in neuronal tissue. NOS-2, also referred to as inducible NOS (iNOS) is expressed in macrophages, hepatocytes, smooth-muscle cells and others. NOS-3, also called endothelial NOS (eNOS), is present in the endothelium of a variety of tissues.[5-7]

The mammalian NO-GC is a heterodimeric hemoprotein that consists of a larger α subunit and a smaller heme-containing β subunit. Currently, two isoforms for each subunit are known. They are termed α_1, α_2 and β_1. The functional relevant and most abundant combinations are $\alpha_1\beta_1$ (termed NO-GC1) and $\alpha_2\beta_1$ (termed NO-GC2). The $\alpha_1\beta_1$ isoform is ubiquitiously expressed in mammalian tissues like lung, heart, kidney, spleen, muscle and brain while the $\alpha_2\beta_1$ isoform is most prominent in the brain, uterus and placenta. A functional role for the β_2 subunit still remains to be elucidated.[3,8-10] The prosthetic heme group of NO-GC is bound to the β subunit through the axial ligand histidine 105 and the heme-binding motif tyrosine 135 and arginine 139.[11] NO binding to the heme Fe^{2+} leads to the formation of nitrosyl heme. This disrupts the histidine 105-iron bond and leads to the activation of the enzyme.[10]

The pGC family comprises at least seven enzymes (GC-A to GC-G), each of them functions as a homodimer. All of them consist of an extracellular ligand-binding domain, a single transmembrane region and an intracellular cyclase domain.[12] Until now, ligands for GC-A, GC-B and GC-C have been identified. While atrial natriuretic peptide (ANP) and B-type natriuretic peptide (BNP) preferentially bind GC-A, C-type natriuretic peptide

(CNP) activates GC-B. GC-C mediates the effects of guanylin, uroguanylin and heat-stable enterotoxins.[13-15] GC-A is mainly expressed in brain, kidney, lung, vasculature, liver, endothelial and adipose tissues.[16] GC-A-mediated signaling is crucial for maintenance and regulation of cardiovascular homeostasis, since GC-A null mice exhibit cardiac hypertrophy, high blood pressure and ventricular fibrosis.[17] Genetic ablation of ANP results in hypertensive mice with cardiac hypertrophy, while BNP disruption in mice leads to ventricular fibrosis, but not to increased blood pressure or cardiac hypertension.[18-21] GC-B is highly expressed in brain, dorsal root ganglion neurons of the spinal cord (for more details see also chapter 1.1.1), lung, bone, heart and ovary tissue.[22]

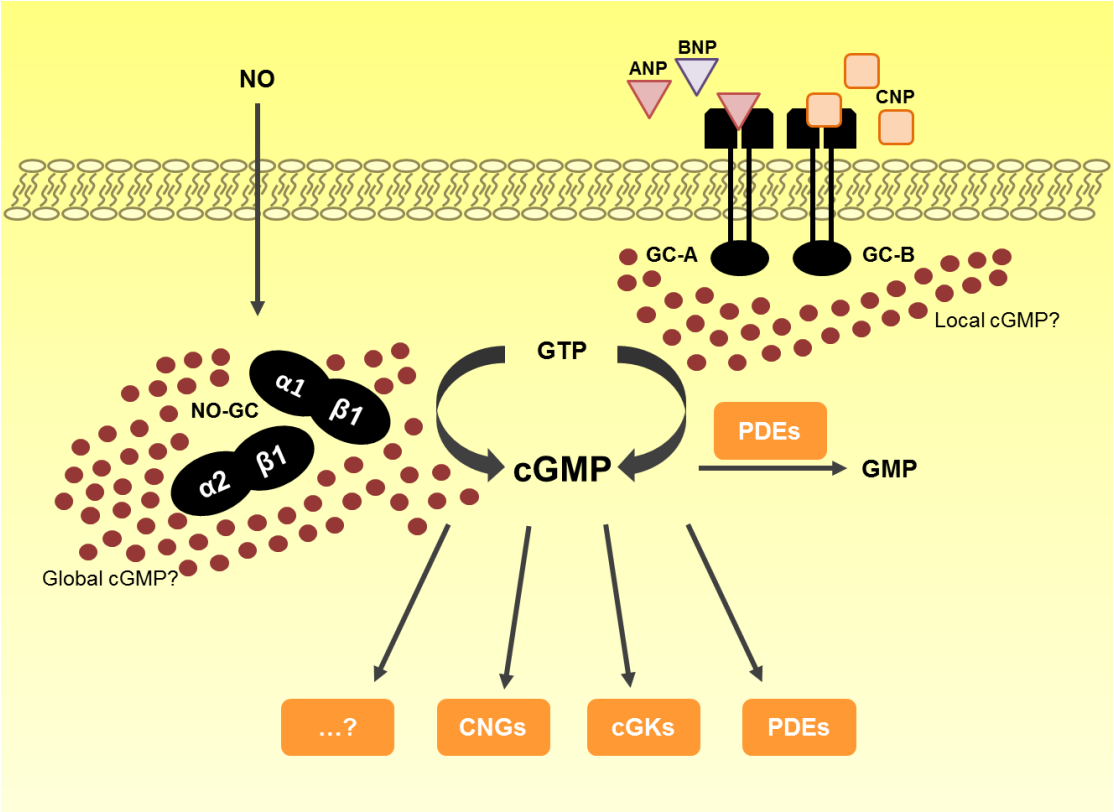

Figure 1-1: The cGMP signaling pathway. Cyclic 3',5' guanosine monophosphate (cGMP) can be generated from guanosine triphosphate (GTP) by either nitric oxide (NO)-activated soluble guanylyl cyclases (NO-GCs) or by natriuretic petptide-activated particulate guanylyl cyclases, such as GC-A (activated by atrial natriuretic peptide, ANP and B-type natriuretic peptide, BNP) and GC-B (activated by C-type natriuretic peptide, CNP). Two functional isoforms of NO-GCs are known: NO-GC1 ($\alpha_1\beta_1$) and NO-GC2 ($\alpha_2\beta_1$). It is hypothesized that NO-GCs produce a global cGMP pool in the cytosol of a cell, while pGCs produce a local membrane-located cGMP pool. cGMP activates several downstream effectors, such as cyclic nucleotide-gated channels (CNGs), cGMP-dependent protein kinases (cGKs) and phosphodiesterases (PDEs) that also regulate the degradation of cGMP. Besides those, there might be several additional downstream targets of cGMP that have not been discovered yet.[1, 2, 23]

Once generated, cGMP acts on several downstream effectors including cyclic nucleotide-regulated channels (CNGs) and hyperpolarization-activated cyclic nucleotide-gated channels (HCNs), cGMP-dependent protein kinases (cGKs) and cyclic adenosine 3',5' monophosphate (cAMP)- and/or cGMP-degrading phosphodiesterases (PDEs).[2] The cGMP signaling cascade is summarized in Figure 1-1.

CNGs and HCNs belong to the family of cyclic nucleotide-binding domain-containing ion channels.[24-26] They hardly differ in their structural architecture, but possess different ion selectivities.[27,28] While CNGs let Na^+, K^+ and Ca^{2+} pass and are strictly regulated by cyclic nucleotides, voltage-operated HCNs mainly carry Na^+ and K^+ and some HCN isoforms seem to be unaffected or even inhibited upon cAMP binding.[29-31] A well understood role of cGMP-gated CNG signaling is the signal transduction of photoreceptors. In the dark, CNG channels are kept open by cGMP binding which leads to an influx of Na^+ and Ca^{2+} that depolarizes the plasma membrane. Ca^{2+} interacts with calmodulin and other potential, not yet identified Ca^{2+}-binding proteins. Light activates a signaling cascade that in turn activates PDE6 that hydrolyses cGMP. This leads to the closure of the CNG channel and a hyperpolarization of the plasma membrane.[26,28] HCNs were found to play a role in the cardiac system. They contribute to pacemaking in sinoatrial pacemaker cells as well as to ventricular action potential waveform in the murine heart.[32,33] Moreover, HCNs are involved in different neuronal signaling cascades and are highly discussed as potential targets to treat neuropathic pain.[34,35]

The cGKs belong to the family of serine/threonine kinases. In vertebrates, the prkg1 and prkg2 genes encode three cGK isoforms: cGK type Iα, cGK type Iβ (cGKIα/β) and cGK type II (cGKII), respectively.[2,36,37] The cGK enzymes are homodimers and have a rod like structure. They are composed of two functional domains: a regulatory (N-terminal) and a catalytic (C-terminal) domain. The regulatory domain contains two cGMP-binding pockets, while the catalytic domain has the MgATP- and a substrate-binding pocket. The dimerization is mediated by a leucine zipper motif in the N-terminal region. An additional important function of the N-termini of cGK enzymes is the targeting to different subcellular compartments.[38,39] cGKI is expressed in various tissues such as smooth muscle cells, dorsal root ganglia (chapter 1.1.1), cerebellum, hippocampus (chapter 1.1.3), and others.[40-43] In contrast, cGKII is more prominent in intestinal mucosa, kidney and several brain regions.[44,45] It is well accepted that cGKI plays an important role in

vasorelaxation.[39] Mice deficient for cGKI show impaired NO/cGMP-dependent dilation of large and small arteries.[46,47]

The cytosolic concentration of cGMP crucially depends on the activity of PDEs. The mammalian PDEs are subdivided into 11 families (PDE1 – PDE11). Within these families multiple isoforms are expressed.[48] There are PDE families with a high substrate preference for either cAMP (PDE4, 7, 8) or cGMP (PDE5, 6, 9). 5 families (PDE1, 2, 3, 10, 11) hydrolyze both cAMP and cGMP.[49-51] All mentioned PDEs hydrolyze the 3' cyclic phosphate bonds of cAMP and/or cGMP resulting in 5'AMP and 5'GMP. A cross talk between the two cyclic nucleotides is achieved, e.g. through cGMP-mediated stimulation and inhibition of the cAMP-hydrolyzing enzymes PDE2 and PDE3, respectively. PDE5 was found to be cGMP-modulated and -specific. cGMP accelerates the PDE5-dependent degradation by activating cGKI that phosphorylates PDE5. cAMP can bind to the GAF domain of PDE10 and thus inhibit the hydrolysis of cGMP.[50-54]

1.1.1 The role of cGMP in establishing DRG axonal projections

Dorsal root ganglia (DRGs) are structures of the peripheral nervous system. They transduce peripheral stimuli and convey their information to the central nervous system through their central fibers entering the spinal cord.[55] In mice, between embryonic day 10-13 (E10-E13), axons of sensory neurons that reside in DRGs enter the spinal cord at the dorsal root entry zone. Once entered, axons bifurcate which means they form two daughter branches that grow in rostral and caudal direction, respectively (Figure 1-2 A). This branching process takes place at the growth cone, a highly motile sensorimotor structure at the tip of an outgrowing neurite.[56,57] The growth cone is the leading edge of the axon, directing the axon along its intended path by detecting attractive and repulsive signals from the environment.[58,59] Besides bifurcation, there are two additional branching mechanisms that DRG axons can undergo: (1) interstitial branching or collateral formation – collaterals branch off from a stable axon shaft penetrating the grey matter – and (2) terminal branching or arborization – the terminal arborization of collateral terminals (Figure 1-2 B).[60-64] The bifurcation of embryonic DRG sensory axons was shown to depend on a specific cGMP signaling cascade including CNP, GC-B and cGKIα (Figure 1-2 C).[43] While GC-B and cGKIα are expressed in sensory neurons of DRGs, CNP localizes to the dorsal site of the spinal cord (Figure 1-2 A). In the absence of one of these signaling partners, bifurcation of DRG sensory axons is largely impaired. Axons turn either rostrally or caudally, but hardly form two daughter branches (Figure 1-2

D).[43,65,66] Other cGMP generators, such as GC-A and NO-GCs as well as the cGMP effectors cGKIβ and cGKII are not expressed in E12 DRG neurons.[65] Therefore, there was no bifurcation error found in the absence of NO-GC in murine embryonic DRG neurons (Figure 1-2).[66]

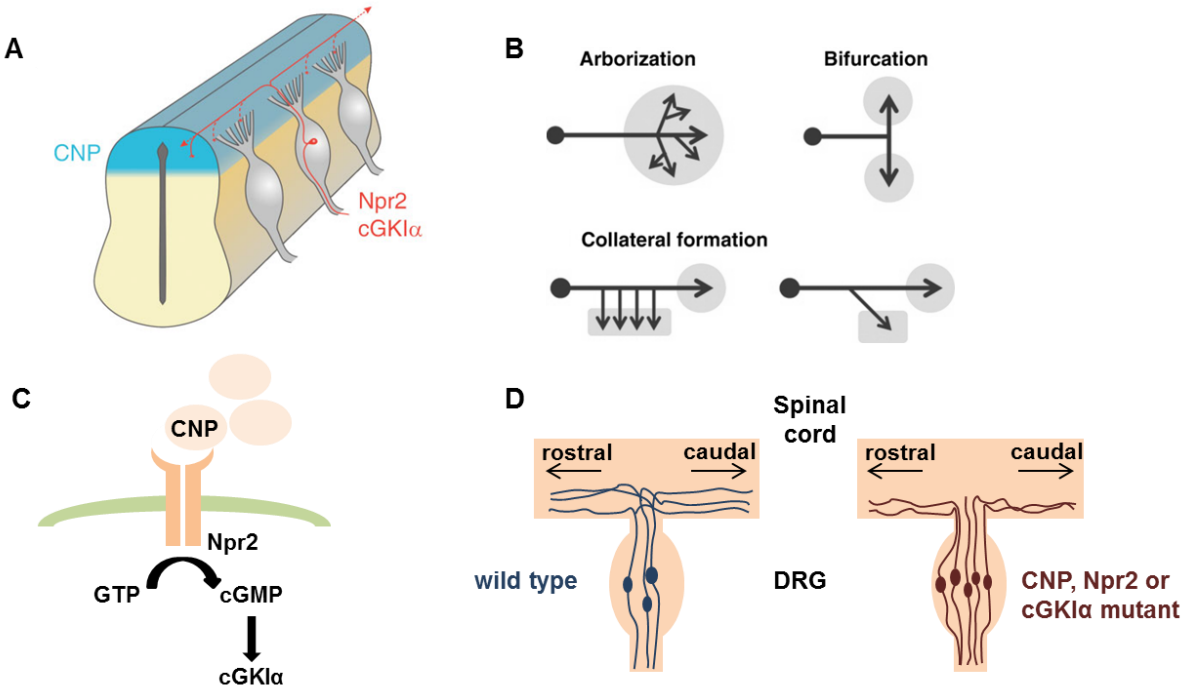

Figure 1-2: The role of cGMP signaling in embryonic sensory axon bifurcation of mice. (A) Illustration of the murine, embryonic spinal cord with attached dorsal root ganglions (DRGs, gray). Inside the DRGs reside sensory neurons (red) that grow axons inside the spinal cord. Upon entering the spinal cord at the dorsal root entry zone during embryonic day 10-13, axons bifurcate and form two stem axons, one growing in rostral and one into caudal direction (indicated by two red arrows along the spinal cord). While Npr2 and cGKIα are expressed in sensory neurons (red), CNP is exposed along the dorsal part at the spinal cord (blue). Picture taken from Schmidt et al., 2010.[56] (B) Besides bifurcation, DRG sensory axons undergo two additional forms of branching: (1) terminal branching/arborization – terminal branching or arborization of collaterals and (2) interstiatial branching/collateral formation – the outgrowth of collaterals from a stable axon shaft that penetrate the gray matter. Pictures taken from Gibson et al, 2011.[64] C) It was found that bifurcation of DRG sensory axons is dependent on a cGMP signaling cascade including CNP, Npr2 and cGKIα. (D) In the absence of one of the cGMP signaling components (right), bifurcation is largely impaired compared to wildtype axons (left). Axons turn either in rostral or caudal direction and hardly form two daughter branches.[43]

Zhao and Ma could show that CNP not only promotes axonal branching of rat dissociated DRG neurons and the axonal outgrowth of rat DRG explants but also acts as an attractive guidance cue for embryonic DRG growth cones.[67] However, there are several other molecules involved in axon guidance. The best ones understood are netrins, Slits, and semaphorins.[59] Netrin-1 is mostly expressed in the ventral spinal cord and acts as a bifunctional guidance cue, attracting some neuronal populations, such as commissural

axons, while repelling others.[68,69] Masuda et al. showed that netrin-1 is an important repellent guidance cue for embryonic DRG sensory neurons. DRG axons that were exposed to netrin-1 were chemorepelled and thus axonal outgrowth was inhibited in vitro. Moreover, they observed that a subset of DRG axons of netrin-1 knockout embryos did not project to the DREZ, but rather projected aberrantly towards the intermediate and ventral part of the spinal cord.[70] Another multifunctional group of guidance cues are the Slit family members. Originally, they were reported to act as chemorepellents. It was reported that rat DRG axonal outgrowth is inhibited in presence of hSlit2 *in vitro*.[71] However, Slit was also purified as a factor that stimulates sensory axon branching and elongation.[72] Semaphorins are known to act as repulsive guidance cues. *In vitro* experiments with murine sensory DRG neurons revealed that Semaphorin 3a (Sema3a) induces growth cone collapse.[73] Interestingly, it was shown that cGMP counteracts the Sema3a-induced growth cone collapse in murine and rat sensory DRG neurons while cAMP was without effect.[43,74] The cGMP downstream target cGKI is not part of the Sema3a-induced signaling cascade that leads to growth cone collapse, but activation of cGKI can counteract the Sema3a-mediated collapse of sensory neurons.[43] Brown et al. published that the response of murine DRG sensory neurons to Sema3a can be divided into two steps: growth cone collapse and retraction.[75] Taken together, attractive and repulsive guidance cues are crucial for proper axon guidance comprising processes like growth cone steering or branching. It is well accepted that not only the presence, but also a graded distribution of guidance cues controls the direction of axons.[76] When a growth cone approaches a guidance cue gradient it starts turning toward or away from the cue through intracellular generation of second messengers such as cyclic nucleotides or calcium (Ca^{2+}).[67,77] Hong et al. published that netrin-1-induced growth cone turning of cultured *Xenopus* spinal neurons is mediated by Ca^{2+} influx from extracellular space and by Ca^{2+}-induced Ca^{2+} release (CICR). Netrin-1-induced attraction was converted to repulsion when either of these two Ca^{2+} sources was blocked.[78] High amplitude Ca^{2+} is generated from CICR via ryanodine receptors (RyRs) or from inositol-1,4,5-triphophate ($InsP_3$)-induced Ca^{2+} release (IICR) via $InsP_3$ receptors ($InsP_3Rs$) and mediate cue-induced attraction.[79] On the contrary, repulsion is mediated by lower amplitude Ca^{2+} that is generated by Ca^{2+} influx through plasma membrane channels.[80,81]

1.1.2 The role of Ach and ATP in developing DRGs

Acetylcholine (ACh) is a classical neurotransmitter activating nicotinic as well as muscarinic acetylcholine receptors (nAChRs and mAChRs). ACh is considered to act as an algogenic agent since it has been shown to produce burning pain when it was applied to human skin.[82,83] mAChRs comprise 5 isoforms (M1R-M5R). They all are G-protein coupled receptors with seven transmembrane domains.[84,85] It was shown that M2R-M4R are expressed in the dorsal horn of the rat spinal cord.[86,87] However, how different subtypes of mAChRs contribute to nociception is still controversially discussed.[88] Honda et al. showed that injection of formalin into a paw of mice leads to two distinct phases of licking and biting. Formalin injection caused an increase of ACh in the spinal cord. Additionally, they found that the second phase can be inhibited by treatment with M3R antagonists, suggesting a role of ACh/mAChRs in formalin-induced nociception.[89] On the contrary, Iwamoto and Marion reported an antinociceptive effect of agonist-induced mAChRs in rats.[90] Nandigama et al. found that specific mAChR subtypes (M2R-M4R) are expressed in a part of adult DRGs that provide afferents to the bladder. They hypothesize that processing of sensory information from the bladder might be under direct cholinergic control.[85] nAChRs were also reported to participate in the modulation of pain perception. Stimulation of neuronal nAChR excites or sensitizes rat peripheral sensory nerve fibers, but has also been reported to mediate cholinergic antinociception.[91,83,92] Neuronal nAChR are pentameric ligand-gated ion channels consisting of differently assembled α and β subunits.[93] In DRG neurons of postnatal rats mRNA analysis revealed the expression of α2-α7 and β2-β4 subunits.[94] Investigations performed with neuronal cell cultures of *Xenopus* revealed that ACh attracts growth cones of spinal neurons by Ca^{2+} influx.[95] The filopodial outgrowth of B5 neurons of the pond snail *Helisoma trivolvis* was increased when they were treated with ACh. This process was mediated via nAChR and Ca^{2+} influx.[96] Hanson et al. published that in the murine embryonic spinal cord endogenously released ACh – most likely from the motoneurons – acting on nicotinic receptors, is essential for the generation of spontaneous rhythmic activity.[97]

Extracellular ATP plays an important role in the nervous system, e.g. in neurotransmission, neuromodulation, and chemoattraction.[98,99] ATP binds to P_2 receptors which are classified into two families: P_2X ionotropic ligand-gated channel receptors (P_2X_1-P_2X_7) and the metabotropic G-protein-coupled receptors (P_2Y_1, P_2Y_2, P_2Y_4, P_2Y_6, P_2Y_{11}-P_2Y_{14}).[100, 101] P_2X receptors are assembled as homo- or heterotrimers.[102] Purinergic

signaling is involved in pathological processes such as the ability of ATP to evoke pain or to generate fast excitatory action potentials in rat DRG neurons, indicating that ATP acts as a pronociceptive stimulus.[99,103-105] While P_2X_2 and P_2X_3 receptors are preferentially expressed by rat C-fiber neurons, P_2X_5 and P_2X_6 receptors are preferentially expressed by A-fiber neurons. P_2X_4, P_2Y_1 and P_2Y_2 receptors were expressed similarly by rat A- and C-fiber neurons.[106, 107] Boldogköi et al. showed that murine DRGs express P_2X_3 at embryonic stages (E9.5-E14.5).[108] Furthermore, in sensory neurons, ATP is suggested to act as one of the first mediators of cell damage, because all cells produce ATP which is released into the extracellular space when cells are damaged.[99,105]

1.1.3 cGMP signaling and synaptic plasticity

Synaptic plasticity is a biological process by which synapses strengthen or weaken over time to increase or to decrease synaptic activity, due to specific signaling pathways.[109] The second messenger cGMP is considered to play an important role in synaptic plasticity, e.g. in long-term depression (LTD) and long-term potentiation (LTP) in the cerebellum and hippocampus, respectively. Both types of synaptic plasticity are linked to specific forms of learning.[110-116]

Located in the medial temporal lobes of the brain, the hippocampal formation plays a key role in different types of learning and memory.[117] It comprises four cortical regions: the dentate gyrus (DG), the hippocampal proper (Cornu Ammonis 1-3; CA1, CA2, CA3), the subicular complex, and the entorhinal complex.[118] CA1 hippocampal synapses have been extensively studied and have become a major model system for understanding synaptic transmission and plasticity. These synapses are glutamatergic, have vesicle-mediated transmission and represent a model for LTP[119] that includes a *N*-methyl-D-aspartic acid (NMDA) receptor-mediated Ca^{2+} influx that activates Ca^{2+}/calmodulin-regulated nNOS which leads to the synthesis of NO in the postsynapse. NO diffuses as a retrograde messenger through the synaptic cleft into the presynaptic terminal. Here, it is thought to activate its effectors, e.g. NO-GCs followed by a rise of cGMP concentration and the activation of cGK (Figure 1-3).[110] Arancio et al. found that in cultured hippocampal neurons, NO travels across the extracellular space to cause long-lasting enhancement of excitatory postsynaptic currents.[120] Furthermore, application of inhibitors of NO-GCs or cGKs to cultured hippocampal neurons or hippocampal slices blocked potentiation by either tetanic stimulation or low-frequency stimulation paired with postsynaptic depolarization.[121,122,123] Besides LTP at CA1 synapses, cGMP signaling is considered to

be involved in a form of hippocampal LTD.[110] Reyes-Harde et al. showed that a release of Ca^{2+} from ryanodine-sensitive stores is necessary for the induction of LTD. Here, NO-GC-generated cGMP was suggested to activate ADP-ribosyl cyclase, in a cGKI-dependent manner. This leads to the generation of ADP ribose an endogenous activator of RyRs.[124,125]

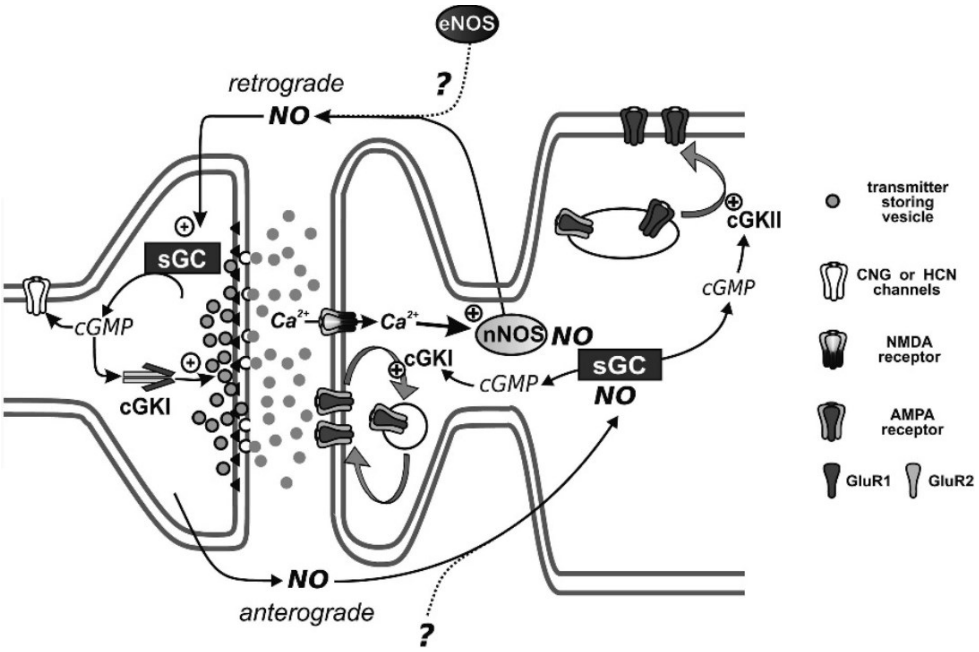

Figure 1-3: Model for the role of cGMP signaling in synaptic plasticity. Depending on the brain region, postsynaptically produced NO diffuses into the presynaptic terminal (retrograde signalling) or *vice versa* (anterograde signalling). NO might be produced by nNOS or by eNOS from nearby vessels and activates NO-GC (sGC) leading to cGMP production. The downstream targets of cGMP in synaptic plasticity are cGKI, cGKII and the ion channels HCN and CGN. In the hippocampus, cGKI is thought to be localized in the presynapse phosphorylating various proteins involved in cytoskeletal and vesicular dynamics leading to an increase in transmitter release and LTP. cGKII has been suggested to be expressed postsynaptically to increase the amount of GluR1 homotetramers at the extrasynaptic surface. Anterograde NO signalling is believed to induce LTD in the cerebellum. In this case, cGKI is expressed post-synaptically, that might lead to an enhanced internalisation of AMPA receptors through phopshporylation of G-substrate (not shown), which acts as inhibitor of protein phosphatases. This increases the level of phosphorylated AMPA receptors, which are removed from the postsynaptic membrane, thus, resulting in LTD. Picture taken from Kleppisch and Feil, 2009.[110]

The cerebellum is responsible for the control of smooth and skillful movements as well as for higher cognitive and emotional functions. It contains many different types of excitatory and inhibitory neurons.[126,127] The excitatory glutamatergic neurons use glutamate as their neurotransmitter. They comprise granule cells, unipolar brush cells, and large neurons from the deep cerebellar nuclei (DCN). The inhibitory GABAergic neurons, including Purkinje cells (PCs), Golgi cells, Lugaro cells, candelabrum cells,

basket cells, stellate cells, and small cells of the DCN, use gamma-aminobutyric acid (GABA) and/or glycine as neurotransmitter. In addition to neuronal cell types, there are the Bergmann glia cells and oligodendrocytes. The cerebellum is organized in a three-layer structure: the molecular layer (ML), the Purkinje cell layer (PCL) and the granule cell layer (GCL).[126,128,129] The large dendritic tree of a Purkinje cell receives excitatory signals from a single climbing fibre (CF) and numerous parallel fibres (PFs). Motor learning is considered to be based on cerebellar LTD of glutamatergic transmission from CFs and PFs onto PCs.[110,111] The increase of both, postsynaptic NO-induced cGMP and Ca^{2+}, is sufficient to induce LTD. An important downstream effector of cGMP in PCs of rodents is cGKI.[130,131] The application of NMDA/NO-GC and cGK inhibitors to cerebellar slices impaired LTD induction.[132] An impairment of LTD was also observed, when cerebellar slices of mice with a PC-specific ablation of cGKI were analyzed.[130]

The striatum serves as the primary input area of basal ganglia. Most of striatal cells are GABAergic, including a large population of principal cells and a small population of interneurons (fast-spiking or low-threshold spiking). Cholinergic interneurons can be found as well. However, the vast majority of neurons in the striatum are medium-sized spiny neurons (MSNs) that can be divided into two classes: (1) striatonigral MSNs express high levels of dopamine D1 and muscarinic M4 receptors and project to the internal globus pallidus and substantia nigra pars reticulata, while (2) striatopallidal MSNs express high levels of dopamine D2 receptors and adenosine A2A receptors and project axons to the external globus pallidus.[133-136] The two forms of synaptic plasticity, LTD and LTP, have been shown in the rodent striatum.[137,138] The MSNs receive cortical information from glutamatergic neurons and transfer them to output structures under control of dopaminergic, cholinergic and nitrergic interneurons. The interplay of these three neurotransmitters determines whether corticostriatal transmission is amplified (LTP) or dampened (LTD) following repetitive activation.[139,140] It was shown that a group of striatal interneurons expressing nNOS forms synaptic contacts with putative MSNs.[141]

1.2 Pharmacological intervention with the cGMP signaling pathway

Aberrant cGMP production and/or signaling had been shown to accompany several disorders and diseases, e.g. in the cardiovascular and neurological field. To treat those,

drugs have been developed that target the cGMP signaling cascade leading to an increased cellular cGMP level.[142]

A therapeutically and frequently used group of drugs are the PDE blockers. The most famous PDE inhibitors might be PDE5 blockers such as Sildenafil (Viagra®), Tadalafil (Cialis®) and Vardenafil (Levitra®). They have been established as first-line therapy for the treatment of erectile dysfunction.[143] Under normal conditions, sexual stimulation causes NO release from nerve endings and endothelial cells into the penile tissue leading to activation of NO-GC and the subsequent generation of cGMP in smooth muscle cells. Here, cGMP activates cGKI, leading to smooth muscle relaxation. Pharmacological inhibition of PDE5 leads to an elevation of cGMP enhancing the effect of sexual stimulation in the penile tissue.[143-145] PDE5 inhibitors are also used to treat pulmonary arterial hypertension or myocardial fibrosis and hypertrophy.[146-151] In the brain, mRNAs of most PDE isoforms are found but their level of expression varies from one region to another and in some cases even between neurons of the same region.[152,53] The subtypes of PDE1 and PDE2 are widely expressed throughout the CNS. The expression of PDE1 and PDE2A in the hippocampus and PDE1 in the cerebral cortex suggests a role in learning and memory formation. Indeed, treatment of rats with learning and memory impairments, using the PDE1 inhibitor Vinpocetine had beneficial effects on cognitive functions.[153-155] Moreover, it was shown that PDE1 plays an important role in synaptic plasticity, as its inhibition with PDE1 inhibitor Lu AF64196 caused increased LTP in rat ventral striatum.[156] Fieblinger et al. showed that excitatory striatal inputs are depressed by PDE1. Blocking the PDE activity boosts presynaptic calcium entry and glutamate release, leading to strongly increased synaptic transmission.[157] Inhibition of PDE2 using Bay 60-7550 enhanced hippocampal LTP of synaptic transmission in rats without altering basal synaptic transmission. Inhibition of PDE2 also improved rats social behavior and object recognition memories.[158] PDE10 transcripts are present in a number of brain regions including hippocampus, hypothalamus and cerebellum with the strongest expression in the striatum, suggesting PDE10 to be a target to treat psychiatric disorders of frontostriatal dysfunction.[154,159,160] In rats, the PDE10 inhibitor Papaverine reversed deficits in attentional set-shifting induced by the NMDA receptor antagonist phencyclidine, which is a model to investigate cognitive deficits of schizophrenics.[161] Additionally, in patients with Huntington's disease, reduced mRNA and protein levels of PDE10A were found, which were most likely caused by the loss of striatal MSNs.[162] In R6/2 mice, a mouse model of Huntington's disease, it was shown that treatment with the

recently developed PDE10A inhibitor TAK-063 prevented striatal neurodegeneration and suppressed elevation in seizure frequency. Furthermore, TAK-063 suppressed the development of clasping behavior and motor deficits.[163] In contrast to the protective effects of several PDE inhibitors in diseases of the brain, heart and lung, the use of the PDE5 inhibitor Sildenafil has been linked to an increased risk of melanoma.[164,165]

It has been reported that cardiovascular diseases are associated with resistances to NO and organic nitrates.[166] NO-GC is the key enzyme in the NO-cGMP signaling pathway and therefore represents a promising therapeutic target. NO-GC stimulators sensitize NO-GC to low levels of bioavailable NO by stabilizing the nitrosyl-heme complex and thus maintaining the enzyme in its active configuration.[167] The so-called stimulators are considered to directly activate NO-GCs, both independent from NO or in synergy with NO.[168-170] The stimulator Bay 41-2272 is a pyrazole-pyridine derivative (Figure 1-4 A) developed by the company Bayer. It stimulates NO-GC independently of NO. It is very potent, stimulating recombinant NO-GC at concentrations ranging from 0.1 nM to 100 µM. Bay 41-2272 acts heme-dependent since it does not stimulate a heme-free variant of NO-GC.[171] In contrast to the first developed NO-GC stimulator YC-1, an inhibitor of platelet aggregation, Bay 41-2272 does not cause any cGMP-independent effects or any inhibition of PDE5 at concentrations necessary to stimulate NO-GC.[172-177] Impaired NO/NO-GC/cGMP signaling is probably a major cause of arterial hypertension.[178,179] It has been shown that YC-1 and Bay 41-2272 significantly reduced mean arterial pressure in hypertensive rats.[171, 180] Furthermore, inhaling Bay 41-2272 resulted in selective pulmonary vasodilation in ovine and rat models of pulmonary hypertension (PH).[181] Taken together, the aforementioned NO-GC stimulators showed beneficial effects in experimental models of PH but were associated with poor pharmacokinetic properties and drug metabolism.[182] Here, Stasch and colleagues went on with the optimization of existing NO-GC stimulators and found Riociguat (Adempas®), the first potent, orally available NO-GC stimulator that was approved in 2013 to treat patients who suffer from PH.[182-184]

A novel NO-GC stimulator, that is structurally different from before mentioned Bay stimulators, is IWP-051. It is a pyrazole-pyrimidine derivative (Figure 1-4 B), developed by Ironwood Pharmaceuticals. It is described to act heme-dependently and in synergy with NO. In normotensive rats, administration of increasing doses of IWP-051 (ranging from 1 –100 mg/kg) decreased mean arterial pressure in a dose-dependent manner.[185]

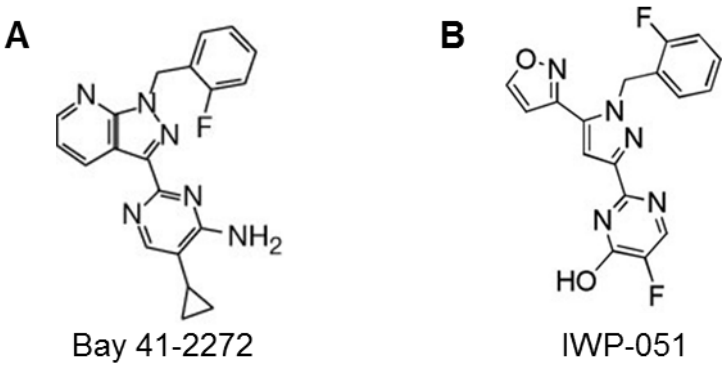

Figure 1-4: Structures of the two NO-GC stimulators Bay 41-2272 and IWP-051. (A) Bay 41-2272 is a pyrazole-pyridine derivative developed by the company Bayer. It stimulates NO-GC independently of NO. (B) IWP-051, a pyrazole-pyrimidine derivative, is a potent NO-GC stimulator developed by Ironwood Pharmaceuticals. It is described to act heme-dependently and in synergy with NO.[171, 185]

1.3 Second messenger imaging

Live-cell imaging has become an integral part of modern cell biology. Fluorescent protein tags and live-cell dyes provide a wide range of tools to investigate cellular processes in real time.[186] Over the last few decades the number of available genetically encodable biosensors and the types of processes they can monitor has increased rapidly.[187] Early optical sensors included small molecules that changed their fluorescence properties after binding of the analyte, such as the Ca^{2+} indicator Fura-2.[188] Fura-2 is an UV-excited Ca^{2+} indicator that allows for ratiometric measurements. The compound combines an 8-coordinate tetracarboxylate chelating site with stilbene chromophores.[189] Its absorbance peak shifts from 340 nm in the Ca^{2+}-bound state to 380 nm in the Ca^{2+}-free state. The emission wavelength is ~515 nm for either of the two excitation wavelengths. Fura-2 was engineered as acetoxymethyl esters (Fura-2/AM) to offer a more convenient method to load the hydrophilic dye into cells. The hydrophobic Fura2/AM is membrane permeable and can be easily loaded to cells by simply adding it to extracellular medium. Intracellular esterases cleave the AM groups and Fura-2 is trapped in the cytoplasm.[189,190]

Fluorescence resonance energy transfer (FRET)-based biosensors are a powerful tool to investigate cellular dynamics in living cells and tissues.[191,192] FRET is a non-radiative transfer of energy from one fluorophore to another via dipole-dipole interactions.[187] The prototypical FRET-based biosensor consists of a recognition element that is fused to two fluorescent proteins. A conformational change of the recognition element and the fluorescent proteins will lead to a change in FRET efficiency which results in changes of

the fluorescence intensity of the two fluorescent proteins.[193] That is exactly the working principle of the cGi (cGMP indicator) sensors developed by Russwurm and colleagues in 2007 (Figure 1-5 A). The biosensor cGi500 consists of the tandem cGMP-binding sites of the bovine cGKI that are flanked by cyan fluorescent protein (CFP) and yellow fluorescent protein (YFP). Its half-maximally effective cGMP concentration was reported to be 500 nM. In the absence of cGMP, both fluorophores are in close proximity. FRET occurs from excited CFP to YFP resulting in increased fluorescence of the latter. When cGMP is bound, the sensor undergoes a conformational change that increases the distance between CFP and YFP, thereby decreasing FRET efficiency. This leads to an increased emission of CFP at 480 nm and a decreased emission of YFP at 535 nM. The ratio of CFP/YFP emission can directly be correlated to the produced cGMP concentration (Figure 1-5 B).[194] In-cell calibration of β-escin-permeabilized vascular smooth muscle cells revealed that cGi500 detects cGMP levels as low as 100 nM cGMP and is saturated at ~ 3 µM cGMP.[195] Comparable experiments have shown that the sensor cGi500 detects cAMP levels higher than 30 µM which is not in the range of physiological cAMP concentrations (Wolters and Feil 2017, unpublished data).

In 2013, Thunemann and Wen et al. generated a mouse that expresses the cGi500 sensor globally in all tissues and cells (Figure 1-5 C). It is named R26-CAG-cGi500(L1). Therefore, real-time monitoring of cGMP is no longer restricted to transfected cultivated cells, but also possible in living tissues and animals. They showed that different types of smooth muscle cells had different sensitivities to the NO donor 2-(N,N-diethylamino)-diazenolate-2-oxide diethylammonium salt (DEA/NO), ANP and CNP. Moreover, they recorded robust NO-induced cGMP signals in blood vessels of isolated retina and in the cremaster microcirculation of anesthetized mice. With the use of a dorsal skinfold chamber and multiphoton microscopy, NO-induced vascular cGMP signals associated with vasodilation were detected *in vivo*.[195-197] A second Cre-activatable transgenic mouse line (Figure 1-5 D), named R26-CAG-mT/cGi500(L2), carries a floxed stop cassete in front of the cGi500 sensor. This leads to the expression of membrane-targeted tandem dimer tomato (td tomato) before Cre recombination. The construct is based on the R26-mT/mG construct published by Muzumdar et al in 2007. Depending on where Cre is expressed, a tissue-specific expression of cGi500 can be achieved.[197,198]

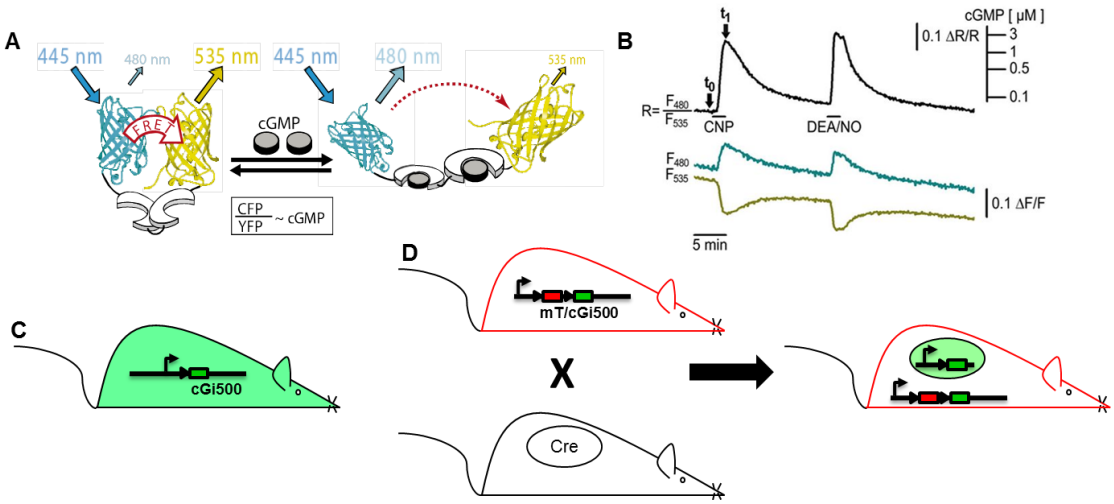

Figure 1-5: Transgenic mice for cGMP imaging. (A) The cGMP biosensor cGi500 consists of the tandem cGMP binding site of bovine cGKI (white) that is flanked by CFP (cyan) and YFP (yellow). In the absence of cGMP, CFP and YFP are in close proximity (less than 10 nm, left) and FRET occurs from excited CFP leading to light emission of YFP. Upon cGMP binding (gray, right), the sensor undergoes a conformational change that leads to a decrease in FRET efficiency. Thus, CFP emission is increased and YFP emission is decreased. Pictures taken from Thunemann and Wen et al., 2013.[197] (B) Representative FRET-based cGMP measurement performed in vascular smooth muscle cells. Cells were superfused with 50 nM CNP and 100 nM DEA/NO (black horizontal lines). Cyan, yellow and black trances represent CFP emission (F_{480}), YFP emission (F_{535}) and CFP/YFP ratio (F_{480}/F_{535}), respectively. CFP/YFP ratio can be directly correlated with the cGMP concentration that is built in the cell (black scale at top right). Picture taken from Thunemann and Wen et al., 2013.[197] Based on the cGMP biosensor cGi500 two mouse lines were generated. They either show ubiquitious expression of cGi500 (C) or can be used for Cre/loxP-dependent, tissue-specific sensor expression (D).[197]

1.4 Aim of the work

The second messenger cGMP is involved in various physiological processes. The identified CNP – GC-B – cGKI signaling pathway is necessary for axon bifurcation of murine DRG neurons in the spinal cord. One aim of this work was to further analyze the cGMP signaling cascade that has an impact on murine axon bifurcation during embryogenesis. FRET-based cGMP imaging as well as Ca^{2+} imaging of primary DRG neurons and explants should be used to gain mechanistic insights as well as to unravel a potential signaling cross talk. Moreover, another animal model – the chicken embryo – should be evaluated for investigation of the role of cGMP on axon pathfinding and nervous system development.

NO-GC stimulators that work synergistically with NO, are promising drug targets to treat various diseases. Their role regarding brain diseases is largely unknown. Thus, the second aim of this work was to characterize the role and impact of two structurally different NO-GC stimulators – Bay 41-2272 and IWP-051 – on murine brain. Acute brain slices and primary neuronal cell cultures and real-time cGMP imaging should be used to investigate if the two NO-GC stimulators would be able to potentiate DEA/NO-induced cGMP in hippocampus, striatum, and cerebellum. The results might suggest novel approaches to treat brain diseases, since Bay 41-2272 and IWP-051 were already shown to have a positive impact on non-neuronal diseases in preclinical studies.

2 MATERIALS AND METHODS

2.1 Common solutions and buffers

2.1.1 Solutions

- 0.5 M EDTA (pH 8.0): Dissolve 186.1 g/L disodium ethylenediaminetetraacetic acid dihydrate ($Na_2EDTA \times 2H_2O$, Roth) in 800 mL H_2O, add NaOH pellets until the solution reaches pH 8.0 and EDTA is dissolved. Adjust volume to 1 L with H_2O.
- 10 mM sodium hydroxide (NaOH, Roth): Weigh 0.3 g NaOH in 0.5 L H_2O.
- 1 M Tris-Cl (pH 8.0): Dissolve 121.14 g tris(hydroxymethyl)aminomethane (Tris, Roth) in 1 L H_2O, adjust pH to 8.0 with HCl.

2.1.2 Buffers

Table 2-1: Phosphate-buffered saline (PBS, pH 7.4)

NaCl	135 mM (8 g/L)
KCl	3 mM (0.2 g/L)
Na_2HPO_4	8 mM (1.42 g/L)
KH_2PO_4	2 mM (0.24 g/L)
H_2O	add 1L

Table 2-2: 5x TBE

Tris-borate	450 mM (54 g/L Tris, 27.5 g/L boric acid)
EDTA	10 mM (20 mL/L 0.5 M EDTA, pH 8.0)

Table 2-3: 10x TE

Tris-CL	100 mM (100 mL/L 1 M Tris-CL, pH 8.0)
EDTA	10 mM (20 mL/L 0.5 M EDTA, pH 8.0)

2.2 Mice

All mouse lines are housed in the animal facility of the Interfaculty Institute for Biochemistry (University of Tuebingen) at 22°C and 50 – 60 % humidity in a 12 h light/12 h dark cycle. Animals have access to standard rodent chow (Altromin Spezialfutter GmbH & Co. KG, Lage, Germany and Sniff Spezialdiaten GmbH, Soest, Germany) and tap water. Single animals or groups of 2 – 3 animals are housed in type II cages (360 cm^2) while groups of four up to eight animals live in type III cages (810 cm^2). The bedding consists of autoclaved shredded wood chips (Tapvei). Environmental enrichments are wooden tunnels and tissues (Tapvei). For breeding, one male mouse is placed together with 1 – 2 females in a type II cage for max. 20 days. Before birth, females are separated into type III cages with access to special breeding chow (Altromin and Sniff). Separation of males and females and ear tagging for identification takes place three weeks after birth. The tissue received by ear tagging is used for mouse genotyping. All animal procedures were approved by the Regierungspraesidium Tuebingen and performed in compliance with the humane care and use of laboratory animals.For brain tissue preparation, mice were killed according to the guidelines.

2.2.1 PCR-based mouse genotyping

- LE Agarose (Biozym); store at RT.
- 2 % Agarosegel: Weigh 0.75 g of agarose and add 37.5 mL 1x TBE buffer. Heat it until agarose is completely dissolved. Let it cool down and add 1 µL Midori Green (Nippon Genetics). Poor it to a gel chamber to polymerize.
- 6x DNA loading dye: Glycerol 30 %, 10x TE 10 %, bromphenol blue 0.05 %, xylene cyanol 0.05 %; store at 4 °C.
- dNTP stocks: 100 mM dATP, 100 mM dCTP, 100 mM dGTP, 100 mM dTTP (Genaxxon); store at -20 °C.
- Midori Green (Nippon Genetics); store at 4 °C.
- Molecular size marker: Add 250 µL 1 kb plus ladder (Life Technologies) to 8.25 mL 1×DNA loading dye; store in 500 µL aliquots at 4 °C.
- Primer (see Table 5-1): 25 pmol/µl (Eurofins Genomics); store at -20 °C.
- Proteinase K (Genaxxon): 50 mg/mL proteinase K in 1x TE, store at -20 °C.
- 10x Reaction buffer S (Bioron); store at -20 °C.
- 10x RT buffer: 100 mM Tris-HCl pH 8.0, 500 mM KCl, 15 mM $MgCl_2$, 2 mM of each dNTP (dATP, dCPT, cGTP, cTTP), in H_2O; store at −20 °C.
- Taq polymerase (Bioron); store at -20 °C.
- 1x TBE buffer: Dilute 2 L 5x TBE with 8 L H_2O. Store at RT.

Table 2-4: Pipetting scheme for PCR lysis buffer (one reaction)

10x Reaction buffer S	5 µL
Proteinase K	1 µL
H_2O	44 µL

PCR is used for mouse genotyping. Ear punches of mice are taken as DNA template.

A. Prepare PCR lysis buffer (see Table 2-4). Incubate each ear punch in 50 µL PCR lysis buffer and incubate overnight at 55 °C.
B. Vortex samples and centrifuge for 3 min at 11,000 rpm. Transfer the supernatant into a 0.5 mL PCR tube.
C. Inactivate proteinase K and denature DNA for 15 min at 95 °C. Briefly centrifuge at 3,000 rpm.
D. Use 1-2 µL DNA for PCR and store remaining solution at -20 °C.
E. Prepare a master mix (see Table 2-5) in an appropriate amount and pipette 23 µL master mix to 2 µL of DNA.
F. Spin down the sample and transfer it to the thermocycler (PEQLAB Peqstar 2x; PEQLAB Primus 96 Advanced). PCR conditions depend on annealing temperature and product length (Table 5-2).
G. Analyze PCR products on a 2 % agarose gel.

Table 2-5: Master mix pipetting scheme for PCR (one reaction)

H_2O	19.4 µL
10x Reaction buffer	2.5 µL
Primer 1	0.3 µL
Primer 2	0.3 µL
Primer 3	0.3 µL
Taq polymerase	0.2 µL

2.2.2 Mouse lines

In the present study, the following mouse lines were utilized: R26-CAG-cGi500(L1)[197], R26-CAG-cGi500(L2)[197], L7Cre[199], NesCre[200], NO-GC1 KO[201], and NO-GC2 KO[201]. R26-CAG-cGi500(L1) mice were directly used for experiments. Other experimental animals were generated by crossing of mouse lines to obtain the following cross mice: L7Cre;R26-CAG-cGi500(L2), NesCre;R26-CAG-cGi500(L2), NesCre;R26-CAG-cGi500(L2);NO-GC1 KO, and NesCre;R26-CAG-cGi500(L2);NO-GC2 KO.

2.3 Neuronal cell culture

- 100 mM Cytosine-β-D-arabinofuranoside hydrochloride (Ara-C, Sigma Aldrich): Dissolve 100 mg Ara-C in 3.58 mL in H_2O. Store in 500 µL aliquots at -20 °C.
- 50x B27 supplement (Life Technlologies): Store in 2 mL aliquots at -20 °C.
- Cell Strainer (Corning B.V. Life Sciences): 24 mm netwell insert 74 µm mesh size.
- Dulbecco's modified eagle medium (DMEM, Life Technologies); store at 4 °C.
- F12 medium (Life Technologies); store at 4 °C.
- Glass cover slips (12 mm diameter, VWR)
- Heat-inactivated Fetal Calf Serum (FCS, Life Technologies): Store in 50 mL aliquots at -20 °C.
- Heat-inactivated Fetal Bovine Serum (FBS, Life Technologies): Store in 50 mL aliquots at -20 °C.
- Heat-inactivated Horse Serum (HS, Life Technologies): Store in 15 mL aliquots at -20 °C.
- 200 mM L-glutamine (Life Technologies): Store in 2 mL aliquots at -20 °C.
- Minimum essential medium (MEM) without L-glutamine (Life Technologies); store at 4 °C.
- 100x Penicillin/Streptomycin (Pen/Strep, Life Technologies): Store in 5 mL aliquots at -20 °C.
- 50 µg/mL Poly-D-lysine hydrobromide (PDL, Sigma Aldrich): Dissolve 5 mg PDL in 100 mL H_2O and shake it overnight at 4 °C. Store in 2 mL tubes at -20 °C.
- 0.4% Trypan blue (Life Technologies); store at 4 °C.
- 10x Trypsin/EDTA (Life Technologies); store at 4 °C.
- 2.5x Trypsin/EDTA: Dilute 1 mL 10x Trypsin/EDTA with 3 mL PBS. Store at -20 °C.

2.3.1 DRG dissociated culture and explants

DRGs reside in the spinal cord. In mice, during embryonic day 10 – 13 (E10 – 13) outgrowing axons of sensory neurons enter the spinal cord at the dorsal root entry zone and bifurcate in one rostral and one caudal arm. E12.5 DRGs were used for the preparation of either dissociated DRG neurons or DRG explants.

- 96% Ethanol: Mix 48 mL of 99.9% ethanol (Sigma) with 2 mL H_2O.
- 20 µg/mL laminin (Sigma): Dissolve 1 mg laminin in 50 mL PBS. Store in 2 mL aliquots at -20 °C.
- 25 ng/µL NGF (Alomone labs): Dissolve 25 µg NGF in 1 mL H_2O. Store in 50 µL aliquots at -80 °C.

Table 2-6: DRG medium

DMEM	4.5 mL
F12	4.5 mL
Horse serum	1 mL
Pen/Strep	0.1 mL
100x L-glutamine	0.1 mL
Glucose (400 mg/mL in DMEM)	0.2 mL
NGF (25 ng/µL)	0.04 mL

2.3.1.1 Treatment of glass coverslips

A. Dissolve 4 pellets of NaOH (Roth) in 10 mL H_2O.
B. Add 35 mL of 96 % Ethanol.
C. Use a plastic beaker, put 50 – 100 glass coverslips inside and fill up with the NaOH/EtOH solution. Agitate overnight at RT.
D. Wash 10 x 3 min with H_2O. Add 50 mL 1 M HCl (Roth) and agitate overnight at RT.
E. Wash 10 x 3 min with H_2O. Add 50 ml 96 % EtOH and agitate for 1 h at RT.
F. Let coverslips dry before use.

2.3.1.2 Coating of glass coverslips

One day before preparation of culture, coat coverslips with PDL and laminin.

A. Place the required number of pretreated coverslips into a culture plate and add 50 µg/mL PDL on top. Incubate for 4 h at 37 °C.
B. Wash 3 times with ddH_2O. Let the coverslips dry.
C. Add 20 µg/mL laminin on the coverslips and incubate overnight at 37 °C.
D. On the next day, before use, wash 2 times with H_2O and once with PBS. Do not let the coverslips dry.

2.3.1.3 Preparation of DRG cultures

A. Mate 6 – 10 female wildtype mice with 2 – 4 transgenic or wildtype males.
B. Separate plug-positive females 0.5 days *post coitum* (dpc).
C. On the day of preparation (12.5 dpc), prepare an ice-box with cold PBS.
D. Sacrifice the pregnant animal by using CO_2. Take out the embryos and put them in a 10 cm petri dish with ice-cold PBS.
E. Open the uterine wall, peel away the amniotic sac and cut the umbilical cord. Transfer the embryo to a new petri dish with ice-cold PBS.

F. Decapitate the embryo and remove tail and limbs. Tear apart the thin skin above the spinal cord and remove the surrounding tissue and cartilage to free the DRGs.

2.3.1.3.1 DRG dissociated neurons

A. Rip of 30 – 40 DRGs and transfer them to a 2 mL tube with 900 µL ice-cold PBS.
B. Add 100 µL 10x trypsin/EDTA to the tube with DRGs.
C. Incubate for 20 min at 37 °C in a water bath (Memmert GmbH & Co. KG, Schwabach) and swirl the tube every 5 min. After trypsinization pipette 10 times up and down using a 200 µL pipette.
D. Add 1 mL DRG medium without NGF.
E. Centrifuge for 4 min at 200 x g at RT.
F. Remove the supernatant carefully and suspend the cells in 800 µL DRG medium with NGF. Plate 100 µL cell suspension per coverslip. Add 300 µL DRG medium with NGF to each well.
G. Incubate cells at 37 °C and 6 % CO_2 for at least 12 h.

2.3.1.3.2 DRG explants

A. After coating and washing of coverslips (2.3.1.2), add 400 µL DRG medium with NGF on the coverslips.
B. Rip of one DRG and cut it into halves using a small razor blade. Transfer two halves to one medium-covered coverslip.
C. Incubate at 37 °C and 6 % CO_2 for at least 12 h.

2.3.2 Hippocampal neurons

- 1 M HEPES pH 7.3: Dissolve 23.8 g HEPES (Roth) in 100 mL H_2O. Adjust pH with NaOH, sterilize by filtration and store at 4°C.
- 1% DNase: Dissolve 100 mg DNase (Roche) in 10 mL H_2O. Store in 0.3 mL aliquots at −20°C.
- 10× Hank's balanced salt solution (HBSS, Life Technologies); store at 4 °C.
- 12% D-Glucose: Dissolve 3 g D-glucose (Sigma) in 25 mL MEM and sterilize by filtration. Store at 4 °C.
- 20 mM Na pyruvate: Dissolve 56 mg Na pyruvate (Roth) in 25 mL MEM and sterilize by filtration. Store at 4°C.
- Horse serum (HS, Life Technologies) heat-inactivated. Store in 15 mL aliquots at -80 °C.
- DMEM + 10 % HS: 27 mL DMEM + 3 mL HS.

Table 2-7: Calcium/magnesium-free HBSS

10x HBSS	10 mL
1 M HEPES	1 mL
H_2O	89 mL

Table 2-8: HN medium

MEM	26.1 mL
20 mM Na pyruvate	1.5 mL
12 % D-Glucose	1.5 mL
200x L-glutamine	0.3 mL
50x B27	0.6 mL

Postnatal day 0 – 2 (P0 – P2) mice are used for the preparation of primary hippocampal neurons (HNs).

2.3.2.1 Coating of glass coverslips

A. Place coverslips to a 24-well plate and cover them with 400 µL 50 µg/mL PDL. Incubate overnight at RT.
B. On the next day, before use, remove PDL and wash 3 times with PBS. After washing, let the coverslips dry.

2.3.2.2 Preparation of HNs

A. Prepare several petri dishes with CMF-HBSS. Keep them on ice.
B. Clean dissection instruments with 70 % ethanol and rinse once with water afterwards.
C. Use 7-10 mouse pups of P0 – P2. Dip the pup's head into a beaker filled with 70 % ethanol. Cut the neck with a scissor and collect the heads in a CMF-HBSS-filled petri dish.
D. Under a stereomicroscope, remove the skin of the head and open the skull. Take out the brain and place it to a new CMF-HBSS-filled petri dish and keep it on ice while preparing remaining brains.
E. After all brains have been dissected, take one brain and separate the two hemispheres. Remove meninges and the inner part of the brain. Separate the hippocampi from cortex and put them to a new petri dish filled with CMF-HBSS. Continue with separation of remaining hippocampi.

F. While removing remaining meninges and blood vessels from hippocampi, tear them into small pieces.
G. Transfer the tissue into a 50 mL tube filled with 2 mL CMF-HBSS. Add 40 µL of 2.5x trypsin and incubate for 15 min in a 37 °C water bath (Memmert GmbH & Co. KG, Schwabach).
H. Add 50 µL DNase and wait for 1 min. Add 10 mL pre-warmed DMEM + 10 % HS. Allow the tissue pieces to settle down and aspirate the supernatant carefully using a 10 mL pipette. Repeat this washing step once, then add 2 mL DMEM + 10 % HS.
I. Dissociate the tissue by slowly pipetting through a regular Pasteur pipette for at least 10 passes. Repeat this step by using a flame-polished Pasteur pipette.
J. When the solution becomes turbid and all tissue pieces disappear, centrifuge for 5 min at 600 rpm. Remove the supernatant and resuspend the pellet in 1 mL pre-warmed HN medium.
K. Mix 18 µL of cell suspension with 2 µL trypan blue. Count viable cells using a Neubauer chamber. Seed $1x10^5$ cells per well. Grow cells at 37 °C and 6 % CO_2 (Hera Cell incubator, Thermo Fisher).
L. Add Ara-C with a final concentration of 5 µM to the cells 24 h after plating. Imaging experiments can be started from day 5 after plating.

2.3.3 Cerebellar granule neurons

- 1.2% $CaCl_2$: Dissolve 1.2 g $CaCl_2 \times 2\ H_2O$ (Roth) in 100 mL H_2O. Sterilize by filtration and store at 4°C.
- 1 M D-glucose (198.17 g/L D-glucose×H_2O, Sigma), sterilize by filtration and store at 4°C.
- 50 mg/mL Gentamicin (Life Technologies).
- High K+ (HK) medium: Weigh 825 mg KCl (Roth) into an autoclaved beaker glass. Add 50 mL from a medium bottle with 500 mL MEM. After the KCl has dissolved, sterilize the solution by filtration and transfer it back into the original medium bottle. Add 1 mL of gentamicin (50 mg/mL). Store at 4°C.
- 3.82% $MgSO_4$: Dissolve 3.82 g $MgSO_4 \times 7\ H_2O$ (Roth) in 100 mL H_2O, sterilize by filtration and store at 4°C.
- Trypsin inhibitor (Life Technologies). Store at -20 °C.

Table 2-9: 10x Krebs buffer (pH 7.4)

NaCl	1.24 M (72.5 g/L)
KCl	54 mM (4 g/L)
NaH_2PO_4	5 mM (0.7 g/L)

Table 2-10: 0.3 % BSA solution

BSA	450 mg
H_2O	132.84 mL
10x Krebs buffer	15 mL
1 M D-glucose	2.16 mL
3.82 % $MgSO_4$	1.2 mL

Table 2-11: CGN medium

HK medium	88 mL
FBS	9 mL
100x L-glutamine	0.9 mL
50x B27	2 mL

P7 mice are used for the preparation of primary cerebellar granule neurons (CGNs).

2.3.3.1 Coating of glass coverslips

A. Place coverslips (12 mm) to a 24 well plate and cover them with 400 µL 50 µg/mL PDL. Incubate overnight at RT.
B. On the next day, before use, remove PDL and wash 3 times with PBS. After washing, let coverslips dry.

2.3.3.2 Preparation of solutions

On the day of preparation, prepare 5 x 50 mL falcons in the culture hood:

- Tube 1: Add 30 mL 0.3 % BSA solution.
- Tube 2: Add 30 mL 0.3% BSA solution and, shortly before use, 300 µL 2.5x trypsin.
- Tube 3: Dissolve 7.8 mg trypsin inhibitor in 15 mL 0.3% BSA solution, add 150 µL 3.82% $MgSO_4$ and, shortly before use, 150 µL 1% DNase.
- Tube 4: Add 17 mL 0.3% BSA solution and 8 mL from tube 3; discard 10 mL, so that 15 mL remain in the tube.
- Tube 5: Add 12.5 mL 0.3% BSA solution, 100 µL 3.82% $MgSO_4$ and 15 µL 1.2% $CaCl_2$.

2.3.3.3 Preparation of CGNs

A. Isolate brains from 3-5 pups (P7) according to chapter 2.3.2.2 but use 0.3 % BSA solution instead of CMF-HBSS.
B. Under a stereomicroscope remove cerebella from brains after all brains have been dissected. Remove meninges and blood vessels and place cerebella into a new petri dish.
C. In the tissue culture hood, mince cerebella using a razorblade until the solution becomes turbid. Transfer the minced tissue into tube 1 using a pasteur pipette.
D. Centrifuge for 5 min at 1,100 rpm. Remove the supernatant and resuspend the pellet in 30 mL solution from tube 2 (with trypsin). Incubate for 15 min in a 37°C water bath (Memmert GmbH & Co. KG, Schwabach). Invert tube after 5 and 10 min.
E. Using a 25 mL pipette, resuspend the cells and transfer the suspension into tube 4 (with diluted trypsin inhibitor and DNase). Centrifuge for 5 min at 1,100 rpm. Remove the supernatant and resuspend the cell pellet with a 25 mL pipette in 7 mL solution from tube 3 (with trypsin inhibitor and DNase). Resuspend 20 times with a 10 mL pipette and then 10 times with a Pasteur pipette. Add 12 mL solution from tube 5.
F. Pass the cell suspension through a netwell mesh into a new 50 mL tube. Centrifuge for 5 min at 1,100 rpm. Remove the supernatant and resuspend the cell pellet in 5 mL CGN medium. Mix 18 µL of the cell suspension with 2 µL trypan blue and count viable cells in a Neubauer chamber. Plate $1x10^5$ cells per well. Grow the cells at 37 °C and 6 % CO_2.
G. Add Ara-C to a final concentration of 5 µM to the medium 24 h after plating. Imaging experiments can be started 3 days after plating.

2.4 Immunofluorescence staining of mouse tissue

- Normal Donkey Serum (NDS, Millipore): Store in 1 mL aliquots at 4 °C.
- 1000x Hoechst 33258 (1 mg/mL, Sigma): Store in 1 mL aliquots at -20 °C.
- Immu-Mount (Shandon, Thermo Scientific): Store at RT.

2.4.1 Cells

- Acetone (AnalaR, VWR): Pre-chill to -20 °C.
- 0.5 % BSA-PBS: Weight 0.5 g BSA (Roth) and dissolve it with 100 mL PBS.

- Immunofix: Dilute 1 mL 37 % formaldehyde (Chem solute, Th. Geyer) in 9 mL PBS.
- 5 % Serum-PBS: Dilute 25 µL NDS in 475 µL PBS.
- Primary antibody solution: Dilute primary antibody in Serum-PBS. For dilution factors and antibody information, see Table 5-3.
- Secondary antibody solution: Dilute secondary antibodies in PBS. For dilution factors and antibody information, see Table 5-4.

A. Wash cells once with 0.5 mL PBS.
B. Fix cells in 0.5 mL Immunofix for 10 min in the hood.
C. Remove Immunofix, permeabilize cells with 0.5 mL Acetone for max. 5 min and wash once with 0.5 mL PBS.
D. Transfer coverslips to a new well plate filled with 0.5 mL BSA-PBS and incubate for 5 min (or store at 4 °C, if necessary).
E. Block unspecific binding with Serum-PBS. Add 70 µL Serum-PBS to parafilm and put the coverslip upside down on the drop by avoiding air bubbles. Incubate for 10 min at RT. Wash once with 0.5 mL BSA-PBS in the well plate.
F. Place a 70 µL drop of primary antibody to parafilm and put the coverslip upside down on the drop by avoiding air bubbles. Incubate for 45 min at RT. Wash 2 times for 3 min with 0.5 mL BSA-PBS in the well plate.
G. Place a 70 µL drop of secondary antibody with Hoechst dye (1:1000) to parafilm and put the coverslip upside down on the drop by avoiding air bubbles. Incubate for 30 min in the dark at RT. Wash 2 times with 0.5 mL PBS in the well plate.
H. For double staining, start again from step E. For mounting, rinse the coverslip once in H_2O, add a drop of Immu-Mount solution on a glass slide and place the coverslip upside down on the glass slide.

2.4.2 Frozen Sections

- Blocking solution: 5 % NDS and 1 % BSA in PBS-T.
- 4 % Paraformaldehyde (PFA, Roth): Dissolve 4 g in 100 mL PBS (heat it to 55-57 °C to facilitate this process). Store in 10 mL aliquots at -20 °C.
- 0.4 % PBS-T: Add 0.4 mL Triton X 100 (Roth) to 100 mL PBS.
- 30 % Sucrose (Roth): Dissolve 30 g Sucrose in 100 mL PBS.
- SuperFrost Plus glass slides (Thermo Fisher)
- Tissue Tek O.C.T. compound (Sakura Finetek Germany GmbH, Staufen, Germany)

A. Sacrifice animal using CO_2 and dissect the brain.
B. Fix the brain in 10 mL ice-cold 4 % PFA for max. 5 h at 4 °C. If you work with fluorescent probes, wrap the falcon tube with aluminum foil for fixation time.
C. After fixation, briefly wash with PBS and then transfer the brain to a 30 % sucrose-filled falcon tube and keep it at 4 °C until it sinks down (1 – 2 days).
D. Embed the tissue in Tissue Tek O.C.T. compound and freeze it at -80 °C and store at -20 °C.
E. Prepare frozen sections (10 µm thickness) using a cryotome (Microm, Thermo Fisher). Mount the slices on SuperFrost glass slides. Dry them at RT, use them immeadiately or store at -20 °C.
F. Incubate slides in PBS for 5 min at RT.
G. Incubate slides in PBS-T for 5 min at RT.
H. Place slides into a staining chamber and block unspecific binding with blocking solution for 45 min at RT.
I. Incubate slices overnight with primary antibody diluted in blocking solution at 4 °C.
J. Wash 3x5 min with PBS-T and incubate slices with secondary antibody with Hoechst dye (1:1000) diluted in PBS-T and 1 % BSA for 2 h at RT in the dark.
K. Wash 3x5 min with PBS-T. Dip slides briefly in H_2O, add a drop of Immu-Mount and cover the slides with a glass coverslip of appropriate size.

2.5 Real-time imaging

- Acetylcholine chloride (**10 mM ACh**, Sigma): Dissolve 10 mg in 5.5 mL H_2O. Store in 500 µL aliquots at -20 °C.
- Adenosine 5'Triphosphoric Acid Disodium (**100 mM ATP**, AppliChem): Dissolve 1 g ATP in 18.15 mL H_2O. Store in 1 mL aliquots at -20 °C.
- A-type natriuretic peptide (**100 µM ANP**, Tocris): Dissolve 1 mg ANP in 3.246 mL H_2O. Store in 50 µL aliquots at -20 °C.
- **BAY 41-2272** (**10 mM**, Santa Cruz): Dissolve 5 mg BAY 41-2272 in 1.39 mL DMSO. Store in 100 µL aliquots at -20 °C.
- B-type natriuretic peptide (**100 µM BNP**, Phoenix Pharmaceuticals): Dissolve 1 mg BNP in 2.887 mL H_2O. Store in 50 µL aliquots at -20 °C.
- C-type natriuretic peptide (**100 µM CNP**, Tocris): Dissolve 1 mg CNP in 4.55 mL H_2O. Store in 50 µL aliquots at -20 °C.
- 2-(N,N-diethylamino)-diazenolate-2-oxide diethylammonium (**100 mM DEA/NO**, Axxora): Dissolve 50 mg DEA/NO in 2.42 mL 10 mM NaOH. Store in 10µL and 30 µL aliquots at -20 °C.

- Sodium L-glutamate monohydrate (**1 M Glu**, Merck Millipore): Dissolve 1.873 g in 10 mL H_2O. Store in 1 mL aliquots at -20 °C.
- Erythro-9-(2-hydroxy-3-nonyl)-adenine: (**10 mM EHNA**, Axxora): Dissolve 10 mg in 3.19 mL DMSO. Store in 100 µL aliquots at -20 °C.
- **Fura-2/AM** (**1 mM**, Calbiochem): Dissolve 1 mg Fura-2/AM in 0.998 mL DMSO. Store in 20 µL aliquots at -20 °C.
- 3-isobutyl-1-methylxanthine (**500 mM IBMX**, Sigma): Dissolve 1 g IBMX in 9 mL DMSO. Store in 1 mL aliquots at -20 °C.
- **IWP-051** (**10 mM**, Ironwood Pharmaceuticals): Dissolve 2.1 mg IWP-051 in 591 µL DMSO. Store at -20 °C.
- **Milrinone** (**10 mM**, Santa Cruz): Dissolve 10 mg Milrinone in 4.73 mL DMSO. Store in 500 µL aliquots at -20 °C.
- **Sildenafil** (**30 mM**, Santa Cruz): Dissolve 50 mg Sildenafil in 25 mL H_2O. Store in 1.5 mL aliquots at -20 °C.
- Uridine 5'triphosphoric acid trisodium salt hydrate (**10 mM UTP,** AppliChem): Dissolve 55 mg UTP in 10 mL PBS. Store in 500 µL aliquots at -20 °C.
- **Vinpocetine** (**5 mM**, Santa Cruz): Dissolve 20 mg Vinpocetine in 11.41 mL DMSO. Store in 1.5 mL aliquots at -20 °C.
- **Zaprinast** (**10 mM**, Santa Cruz): Dissolve 20 mg Zaprinast in 7.37 mL DMSO. Store in 500 µL aliquots at -20 °C.

Table 2-12: Tyrode buffer (pH 7.4)

NaCl	140 mM (8.18 g/L)
KCl	5 mM (0.372 g/L)
$MgCl_2$	1.2 mM (0.244 g/L)
$CaCl_2$	2 mM (0.222 g/L)
HEPES	5 mM (1.192 g/L)
Add 4 mL 2.5 M D-glucose to 1 L Tyrode buffer before use (final concentration 10 mM).	

2.5.1 In vitro measurements

The imaging setup consists of an inverted Axiovert 200 microscope with 1.0/1.6x Optovar lens (Zeiss) equipped with Plan NeoFluar 40×/1.30 oil objective (Zeiss), computer-controlled light source with excitation filter switching device (Oligochrome, TILL Photonics). For FRET-based imaging a DualView beam splitter (Dual View DV, DUAL-View, Photometrics), for separation of CFP and YFP emission, with 516 nm dichroic mirror, 480/50 nm and 535/40 nm emission filters is used. Signals are recorded with a charged-coupled device (CCD) camera (Retiga 2000R, QImaging). Additionally, specific filter sets (see **Table 2-13**) are used to examine cell samples by eye, to record fluorescence images or to perform Fura-2-based Ca^{2+} imaging.

Table 2-13: Filter sets for epi fluorescence imaging

name	excitation filter	dichroic mirror	emission filter
Cy3	543/22 nm	565 nm	610/75 nm
Fura-2 (340)	340/26 nm	410 nm	440 nm LP
Fura-2 (387)	387/11 nm	410 nm	440 nm LP
YFP	497/16 nm	516 nm	535/22 nm

During real-time imaging, cells that are grown on glass coverslips are continuously superfused with buffer or buffer-containing drugs of interest. Therefore, a custom built superfusion system is used that consist of a FPLC pump (Pharmacia P-500, GE Healthcare), FPLC injection valves (Pharmacia V-7, GE Healthcare), a superfusion chamber (RC-25/26, Warner Instruments) and sample loops of different sizes (0.16, 2, 7 mL). To remove the buffer from the system, a vacuum pump with adjustable vacuum (Laboport N86, KNF Neuberger) is connected to the system.[195, 197]

2.5.1.1 FRET-based cGMP imaging

A. The imaging setup is located in a dark room at ~21 °C.
B. Check beam splitter for alignment of YFP and CFP channels before starting a FRET-based imaging session.
C. Assemble appropriate sample loops to injection valves and connect the Tyrode buffer to FPLC pump. Start a solvent change with both injection valves at inject mode. Continue with solvent change in load mode.
D. Assemble the superfusion chamber with a coverslip (use silicon to make the coverslip stick to the chamber). Cover the cells with ~500 µL Tyrode buffer.
E. Place the superfusion chamber on the microscope and connect inlet (provides Tyrode buffer from FPLC pump) and outlet (aspirates Tyrode buffer from superfusion chamber). Start the superfusion with a rate of 1 mL/min and injection valves in load mode.
F. Using the YFP filter set, by eye identify a field of view with appropriate amount of cGMP sensor-expressing cells. Aquire an image of the cells. Select regions of interest (ROIs).
G. Adjust imaging settings (binning, exposure time, cycle interval) and start the measurement. For cGMP imaging, 4x4 binning, a cycle interval of 5 s and an exposure time of 30-100 ms was used.
H. For each measurement, record a baseline for 2 – 5 min.

I. Dilute test compound to an appropriate concentration and load them via injection valves into the sample loops by using a syringe. After loading, switch to inject mode and the test compound will be released to the cells.
J. Observe F_{480}/F_{535} ratio changes as well as changes in F_{480} and F_{535} single traces.
K. After every imaging session, flush the superfusion system with 20 % ethanol (run solvent change) while injection valves are in load mode and afterwards in inject mode. Clean superfusion chamber and outlet needle from remaining silicon.

2.5.1.2 Calcium imaging

For Ca^{2+} imaging, the same microscopy setup as described before (chapter 2.5.1) was used. Here, the beam splitter is not necessary, therefore it is turned off and in bypass mode. Cells have to be loaded with Fura-2/AM since they do not express a Ca^{2+} sensor. For Fura-2-based Ca^{2+} imaging, the Fura-2 (340) and the Fura-2 (387) filter sets are used (see **Table 2-13**).

A. While using Fura-2/AM, all working steps should be performed in the dark.
B. For loading of cells with Fura-2/AM, dilute the dye 1:400 in Tyrode buffer. Vortex.
C. Place a coverslip with cells into a petri dish and add 80 µL of diluted Fura-2/AM. Incubate for 40 min at 37 °C in the dark.
D. During incubation time prepare the setup as described in chapter 2.5.1.1 C. For Ca^{2+} measurement, the 0.16 mL and 2 mL loops are used.
E. Wash the cells with Tyrode buffer. Assemble the superfusion chamber with the coverslip using silicon. Cover the cells with ~ 500 µL Tyrode buffer.
F. Place the superfusion chamber on the microscope and connect inlet (provides Tyrode buffer from FPLC pump) and outlet (aspirates Tyrode buffer from superfusion chamber). Start the superfusion with a rate of 1 mL/min and injection valves in load mode.
G. Using the Fura-2 (340) filter set, by eye identify a field of view with appropriate amount of Fura-2-loaded cells. Aquire an image of the cells. Select regions of interest (ROIs).
H. Adjust imaging settings (binning, exposure time, cycle interval) and start the measurement. For imaging neurons, 4x4 binning, cycle interval of 0.5 s (excitation at 340 nm and 387 nm in 0.5 s) and exposure time of 20-80 ms was used.

I. For each measurement, record a baseline for ~ 3 min.
J. Dilute test compound to an appropriate concentration and load them via injection valves into the sample loops by using a syringe. After loading, switch to inject mode and the test compound will be released to the cells. For testing the effect of cGMP on intracellular Ca^{2+} release, the application of drugs was performed at specific time points (see **Table 2-14**).
K. Observe F_{340}/F_{380} ratio changes as well as changes in F_{340} and F_{380} single traces.
L. After every imaging session, flush the superfusion system with 20 % ethanol (run solvent change) while injection valves are in load mode and afterwards in inject mode. Clean superfusion chamber and outlet needle from remaining silicon.

Table 2-14: Schedule for drug application during Ca^{2+} imaging

Drug	Sample loop size	Time point of injection
Ca^{2+}-releasing drug	0.16 mL	180 sec (720 frames)
cGMP-elevating drug/Tyrode buffer	2 mL	780 sec (3120 frames)
Ca^{2+}-releasing drug + cGMP-elevating drug/Tyrode buffer	0.16 mL	870 sec (3480 frames)

2.5.1.3 Combined Calcium and cGMP imaging

For combined Ca^{2+} and cGMP imaging, the same microscopy setup as described before (chapter 2.5.1) was used. For these experiments the beam splitter with corresponding filter sets as well as the Fura-2 (340) and the Fura-2 (387) filter sets are needed. Cells that express a cGMP biosensor (cGi500 or mcGi500) have to be loaded with Fura-2/AM.

For combined Ca^{2+} and cGMP imaging follow the steps A. – F. as described in chapter 2.5.1.2. Then continue with the following steps:

A. Using the Fura-2 (340) or YFP filter set, by eye identify a field of view with appropriate amount of Fura-2-expressing or cGMP biosensor-expressing cells. Aquire an image of the cells. Select regions of interest (ROIs).
B. Adjust imaging settings (binning, exposure time, cycle interval) and start the measurement. For combined Ca^{2+} and cGMP imaging, 4x4 binning, cycle interval of 1 s (excitation at 340 nm, 387 nm and 445 nm in 1 s) and exposure time of 20-100 ms was used.
C. For each measurement, record a baseline for ~ 3 min.

D. Dilute test compound to an appropriate concentration and load them via injection valves into the sample loops by using a syringe. After loading, switch to inject mode and the test compound will be released to the cells. For testing the effect of cGMP on intracellular Ca^{2+} release, the application of drugs was performed at specific time points (see **Table 2-15**).
E. Observe changes in F_{480} and F_{535}, F_{340} and F_{387} of respective ROIs.
F. After every imaging session, flush the superfusion system with 20 % ethanol (run solvent change) while injection valves are in load mode and afterwards in inject mode. Clean superfusion chamber and outlet needle from remaining silicon.

Table 2-15: Schedule for drug application during combined Ca^{2+}/cGMP imaging

Drug	Sample loop size	Time point of injection
Ca^{2+}-releasing drug	0.16 mL	180 sec (540 frames)
cGMP-elevating drug/Tyrode buffer	2 mL	780 sec (2340 frames)
Ca^{2+}-releasing drug + cGMP-elevating drug/Tyrode buffer	0.16 mL	870 sec (2610 frames)

2.5.1.4 Image acquisition and data analysis

For image acquisition and online display, Live Acquisition (TILL Photonics) was used, and for offline analysis Fiji software.[202] For further analysis, Microsoft Excel 2013 (Microsoft Corp.) and OriginPro 2016 (OriginLab Corp.) was used.

For ΔR/R peak area and peak height calculation, Peak Area/Height Analyzer of OriginPro 2016 was used. Peak borders were defined manually. Statistical analysis was performed using Origin software. Statistical differences between more than two groups were analyzed by one-way ANOVA followed by Bonferroni's test. P values <0.05 were significant.

2.5.2 Ex vivo measurements

Ex vivo measurements are performed on acute tissue slices or whole mount preparations. Slicing is performed with a vibratome VT1200 (Leica). The imaging setup (Spinning disk microscope) consists of an upright Examiner.Z1 microscope (Zeiss) equipped with three diode lasers (445 nm, 488 nm and 561 nm) and different objectives (all Zeiss): EC Plan NeoFluar 2.5×/0.0 (air), W Achroplan 10x/0.3 (water immersion), W Plan Achromat

20x/1.0 (water immersion) and W Plan Achromat 40x/1.0 (water immersion). For FRET-based imaging a DualView beam splitter (DUAL-View, Photometrics), with 505 nm dichroic mirror, 470/24 nm and 535/30 nm emission filters is used for simultaneous acquisition of CFP and YFP. Signals are recorded with an electron-multiplying charged-coupled device (EM-CCD) camera (Photometrics QuantEM 512SC). For acquisition of CFP, DAPI, YFP, GFP or mCherry fluorescence of fixed or stained samples, a second camera (Spot Pursuit, Diagnostic Instruments) and additional filter sets are used (see **Table 2-16**).

Table 2-16: Filter sets Spinning disk microscope

Fluorophore	Excitation	Dichroic	Emission
CFP/DAPI	445 nm	T445/515/561	ET470/24m
GFP	488 nm	T405/488/568/647	ZET405_488_561_640m
mCherry	561 nm	T405/488/568/647	ZET405_488_561_640m
YFP	488 nm	T405/488/561	ET535/30m

For the superfusion of tissue samples a custom-build superfusion system was used, as described above (chapter **2.5.1**).

2.5.2.1 Tissue slicing

- Glue (Instant Adhensive, Best-CA 221, BEST Klebstoffe)
- Razor blades (Wilkinson)

Table 2-17: Ringer buffer

NaCl	126 mM (7.4 g/L)
KCl	2.5 mM (0.186 g/L)
$MgCl_2$	1 mM (0.096 g/L)
$CaCl_2$	1 mM (0.12 g/L)
NaH_2PO_4	1.25 mM (0.15 g/L)
D-glucose	20 mM (3.6 g/L)
$NaHCO_3$	26 mM (2.2 g/L)
Gas with Carbogen (5 % CO2, 95 % O2, Westfalia) to adjust pH.	

A. Fill a beaker with ~ 300 mL Ringer buffer (Reservoir 1), place it on ice and gas it with Carbogen for at least 20 min. Prepare a second beaker with ~ 450 mL Ringer buffer (Reservoir 2) and warm it to 37 °C using a water bath. Gas Ringer buffer that is used for superfusion of tissue samples. Fill ice to the ice tray of the vibratome.

B. Sacrifice the mouse with CO_2, take out the tissue of interest and place it to a petri dish filled with ice-cold, gassed Ringer buffer. Place the Carbogen gas apparatus from Reservoir 1 to Reservoir 2.
C. Using a scalpel, cut a small piece of the tissue to create a flat surface. Put a piece of tape to the specimen plate and add a small drop of glue on it.
D. With the help of a spoon-like tool take the tissue out of the buffer, dry excess liquid with a paper towel and mount the tissue with the flat site to the glue.
E. Transfer the plate with mounted tissue to the buffer tray. Fill it with remaining ice-cold, gassed Ringer buffer. Make sure the tissue is completely covered with buffer.
F. Place a razor blade to the blade holder and adjust the position for slicing. For the preparation of brain slices, the following settings are used: thickness 300 µm, amplitude 1.2 mm, frequency 0.3 mm/s.
G. An initial slice hast to be made that is not used for imaging. Subsequent slices should be cut 300 µm and can be used for imaging. Using a Pasteur pipette, transfer the brain slices to Reservoir 2. Incubate slices for at least 40 min before starting the measurements.

2.5.2.2 Imaging using Spinning Disk

A. The imaging setup is located in a dark room at ~21 °C.
B. Check beam splitter for alignment of YFP and CFP channels before starting a FRET-based imaging session.
C. Assemble appropriate sample loops to injection valves and connect the gassed Ringer buffer to FPLC pump. Start a solvent change with both injection valves at inject mode. Continue with solvent change in load mode.
D. Assemble the superfusion chamber with a coverslip (use silicon to make the coverslip stick to the chamber). Fill ~500 µL Ringer buffer to the superfusion chamber. Place the tissue slice/whole-mount preparation into the superfusion chamber and fix them with a slice hold-down (SHD26H/10, Warner Instruments).
E. Place the superfusion chamber on the microscope and connect inlet (provides Ringer buffer from FPLC pump) and outlet (aspirates Ringer buffer from superfusion chamber). Start the superfusion with a rate of 1 mL/min and injection valves in load mode.
F. Using the YFP filter set (laser power ~30 – 50 %) and the 2.5x objective, identify the area of interest. In the preview mode, select regions of interest (ROIs).

G. Adjust imaging settings (exposure time, cycle interval, gain) and start the measurement. For cGMP imaging in brain slices, a cycle interval of 5 s, exposure time of 300 ms and gain 500 was used.
H. For each measurement, record a baseline for 2 – 5 min.
I. Dilute test compound to an appropriate concentration and load them via injection valves into the sample loops by using a syringe. After loading, switch to inject mode and the test compound will be released to the cells.
J. Observe F_{480}/F_{535} ratio changes as well as changes in F_{480} and F_{535} single traces.
K. After every imaging session, flush the superfusion system with 20 % ethanol (run solvent change) while injection valves are in load mode and afterwards in inject mode. Clean superfusion chamber and outlet needle from remaining silicon.

2.5.2.3 Image acquisition and data analysis

For image acquisition and online analysis, VisiView (Visitron) was used, and for offline analysis Fiji software (NIH). For further analysis, Microsoft Excel (Microsoft Corp.) and Origin (OriginLab Corp.) was used.

For ΔR/R peak area and peak height calculation, Peak Area/Height Analyzer of Origin was used. Peak borders were defined manually. Statistical analysis was performed using Origin software. Statistical differences between more than two groups were analyzed by one-way ANOVA followed by Bonferroni's test. P values <0.05 were significant.

2.6 Chicken embryo

Electroporation and staining procedures were supervised by Dr. Andrea Wizenmann, and performed at Institute for Clinical Anatomy and Cell Analytics, University of Tuebingen.

2.6.1 *In ovo* electroporation with CMV-cGi500 plasmid

- 100x Penicillin/Streptomycin (Pen/Strep, Life Technologies): Store in 1 mL aliquots at -20 °C.
- Borosilicate glass capillaries (length to outer diameter: 100 mm x 0.9 mm, World Precision Instruments, WPI).
- CMV-cGi500 plasmid: 1 µg/µL.
- FastGreen (Sigma-Aldrich): 10 mg/mL.
- Ink (Pelikan®): Dilute 200 µL Ink in 800 µL Ringer solution. Store diluted ink for max. 1 week at 4 °C.
- PUL-1 puller (WPI, Berlin).

- Ringer solution (Plastipur®, Fresenius): 0.9 % NaCl.

A. Incubate fertilized Lohman and Hisex chicken eggs (LSL Rhein-Main, Geflügelvermehrungsbetriebe) on their sides at 37 °C until Hamburger and Hamilton stage 10-12 (H10-12, ~36-48 h).[203] Label the top of the embryo with a pencil to recognize where the embryo lies.
B. Sterilize all scissors, forceps, tungsten needle and electrodes with 70% ethanol.
C. Prepare 35 cm dish with cold Ringer solution supplemented with antibiotics (1:100).
D. Dilute ink with Ringer solution (1:5) and supplement with antibiotics 1:100.
E. Pierce the egg at its broader side, where the air cavity should be. Using a 5 mL syringe with attached 21G needle, remove 2 mL of egg white to detach the embryo from the egg shell. Afterwards seal this hole with a small piece of cello tape.
F. Open egg shell carefully by cutting a hole with a small scissor. The hole must be big enough to visualize the embryo and to place needle and electrodes. Carefully pipette Ringer solution on top of the embryo.
G. Inject antibiotic-containing ink solution underneath the area opaca to make the embryo visible using a 1 mL syringe with attached 26G needle.
H. Carefully cut the vitelline membrane on top of the embryo using a sterile tungsten needle. Carefully pipette Ringer solution on top of the embryo.
I. Mix 2-5 µg/µL DNA construct with 18 µL of a 1:20 Fast Green/sterile water mixture. Fill a freshly pulled capillary with DNA construct/Fast Green mix using a mouth pipette.
J. Carefully insert the DNA construct/Fast Green mix into the neural tube of the embryo.
K. Place the plus electrode dorsally and the minus electrode ventrally (distance 3-5 mm). Use an Intercept TSS10 (Intracell, Cambridge) to induce 3-5 pulses (15 V) of 20 ms duration at 50 ms intervals.
L. Carefully pipette Ringer solution on top of the embryo. Seal the egg with cello tape. Place the egg back at 37 °C into a humidified incubator until HH18-20 is reached (~36-48 h).

2.6.2 Immunofluorescence staining

- Blocking solution: 5 % NDS and 1 % BSA in PBS-T.
- 4 % Paraformaldehyde (PFA, Roth): Dissolve 4 g in 100 mL PBS (heat it to 55-57 °C to facilitate this process). Store in 10 mL aliquots at -20 °C.
- 0.4 % PBS-T: Add 0.4 mL Triton X 100 (Roth) to 100 mL PBS.
- 30 % Sucrose (Roth): Dissolve 30 g Sucrose in 100 mL PBS.
- SuperFrost Plus glass slides (Thermo Fisher)
- Tissue Tek O.C.T. compound (Sakura Finetek Germany GmbH, Staufen, Germany)

A. After 36-48 h of incubation, remove the cello tape from the egg shell and dissect the chicken embryo.
B. Fix the brain in 10 mL ice-cold 4 % PFA for max. 30 min at 4 °C. If you work with fluorescent probes, wrap the falcon tube with aluminum foil for fixation time.
C. Continue with fixation and preparation of frozen sections as described in chapter 2.4.2.

2.6.3 In ovo measurements

For *in ovo* measurements, buffers, solutions and spinning disc microscope setup from chapter 2.5.2 are needed.

A. After 36-48 h of incubation real-time imaging was performed.
B. Remove the cello tape from the egg shell and carefully add some gassed Ringer buffer (**Table 2-17**).
C. Assemble the superfusion chamber with the egg (opened site upward) on it under the spinning disc microscope and superfuse with gassed Ringer buffer.
D. Continue with imaging and data analysis as described in chapters 2.5.2.2 and 2.5.2.3.

3 RESULTS

3.1 Second messenger imaging in embryonic DRG neurons

In the past years, the use of fluorescently labeled biosensors became more and more important. In comparison to end-point measurements, biosensors allow the investigation of basic molecular mechanisms in real-time in living cells, tissues and animals. In this study, mice or chicken embryos expressing the cGMP biosensor cGi500 were used to investigate cGMP signaling. In combination with Fura-2/AM, a fluorescent dye to investigate Ca^{2+} dynamics, a potential crosstalk between the two second messengers was explored to better understand molecular mechanisms behind neuronal bifurcation.

3.1.1 FRET-based cGMP imaging in primary DRG neurons

By the use of genetic mouse models, labeling of axons and expression studies it was shown that the bifurcation of sensory neurons, residing in the dorsal root ganglia (DRGs), is dependent on a cGMP signaling cascade including CNP, its receptor GC-B and cGKIα.[43, 65, 66] Since the cGMP sensor mouse R26-CAG-cGi500(L1) was developed, it is possible to prepare cell cultures from these mice and measure cGMP dynamics.[197] Here, primary dissociated neurons and explant cultures from DRGs were prepared and FRET-based cGMP imaging was performed. Figure 3-1 A shows soma and axon of a single dissociated DRG neuron (upper panel) as well as axon and growth cone of a DRG explant culture (lower panel), both expressing the cGi500 biosensor (yellow). For FRET-based cGMP imaging the somata of dissociated neurons (Figure 3-1, upper panel) and the growth cones of explant cultures (Figure 3-1, lower panel) were chosen. An increase of the CFP/YFP ratio (black trace in Figure 3-1 B and C, respectively) represents the production of cGMP in a cell. In the soma of a DRG neuron (Figure 3-1 B), only CNP, but neither the NO donor DEA/NO, nor the natriuretic peptides ANP or BNP (100 nM each, black horizontal lines), elevated the cGMP level, which was confirmed by the opposing development of CFP and YFP emission traces (cyan and yellow traces). Additionally, cGMP imaging of explant cultures (Figure 3-1 C) revealed that CNP increases cGMP in the growth cone of DRGs as well. These results confirm the published data pointing out the CNP/GC-B/cGMP pathway to be present in DRG neurons.[43, 65, 66] Now, using this imaging technique, it is possible to observe cGMP dynamics – cGMP production and degradation – in real-time.

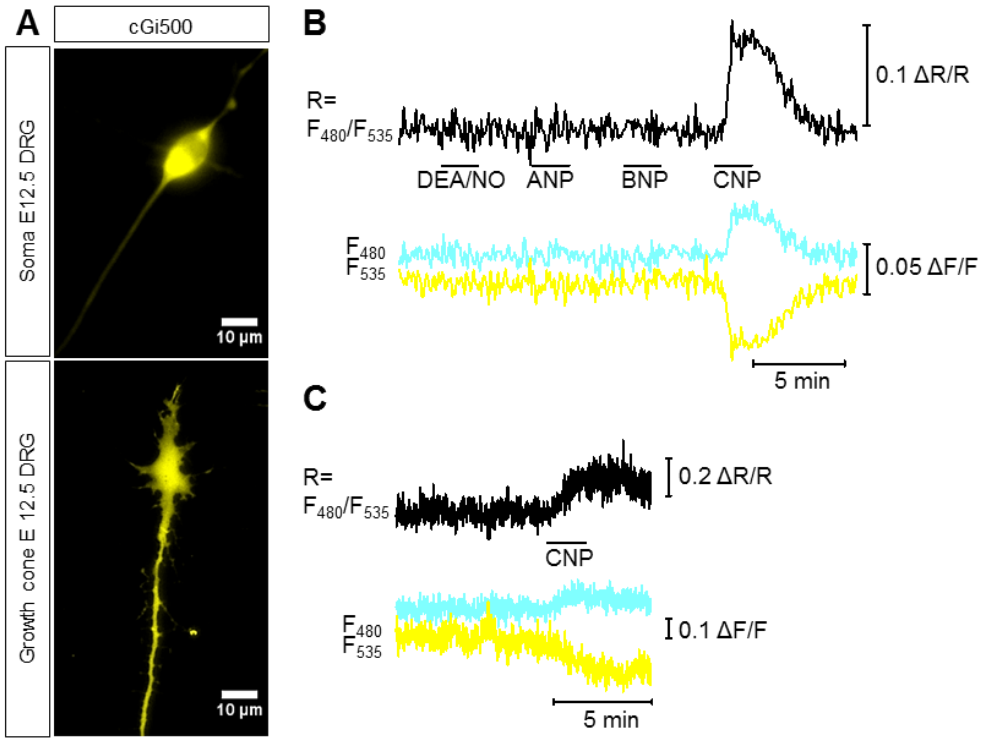

Figure 3-1: CNP elevates cGMP levels in somata and growth cones of primary embryonic DRG neurons. (A) Representative images of DRG neurons showing soma and axon of dissociated DRG neurons in a culture (yellow, upper panel) as well as axon and growth cone of a neuron in a DRG explant culture (yellow, lower panel). FRET-based cGMP imaging was performed in (B) somata and (C) growth cones of DRG neurons isolated from E12.5 R26-CAG-cGi500(L1) embryos. Several drugs were applied such as NO donor DEA/NO (100 nM), and the natriuretic peptides ANP, BNP and CNP (100 nM each, black horizontal bars). Black, cyan and yellow traces represent CFP/YFP ratio, CFP and YFP traces, respectively.

To unravel the functionally active phosphodiesterases (PDEs) that are responsible for the degradation of cGMP in DRG neurons, a FRET-based cGMP imaging study was performed. Here, three consecutive applications of 100 nM CNP– before, during and after incubation with PDE inhibitors – were performed and cGMP signals were recorded from the somata of dissociated DRG neurons. Figure 3-2 summarizes the results obtained from this PDE study. Figure 3-2 A shows F_{480}/F_{535} ratio images of two DRG neurons at different time points ($t_0 - t_3$). Here, IBMX, a PDE inhibitor that blocks several PDEs, was tested. T_0 represents the baseline cGMP signal before a drug was applied. Compared to baseline, the application of CNP (100 nM) led to an increase of cGMP in DRG neurons (t_1) that was even more elevated in presence of 100 µM IBMX (t_2) indicating that there must be at least one PDE that is responsible for cGMP degradation. A 5 min preincubation with IBMX alone did not increase the basal cGMP level (data not shown). The control

stimulus with 100 nM CNP after wash out of IBMX (t_3) led to an increased cGMP level comparable to t_1. The effect of IBMX on cGMP levels was assessed by analysis of the peak area of cGMP-induced ratio changes and IBMX measurements are summarized in Figure 3-2 B.

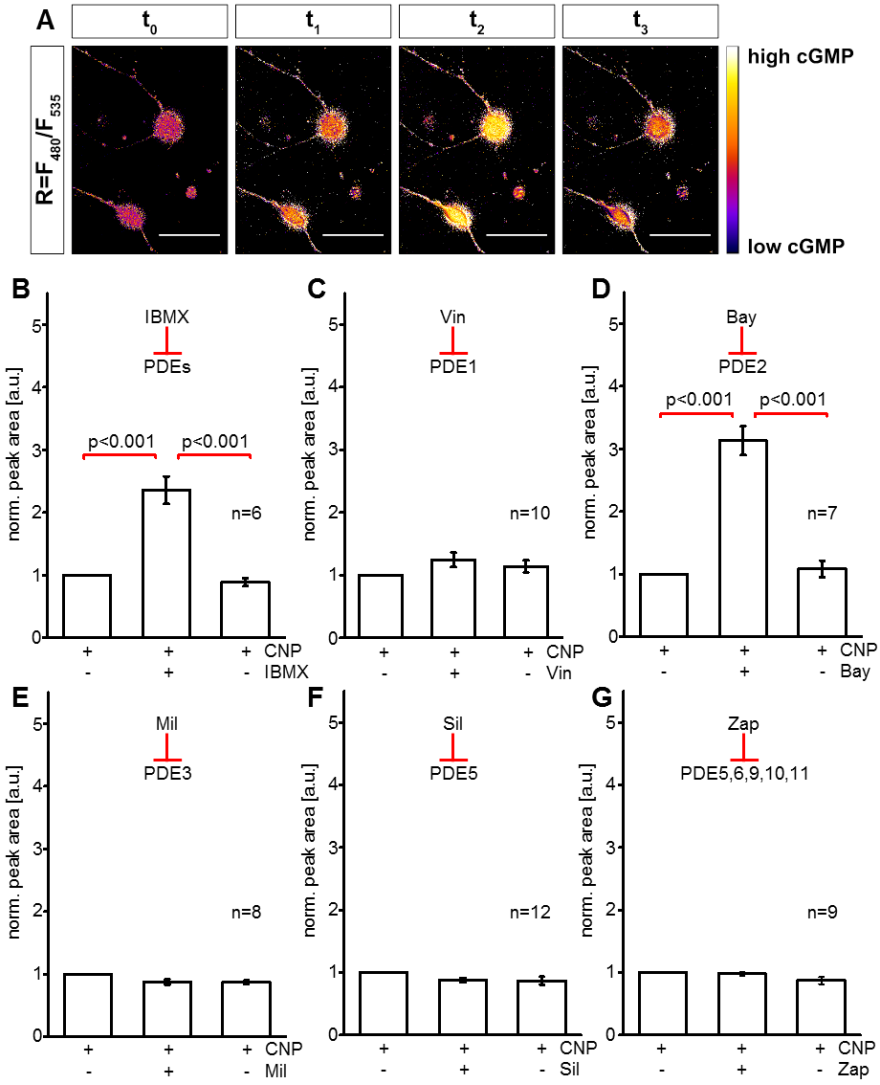

Figure 3-2: PDE2 is mainly responsible for cGMP degradation in embryonic DRG neurons. FRET-based cGMP imaging was performed in somata of dissociated, embryonic DRG neurons. Cells were superfused three times with 100 nM CNP. The second application was performed in the presence of a PDE inhibitor indicated in the respective plots. For concentrations of PDE inhibitors, see main text. (A) Representative ratio images of DRG neurons during cGMP measurement with CNP±IBMX (100 µM) application. ΔR/R values reflect changes of intracellular cGMP levels. Time points t_0 - t_3 show ΔCFP/YFP ratios before (t_0) and after (t_1, t_3) application of CNP. T_2 shows cGMP levels after CNP application in the presence of the PDE inhibitor IBMX. (B-G) Statistical analysis of the effects of several PDE inhibitors (for full names and concentrations, see main text) on the CNP-induced cGMP signals was performed calculating peak areas of respective cGMP images. Depicted in the bar graphs are mean values of peak area (+SEM) for each drug application. Values of second and first application were normalized to the first one. N-number represents number of measured somata. P-values <0.05 were considered to be significant. [204]

To narrow down which PDEs are responsible for cGMP breakdown in DRGs, five specific PDE inhibitors were tested with the same experimental setup and analysis as for IBMX. The results are summarized in Figure 3-2 C-G and show that only the PDE2 blocker Bay 60-7550 (Bay, 10 nM) elevates CNP-induced cGMP in DRG neurons while inhibitors of PDE1 (Vinpocetine – Vin, 5 µM), PDE3 (Milrinone – Mil, 10 µM), PDE5 (Sildenafil – Sil, 20 µM) and PDE5,6,9,10,11 (Zaprinast – Zap, 20 µM) do not. The 5 min pre-incubation with any of these PDE inhibitors alone did not affect the basal cGMP levels, respectively (data not shown). These results show that PDE2 is the major enzyme responsible for the degradation of CNP-induced cGMP in embryonic DRG neurons. These results correlate well with published mRNA and protein expression data showing PDE2A expression in E12.5 DRG neurons.[204]

3.1.2 Ex vivo cGMP imaging in embryonic DRGs

3.1.2.1 Mouse DRGs

Acute whole mount spinal cord preparations with attached DRGs were isolated from E12.5 R26-CAG-cGi500(L1) mouse embryos to perform real-time cGMP imaging. Figure 3-3 A shows the spinal cord with attached DRGs expressing the biosensor cGi500 globally. Figure 3-3 B shows FRET-based cGMP imaging in DRGs with applications of CNP (100 nM and 250 nM), DEA/NO (500 nM) and ANP (250 nM). Only CNP, but neither DEA/NO nor ANP, was able to induce cGMP production in ex vivo spinal cord/DRG preparations of E12.5 embryos. This data confirms the in vitro data described in chapter 3.1.1 as well as the published data from Schmidt et al.[66, 204] and clearly shows that the recently generated cGMP sensor mouse R26-CAG-cGi500(L1)[197] is an excellent model to study cGMP dynamics in the developing spinal cord.

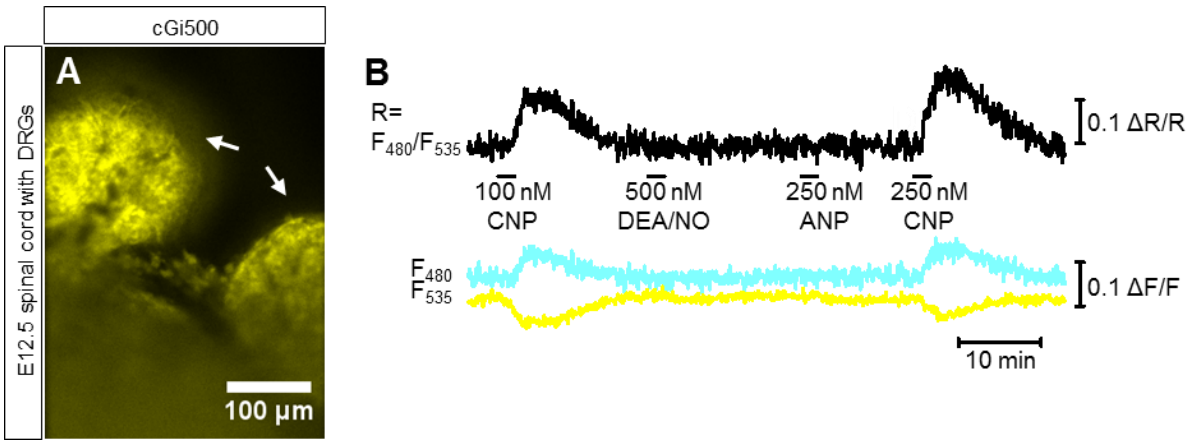

Figure 3-3: CNP elevates cGMP in DRGs of ex vivo whole mount spinal cord preparations, while DEA/NO and ANP do not. (A) Representative picture of ex vivo whole mount preparation of murine spinal cord with attached DRGs expressing the cGMP biosensor cGi500 globally [yellow, mouse line: R26-CAG-cGi500(L1)]. (B) FRET-based cGMP imaging was performed in DRGs (indicated by white arrows in panel A) of acute spinal cord/DRG preparations. Several drugs were applied (black horizontal bars): DEA/NO (500 nM), ANP (250 nM), and CNP (100 nM and 250 nM). Black, cyan and yellow traces represent CFP/YFP ratio, CFP and YFP traces, respectively.

3.1.2.2 Chicken DRGs

Another widely used animal model to study the developing nervous system ex vivo and in vivo is the chicken embryo. The goal of this study was to test if the chicken embryo is a suitable model for investigating the cGMP signaling pathway in the developing spinal cord including DRGs. Thus, the presence and functionality of members of the cGMP signaling cascade were investigated by performing immunofluorescence stainings and FRET-based cGMP imaging.

An embryo at Hamburger and Hamilton stage 24 (HH24) was fixed and frozen sections (10 µm) were prepared. Immunofluorescence staining revealed a strong cGKI expression (green) in cells of DRGs including somata as well as axons that entered the dorsal root entry zone (white arrows, Figure 3-4 A and A'). The sections were co-stained for the axonal marker RMO (red, Figure 3-4 B and B'). Nuclei were stained with Hoechst 33258 (cyan, Figure 3-4 C and C'). The overlaid stainings of cGKI and RMO (Figure 3-4 D and D') show clearly that cGKI is expressed in axons of DRG neurons. cGKI expression was also found in the somata of DRG cells as highlighted by an arrowhead in the magnified picture (Figure 3-4 A'). All in all, this staining pattern shows that the downstream target of cGMP – cGKI – that is necessary for bifurcation of DRG sensory neurons in mice[43], is also expressed in DRGs of chicken embryos.

In mice, CNP and its receptor GC-B are upstream members of the cGMP signaling cascade responsible for DRG axon bifurcation.[65, 66] To investigate if these signaling partners are also present in DRGs of chicken, FRET-based cGMP imaging was performed with whole-mount spinal cord preparations from chicken embryos. There is no transgenic chicken expressing the cGMP biosensor cGi500. For that reason, a strategy to express the sensor in DRG neurons was developed: During early embryonic stages (HH11-HH13) a vector encoding cGi500 (CMV-cGi500) was injected into the neural tube of the embryo. Then, electrodes were applied along the dorso-ventral axis and electroporation was performed. The eggs were incubated at 37 °C for two more days. By performing

electroporation at early embryonic stages, neural crest cells are transfected which will later, during develeopment, migrate and differentiate into neurons. Applying the plus electrodes to the dorsal site and the minus electrode to the ventral site of the embryo increases the chance to get sensor expressing DRG neurons. To validate this method, electroporated chicken embryos were dissected after 2 days of incubation. Transversal cryosections were prepared and the expression of the cGi500 biosensor in DRGs was investigated. Figure 3-4 E shows a transversial section of a chicken embryo, with a focus on the spinal cord and DRGs, two days after it was transfected with the CMV-cGi500 plasmid. Expression of cGi500 was detected in cells of the DRGs and in single cells of the neural tube (YFP fluorescence). This result clearly shows that the proposed strategy is appropriate to express the cGi500 biosensor in cells of chicken DRGs.

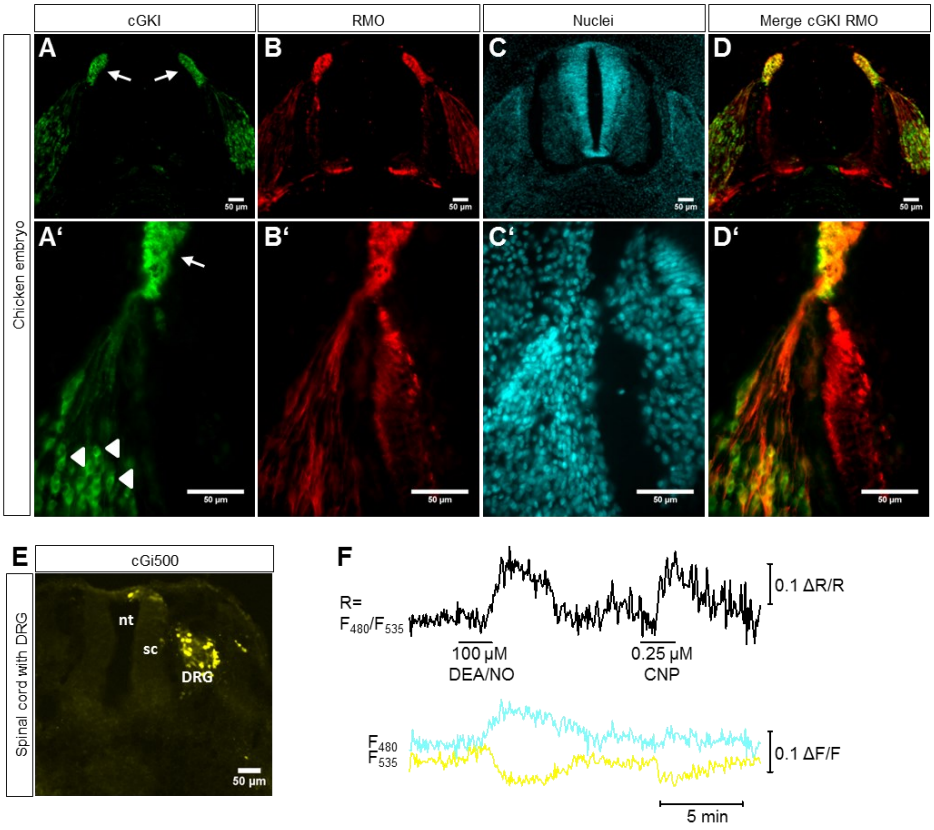

Figure 3-4: The chicken embryo is a suitable system for the investigation of the CNP/cGMP/cGKI signaling cascade in DRGs. Immunostainings were performed with frozen sections (10 µm) investigating the expression pattern of cGKI (A, A') and the axonal marker RMO (B, B') in embryonic chicken (HH18) spinal cord and DRGs. (C, C') Nuclei were stained with Hoechst 33258. (D, D') Merged picture of cGKI and RMO staining. (E) Expression of the cGMP biosensor cGi500 in DRGs of a chicken embryo (HH18). Neural crest cells of the chicken embryo that later differentiate into DRG neurons were transfected by in-ovo electroporation at early embryonic stages (HH10-13). After 2 days of incubation, the embryo was dissected, fixed with PFA, sectioned and checked for cGi500 expression in spinal cord and DRGs. nt neural tube, sc spinal cord. (F) FRET-based cGMP imaging was performed in chicken ex-vivo whole-mount preparation.

Acutely isolated whole mounts of chicken embryos expressing the cGMP biosensor cGi500 were taken for FRET-based cGMP imaging. During measurements, the embryo was continously perfused with Carbogen-gassed Ringer buffer. As shown in Figure 3-4 F, application of the NO donor DEA/NO as well as CNP leds to an elevation of the cGMP level indicating that the NO/NO-GC/cGMP pathway, as well as the CNP/GC-B/cGMP cascade are present in embryonic chicken DRGs. Altogether, these data indicate that the chicken embryo is a usefulmodel to investigate cGMP signaling in DRGs and related physiological processes such as axonal development during embryogenesis in real-time.

3.1.3 Ca^{2+} imaging in DRG somata

One important signaling pathway that is responsible for axon bifurcation of embryonic sensory neurons of DRGs is the well-described CNP/GC-B/cGMP/cGKIα pathway.[43, 65, 66] Other signaling cascades underlying this process are not well known. Ca^{2+} is a second messenger involved in several molecular mechanisms controling the nervous system.[205] The goal of the present study was to analyze if there might be a cross talk between the cGMP signaling cascade and Ca^{2+} signaling. Therefore, Fura-2/AM-based Ca^{2+} imaging was performed which is summarized in Figure 3-5. All signals were recorded at the somata of E12.5 dissociated DRG neurons. Two consecutive applications of 100 µM acetylcholine (ACh) were performed at intervals of ~10 min. Before the second ACh stimulus, cells were preincubated for 1.5 min with either Tyrode buffer (control condition, Figure 3-5 A) or with 100 nM CNP (Figure 3-5 B) to elevate cGMP in these cells (shown before in Figure 3-1, section 3.1.1). The comparison of these two conditions allows to see if CNP-induced cGMP would affect Ca^{2+} transients. While the second Ca^{2+} transient was only slightly reduced under control conditions (Figure 3-5 A), CNP application led to a strong suppression of Ca^{2+} influx (Figure 3-5 B). This indicates a cross talk between cGMP and Ca^{2+} signaling cascades in DRG neurons.

To unravel the underlying mechanism of the cross talk between cGMP and Ca^{2+} signaling, the role of the cGMP downstream effector cGKI was investigated in more detail. Therefore E12.5 DRG neurons from cGKI knockout (KO) embryos were prepared and the same set of experiments as described before was performed. In the control experiments (Tyrode buffer condition, data not shown), two subsequent applications of 100 µM ACh led to Ca^{2+} traces that were comparable to the transients shown in Figure 3-5 A (control condition in wildtype DRG somata). The suppressive effect of CNP-induced cGMP on Ach-induced Ca^{2+} transients was abolished in cGKI KO DRGs (Figure

3-5 C). After measurement, DRG neurons were stained for βIII-tubulin (red) to label neuronal cells and cGKI (green). The overlay of both channels with Hoechst 33258 is presented in Figure 3-5 D showing that wildtype DRG neurons express cGKI while cGKI KO neurons do not.

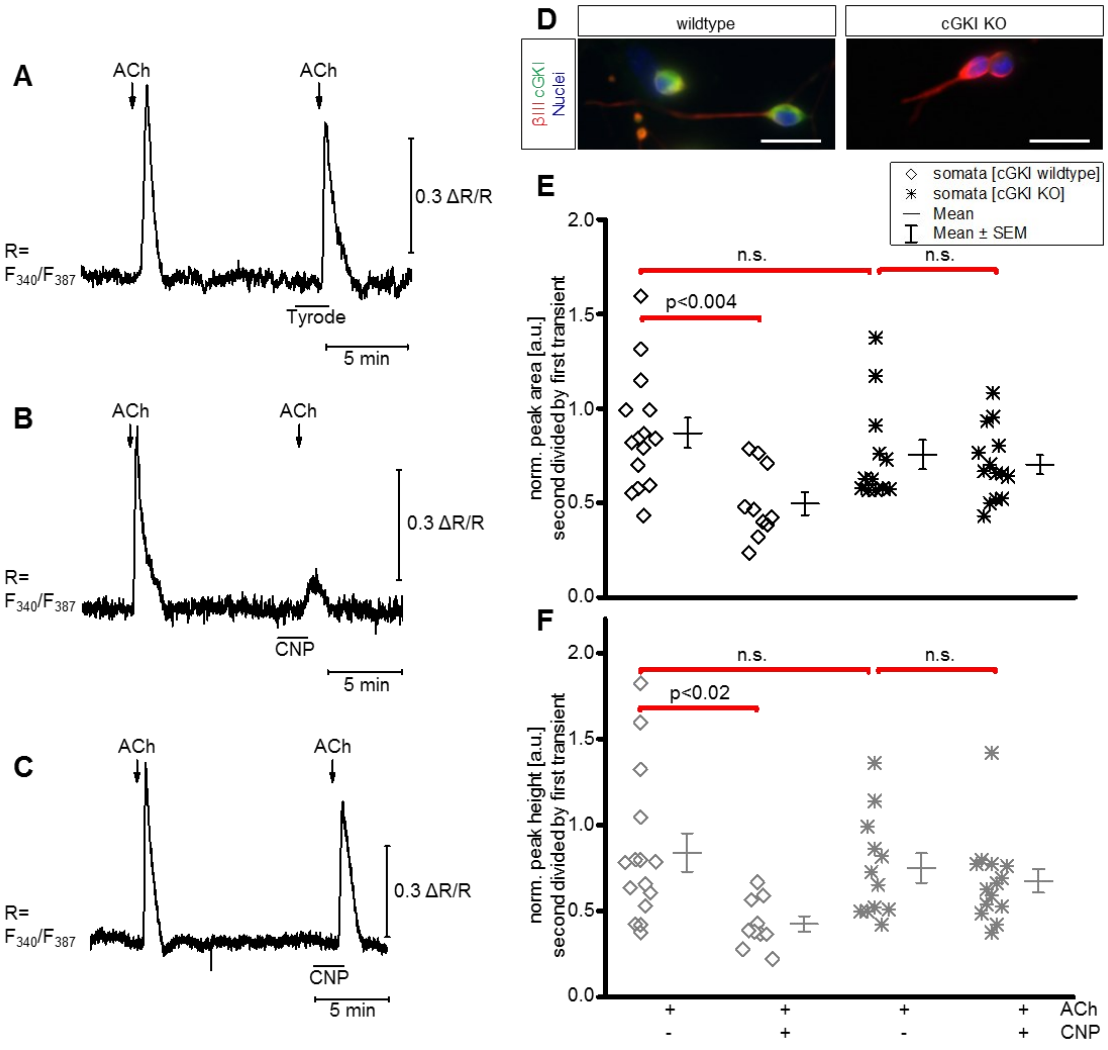

Figure 3-5: In somata of DRG neurons, CNP-induced cGMP suppresses ACh-induced Ca^{2+} transients via cGKI. Fura-2/AM-based Ca^{2+} imaging was performed in dissociated DRG neurons isolated from E12.5 C57BL/6 or R26-CAG-cGi500(L1) embryos. Ca^{2+} signals (ΔR/R) were recorded from the somata of DRG neurons. Two consecutive applications of ACh (100 µM, black arrows) were performed, with the second application in the presence of (A) Tyrode buffer or (B) CNP (100 nM). (C) The same set of experiments was performed in DRG neurons isolated from cGKI KO embryos. Representative Ca^{2+} measurement performed in cGKI KO DRGs showing Ca^{2+} traces after ACh application in the absence (first transient) and presence (second transient) of CNP-induced cGMP. (D) After respective measurements, DRG neurons (wildtype and cGKI KO) were stained for βIII-tubulin (red) and cGKI (green). Statistical analysis of (E) peak area and (F) peak height was performed, comparing values with and without prior application of CNP in cGKI wildtype and cGKI KO DRGs, respectively. For evaluation peak area and peak height were assessed. For normalization, second peak values were divided by first peak values. P-values >0.05 were considered to be not significant (n.s.).

Results from all four conditions are compared in Figure 3-5 E and F. Here, peak areas and peak heights of the Ca^{2+} transients were assessed. To visualize the effect of CNP-induced cGMP on Ca^{2+} signaling, values of the second transient were divided by values of the first transient. Using the normalization procedure, it was found that in control measurements (Tyrode buffer condition) of cGKI wildtype and KO neurons the second transient was already reduced to a small extent (~10 – 20 %, based on peak area) which might be due to desensitization of ACh receptors (Figure 3-5 E and F). Compared to control conditions, application of CNP significantly inhibited Ca^{2+} transients in cGKI wildtype neurons (~50 %). This effect was completely lost in cGKI KO neurons (Figure 3-5 E and F). Therefore, one can conclude that cGKI is mediating the suppressive effect of CNP-induced cGMP on Ach-induced Ca^{2+} signaling in the somata of embryonic DRG neurons.

3.1.4 Combined cGMP/Ca^{2+} imaging in DRG growth cones

To investigate if the above described crosstalk between cGMP and Ca^{2+} signaling in DRG somata (chapter 3.1.3) is also present in growth cones of DRG neurons, the cellular compartment, where bifurcation takes place, DRG explant cultures were cultivated. In explant cultures, DRG neurons develop huge growth cones (see Figure 3-1 A, section 3.1.1), while in dissociated cultures only ~10 % of the neurons develop growth cones at all. Interestingly, in the present study it was found that ATP-induced Ca^{2+} signaling is more prominent in growth cones of murine embryonic DRG neurons than ACh-induced Ca^{2+} signaling (data not shown). For that reason, ATP was used instead of ACh to evoke Ca^{2+} transients in growth cones of E12.5 DRG neurons (Figure 3-6).

For these experiments, DRG explants that express either the biosensor cGi500 or the membrane-targeted version of cGi500 (mcGi500), were loaded with Fura-2/AM. This allowed us to follow cGMP and Ca^{2+} changes simultaneously (Figure 3-6 A and B). Analogous to experiments described in chapter 3.1.3, two subsequent applications of 100 µM ATP were performed. To increase cGMP levels, a 1.5 min pre-incubation with 100 nM CNP (Figure 3-6 B) before second application of ATP was added. Incubation with Tyrode buffer served as a control (Figure 3-6 A). Due to combined cGMP/Ca^{2+} measurements it was possible to follow the change in cGMP in parallel by observing changes in F_{480}/F_{535} ratios (brown traces). While CNP elevated cGMP levels (Figure 3-6 B), Tyrode buffer did not (Figure 3-6 A). Under control conditions, the two consecutive applications of ATP led to two similar Ca^{2+} transients (Figure 3-6 A), while an increased

cGMP level suppressed ATP-induced Ca^{2+} (Figure 3-6 B). These results indicate a cross talk between the CNP/cGMP-pathway and ATP-induced Ca^{2+} signaling.

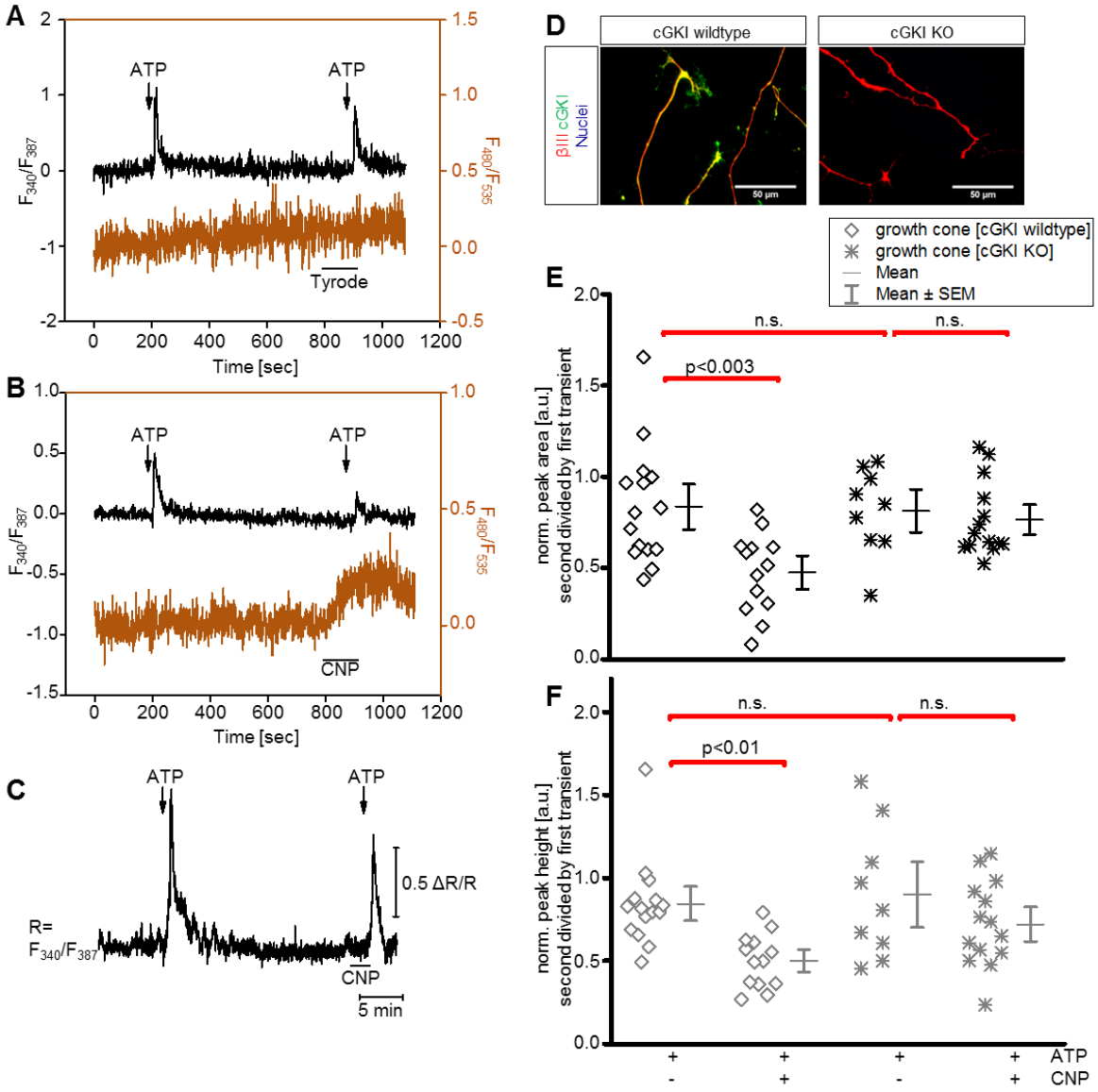

Figure 3-6: In growth cones of DRG neurons, CNP-induced cGMP suppresses ATP-induced Ca^{2+} transients via cGKI. Combined cGMP/Ca^{2+} imaging was performed in embryonic DRG explant cultures isolated from R26-CAG-cGi500(L1) and R26-CAG-mcGi500(L1) embryos. Ca^{2+} (black traces) and cGMP (brown traces) signals were recorded from the growth cones of DRGs. Two consecutive applications of ATP (100 µM) were performed, with the second application in the presence of (A) Tyrode buffer or (B) CNP (100 nM) that elevates cGMP. (C) Fura-2/AM-based Ca^{2+} imaging was performed in DRG growth cones of cGKI KO embryos. Representative Ca^{2+} measurement performed in cGKI KO DRGs showing Ca^{2+} traces after ATP application in the absence and presence of CNP-induced cGMP. (D) After respective measurements, DRG explants (wildtype and cGKI KO) were stained for βIII-tubulin (red) and cGKI (green). Statistical analysis of (E) peak area and (F) peak height of ATP-induced Ca^{2+} transients was performed, comparing values with and without prior application of CNP in cGKI wildtype and cGKI KO DRGs. For evaluation, peak area and peak height were assessed and second peak values were divided by first peak values. P-values >0.05 were considered to be not significant (n.s.).

To investigate if this effect is mediated by the cGMP downstream target cGKI, DRG explant cultures from cGKI KO embryos were prepared and Fura-2/AM-based Ca^{2+} imaging was performed. Two applications of ATP without elevating cGMP levels produced two comparable Ca^{2+} transients in cGKO KO growth cones (data not shown) similar to control conditions in cGKI wildtype growth cones (Figure 3-6 A). Comparable to the results with Ach-induced Ca^{2+} transients in DRG somata, it was observed that the suppressive effect of CNP-induced cGMP on ATP-induced Ca^{2+} was abolished in cGKI KO growth cones (Figure 3-6 C) indicating a cGKI-mediated cross talk between cGMP and Ca^{2+} signaling cascades. Similarly to DRG somata measurements, DRG explants of wildtype or cGKI KO embryos were stained for βIII-tubulin (red) to label neuronal axons and growth cones and for cGKI (green) to confirm that measurements were performed in cGKI-positive or cGKI-negative sensory DRG growth cones. The overlay of both channels showed that wildtype DRG neurons express cGKI, while cGKI KO neurons do not (Figure 3-6 D). For evaluation of all performed experiments, peak area and peak height were assessed, and second area/height values were divided by first values for the respective experiments and depicted in scatter plots (Figure 3-6 E and F). In summary, these results show that ATP induces Ca^{2+} signals in the growth cone of embryonic DRG neurons. The Ca^{2+} transients were suppressed when cGMP was elevated by CNP. This process is mediated by the cGMP downstream mediator cGKI, perhaps due to inactivation of ATP receptors by phosphorylation or other mechanisms.

3.2 Effect of IWP-051 in different brain regions

Aberrant cGMP signaling goes along with several disorders and diseases. The NO-sensitive guanylyl cyclase (NO-GC), of which two isoforms exist – NO-GC1 and NO-GC2 – has been shown to be a promising drug target to increase cGMP in the brain. In this study, two drug-like small molecules – IWP-051 and Bay 41-2272 – that work synergistically with NO to stimulate NO-GC activity, were tested to assess their activity in different brain regions.

3.2.1 Ex vivo FRET analysis in acute brain slices

To visualize cGMP under close-to-nature conditions, acute brain slices were analyzed by FRET-based cGMP imaging with a spinning disk microscope. Slices were carbogen-gassed during slicing and measurements to keep the tissue alive. To investigate the effect of IWP-051 specifically in Purkinje cells of the cerebellum, the L7Cre;R26-CAG-

cGi500(L2) mouse line was used. In these mice, the cGMP biosensor cGi500 is specifically expressed in Purkinje cells of the cerebellum as shown in Figure 3-7 A (yellow). The FRET recording and bar graph depicted in Figure 3-7 A show that the application of 5 µM DEA/NO led to an elevation of cGMP in Purkinje cells, confirming the presence of the NO/NO-GC/cGMP signaling cascade in this cell type. The application of the NO-GC stimulator IWP-051 (0.1 µM) alone did not affect the cGMP level in Purkinje cells. The application of both, 100 nM IWP-051 in combination with 5 µM DEA/NO (third application) significantly potentiated the DEA/NO-induced cGMP level ~2.5 fold (see bar graph in Figure 3-7 A). This experiment demonstrated the potential of IWP-051 for stimulating NO-GC in Purkinje cells of the cerebellum.

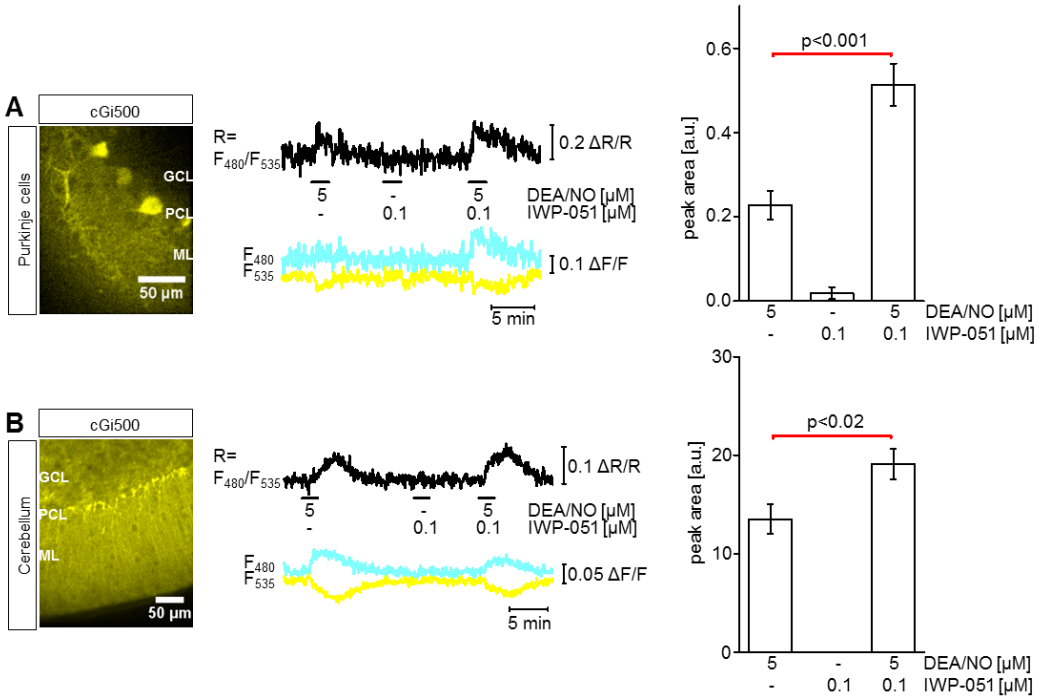

Figure 3-7: IWP-051 potentiates DEA/NO-induced cGMP signals in Purkinje cells and in the granule cell layer of the cerebellum. (A) Fluorescence resonance energy transfer (FRET)-based cGMP imaging was performed in acute cerebellar brain slices from a L7Cre;R26-CAG-cGi500(L2) mice. Crossing a R26-CAG-cGi500(L2) mouse with a L7Cre mouse leads to a Purkinje cell-specific expression of the cGMP biosensor cGi500 (left, yellow). During measurement, DEA/NO, IWP-051 or a combination of both was applied in the indicated concentrations (middle, black horizontal bars). Black, cyan and yellow traces represent CFP/YFP ratio, CFP and YFP traces, respectively. Statistical analysis (right) was performed with integrating peak areas of respective cGMP signals; data are shown as mean ± SEM (n=5 ROIs from one brain slice). (B) FRET-based cGMP imaging was performed in acute cerebellar brain slices from a NesCre;R26-CAG-cGi500(L2) mice. Crossing a R26-CAG-cGi500(L2) mouse with a NesCre mouse leads to a neuronal- and glia-specific expression of the cGMP biosensor cGi500 (left, yellow). A representative measurement of the granule cell layer (GCL) is shown (middle). Statistical analysis (right) was performed by integrating peak areas of respective cGMP signal; data are shown as mean ± SEM (n = 9 ROIs from three brain slices). ML Molecular layer; PCL Purkinje cell layer.

Figure 3-7 B summarizes the measurements performed in the granule cell layer (GCL) of acute cerebellar slices. For this experiment, the cerebellum of a NesCre;R26-CAG-mT/cGi500(L2) mouse was used. In these mice, cGMP sensor cGi500 is expressed in neural tissue including neurons and glia cells (yellow), while excluding small blood vessels in this region (data not shown, for comparison see Figure 3-8 A). The application of 5 µM DEA/NO led to an elevation of cGMP in the GCL of the cerebellum, while IWP-051 (0.1 µM) did not. However, the combination of 5 µM DEA/NO and 0.1 µM IWP-051 (third application) significantly potentiated the magnitude of the cGMP signal in the GCL compared to the signal induced by DEA/NO alone (see bar graph in Figure 3-7 B). These data show that IWP-051 is an effective NO-GC stimulator that potentiates DEA/NO-induced cGMP signals in specific regions of the murine cerebellum.

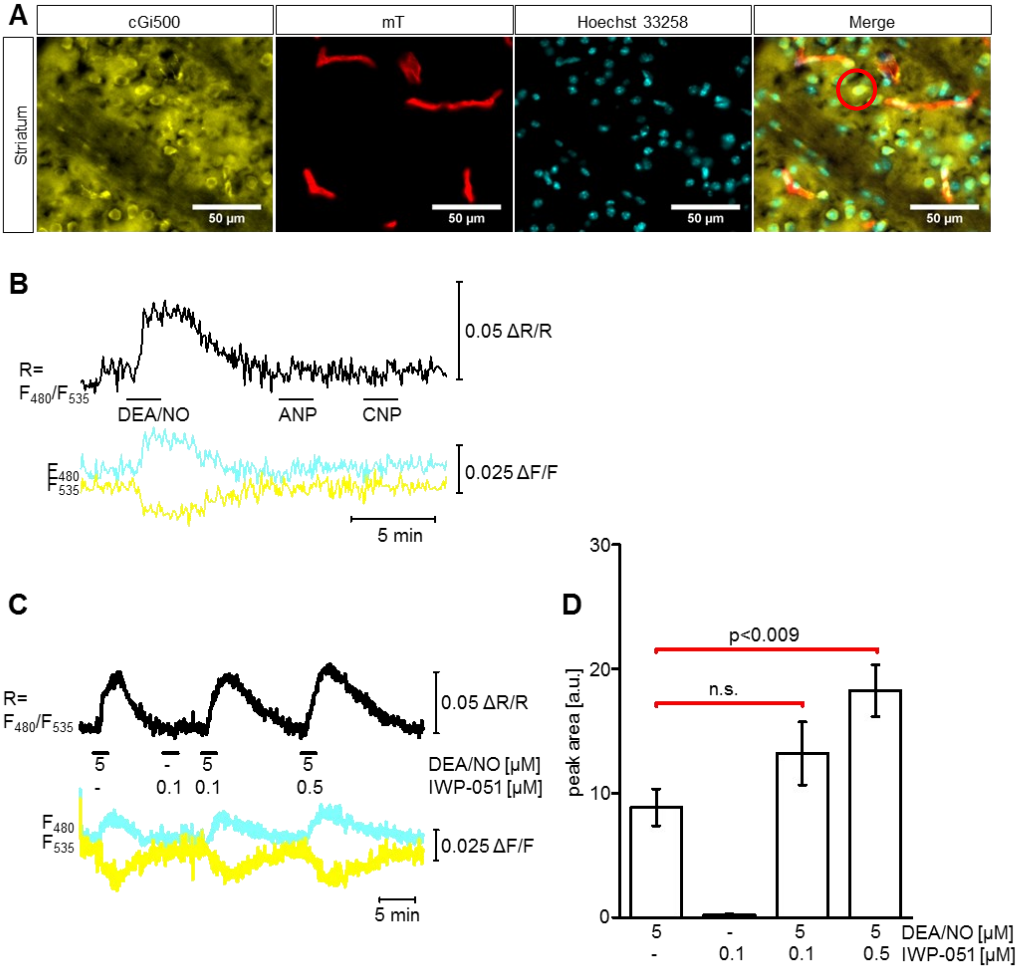

Figure 3-8: IWP-051 potentiates DEA/NO-induced cGMP signals in the striatum. (A) Representative pictures of the striatum in fixed NesCre;R26-CAG-cGi500(L2) brain slices showing cGi500 sensor (yellow) and membrane-targeted tomato expression (mT, red), Hoechst nuclei staining (cyan) and an overlay of all three channels (Merge). The red circle shows a representative ROI chosen for analysis. (B) FRET-based cGMP imaging was performed in acute striatal brain slices from a NesCre;R26-CAG-cGi500(L2) mouse. During measurement 5 µM DEA/NO, 0.25 µM ANP and 0.25 µM CNP (middle, black horizontal bars) were applied (black horizontal bars). Black, cyan and yellow traces represent CFP/YFP ratio, CFP and YFP traces, respectively. (C) Representative cGMP measurement in the striatum with DEA/NO and IWP-051 in the indicated concentrations (black horizontal lines). For imaging studies, striatal cells were chosen that were separated from surrounding blood vessels to avoid false-positive signals. (D) Statistical analysis was performed by integrating peak areas of respective cGMP signals; data are shown as mean ± SEM (n = 6 ROIs from three brain slices). n.s. not significant.

The NesCre;R26-CAG-cGi500(L2) mouse line was used to investigate the potential stimulating effect of IWP-051 on DEA-induced cGMP signals in the striatum and hippocampal CA1 area of the mouse brain (Figure 3-8 and Figure 3-9, respectively). Figure 3-8 A shows the expression of the biosensor cGi500 in recombined neural cells of the striatum (yellow). Small blood vessels of the striatum were not recombined and therefore express membrane-targeted tomato (red). An overlay of both channels with Hoechst staining (blue) showed a high density of neural cells in the striatal area of interest (Merge) that were chosen for FRET-based cGMP imaging experiments in acute brain slices. Figure 3-8 B shows that only DEA/NO but not ANP and CNP were able to induce cGMP in striatal cells of the mouse brain. This is in line with the literature describing the presence of the NO-cGMP pathway in the striatum.[144] The application of 5 µM DEA/NO induced a cGMP signal in murine striatum, IWP-051 (0.1 µM) alone did not. However, the combination of both led to an ~1.5 fold increase of peak areas as compared to the first application with DEA/NO alone and was even more potentiated when 0.5 µM IWP-051 was applied together with DEA/NO (Figure 3-8 D and E).

The cGi500 sensor expression in the hippocampal CA1 area of a NesCre;R26-CAG-cGi500(L2) mouse is shown in Figure 3-9 A (yellow). As in the striatal area, small blood vessels were not recombined and therefore express only membrane-targeted tomato (red). Performing nuclei co-staining with Hoechst dye (blue), visualization of the pyramidal cell layer in hippocampal CA1 area (Merge) was possible which was chosen for FRET-based cGMP imaging experiments (red circle). In the hippocampal CA1 area, cGMP imaging revealed that in contrast to cerebellar and striatal brain areas, IWP-051 did not potentiate DEA/NO-induced cGMP (Figure 3-9 B and C). The application of 5 µM DEA/NO triggered cGMP signals, but these signals where not increased when 0.1 µM or 0.5 µM IWP-051 was added (see peak area evaluation in Figure 3-9 C). IWP-051 (0.1 µM) alone

did not affect the cGMP level. Thus, in contrast to the cerebellum and striatum, IWP-051 did not potentiate NO-induced cGMP signals in the hippocampal CA1 region.

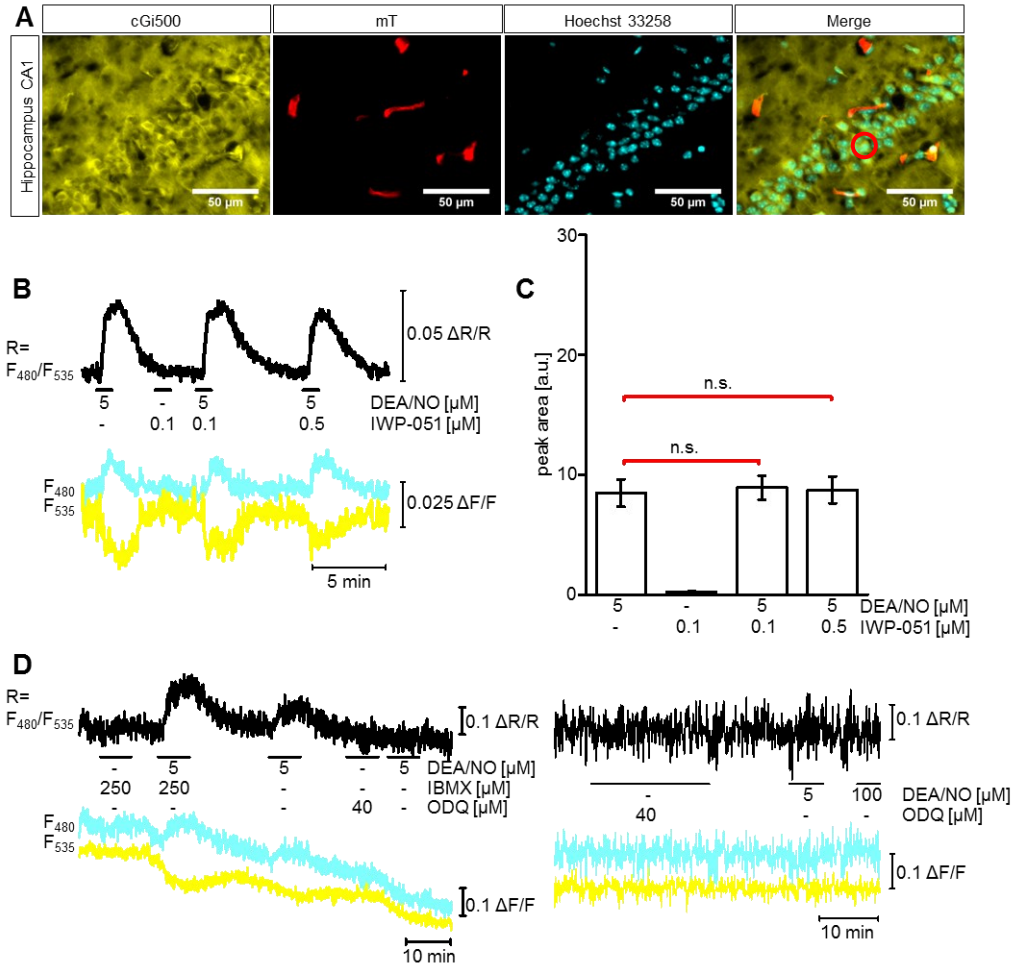

Figure 3-9: IWP-051 does not potentiate DEA/NO-induced cGMP signals in the hippocampal CA1 area. (A) Representative pictures of fixed NesCre;R26-CAG-cGi500(L2) brain slices showing cGi500 sensor (yellow) and membrane-targeted tomato expression (mT, red), Hoechst nuclei staining (cyan) and an overlay of all three channels (Merge) of the hippocampal CA1 area. The circle shows a representative ROI chosen for analysis. (B-D) cGMP imaging of hippocampal cells in the CA1 region was performed in acute brain slices from NesCre;R26-CAG-cGi500(L2) mice. To avoid false-positive signals, only regions of interest that were separated from surrounding blood vessels were analyzed (red circle). Black, cyan and yellow traces represent CFP/YFP ratio, CFP and YFP, respectively. (B) Representative FRET-based cGMP measurement with DEA/NO and IWP-051 applications (black horizontal lines) and (C) statistical analysis (right) of peak areas of respective cGMP signals; data are shown as mean ± SEM (n = 9 ROIs from three brain slices). (D) Representative experiments with 3-isobutyl-1-methylxanthin (IBMX) and 1H-[1,2,4]oxadiazolo[4,3-a]quinoxaline-1-one (ODQ) applications in combination with or without DEA/NO. The respective concentrations are indicated in the graphs. Similar results were obtained in at least three ROIs measured on two brain slices (IBMX and ODQ, left) or one brain slice (ODQ, right). n.s. not significant.

IWP-051 could have been ineffective because the application of 5 µM DEA/NO had already increased the cGMP concentration to the maximum or to a level at which the cGMP sensor was already saturated. To exclude these possibilities, control experiments were performed (see Figure 3-9 D) with the nonspecific PDE inhibitor IBMX. IBMX (250 µM) alone did not affect the baseline cGMP level, but in combination with 5 µM DEA/NO it drastically elevated the cGMP concentration compared to 5 µM DEA/NO alone (Figure 3-9 D, left), thus refuting the possibility that application of NO alone had already resulted in a maximal cGMP response or saturation of the cGMP sensor. Moreover, the baseline FRET/cGMP signal was not altered by application of the NO-GC inhibitor 1H-[1,2,4]oxadiazolo[4,3-a]quinoxaline-1-one (ODQ) or of the PDE inhibitor IBMX (Figure 3-9 D) indicating that basal cGMP production via NO-GC as well as cGMP degradation via PDEs was very low to absent in our acute hippocampal brain slices. The inhibitory potential of applied ODQ was verified by the fact that subsequent application of DEA/NO did not elevate cGMP (Figure 3-9 D, left and right). Taken together, the NO-GC stimulator IWP-051 mediates potentiation of NO donor-induced cGMP signals in Purkinje cells and granule neurons of the cerebellum as well as in neurons of the striatum but not in the hippocampal CA1 area of acute brain slices.

3.2.2 In vitro analysis of cerebellar granule and hippocampal neurons

To support our previous findings from ex vivo/acute brain slice experiments, primary neuronal cell cultures of cerebellar granule neurons (CGNs) and hippocampal neurons (HNs) were analysed. Cells were isolated from pups of R26-CAG-cGi500(L1) mice that express cGi500 globally (Figure 3-10 for CGNs, Figure 3-10 C for HNs). FRET-based cGMP imaging was performed and peak areas of respective signals were evaluated and taken as a measure of produced cGMP. Increasing concentrations of IWP-051 ± DEA/NO were tested. In CGNs (Figure 3-10 B), the application of 0.1 µM IWP-051 alone did not lead to an elevation of cGMP. The very small peak area value was obtained by automated peak area evaluation and represents background noise. However, the application of 3.3 µM IWP-051 led to an increase of the cGMP level that was comparable to the 7.5 nM DEA/NO. Co-treatment with 0.1 µM IWP-051 potentiated the DEA/NO-induced signal ~3 fold, while application of 3.3 µM IWP-051 with DEA/NO elevated the signal ~4.5 fold.

In contrast to CGNs, increasing concentrations of IWP-051 (0.1, 0.5, or 5 µM) in combination with DEA/NO did not potentiate DEA/NO-induced cGMP levels in HNs (Figure 3-10 D, IWP-051 bar graph). The slight elevation of cGMP upon increasing concentrations of IWP-051 was not significantly different from the cGMP increase induced by 10 nM DEA/NO alone. For comparison, another NO-GC stimulator – Bay 41-2272 – clearly potentiated DEA/NO-induced cGMP signals in HNs (Figure 3-10 D, Bay 41-2272 bar graph). Treatment with 3.3 µM Bay 41-2272 alone increased the cGMP level in HNs but 0.1 µM Bay 41-2272 alone did not. Moreover, application of 3.3 µM Bay 41-2272 potentiated DEA/NO-induced cGMP in HNs.

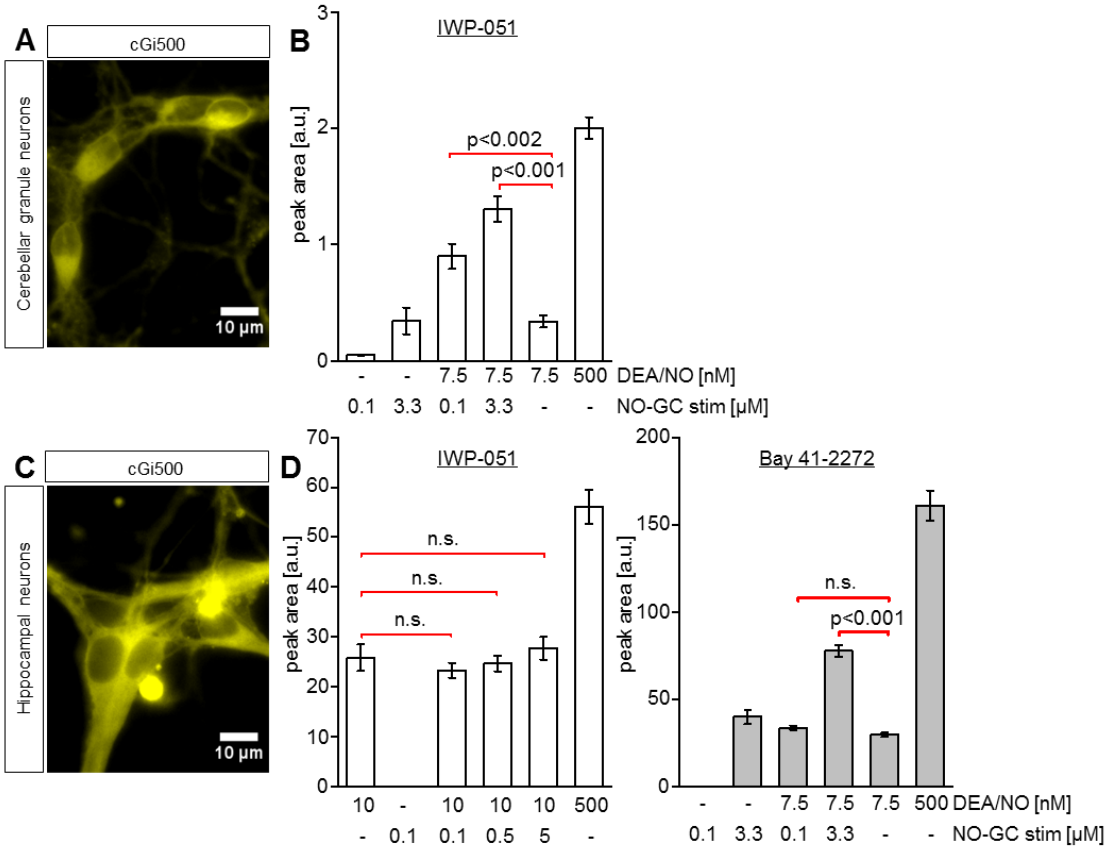

Figure 3-10: IWP-051 potentiates DEA/NO-induced cGMP in primary cerebellar granule neurons (CGNs), but not in hippocampal neurons (HNs). (A) Representative picture of primary cGi500-expressing CGNs (yellow) isolated from postnatal day 7 R26-CAG-cGi500(L1) mice. (B) Statistical analysis of FRET-based cGMP imaging in P7 CGNs, showing peak areas of cGMP signals evoked by DEA/NO and/or IWP-051. Respective concentrations are indicated below the graph; data are shown as mean ± SEM (n = 7 cells from two coverslips). (C) Representative picture of primary HNs expressing the cGMP biosensor cGi500 (yellow). Neurons were isolated from newborn (P0) R26-CAG-cGi500(L1) mice. (D) Statistical analysis of FRET-based cGMP imaging in P0 HNs, showing peak area values for the respective DEA/NO- and/or IWP-051-induced cGMP signals (left, n = 12 cells from two coverslips) or DEA/NO- and/or Bay 41-2272-induced signals (right, n = 6 from one coverslip); data are shown as mean ± SEM. n.s. not significant.

In contrast to IWP-051, Bay 41-2272 had a clear potentiating effect on the NO-induced cGMP signals in HNs. These findings indicated potential differences in the activity profiles of the NO-GC stimulators IWP-051 and Bay 41.2272 in different brain regions.

3.2.3 Comparison of IWP-051 and Bay41-2272 activity in striatum and hippocampus of wildtype and NO-GC1/2 KO mice

The apparent brain region-specific activity profile of IWP-051 could be explained by a NO-GC isoform-specific activity of the compound. According to mRNA *in-situ* hybridization data obtained by us in collaboration with Lea Kennel and Prof. Dr. Achim Schmidtko from the Institute for Pharmacology and Clinical Pharmacy in Frankfurt/Main (data not shown) or published in the Allen mouse brain atlas.[206]

In Figure 3-11 is shown that NO-GC1 is mainly expressed in the striatum (white arrowhead), cerebellar Purkinje cells (yellow arrowhead), and cerebellar granule neurons (red arrowhead), but not in the hippocampus (blue arrowhead). In contrast, only few neurons in the striatum (white arrow) and cerebellum, mainly Purkinje cells (yellow arrow), show NO-GC2 expression, while the hippocampal dentate gyrus and CA1-CA3 area express high levels of NO-GC2 (blue arrow). A similar expression profile of the NO-GC isoforms was found in the rat brain[207], and mRNA analysis by real-time polymerase chain reaction showed that mouse hippocampus expresses a 3-fold higher mRNA level of NO-GC2 vs. NO-GC1.[208] The activity profile of IWP-051 and the expression pattern of NO-GC1 and NO-GC2 in the striatum, cerebellum and hippocampus is consistent with isoform-specific potentiation of NO-GC1 but not NO-GC2 by IWP-051.

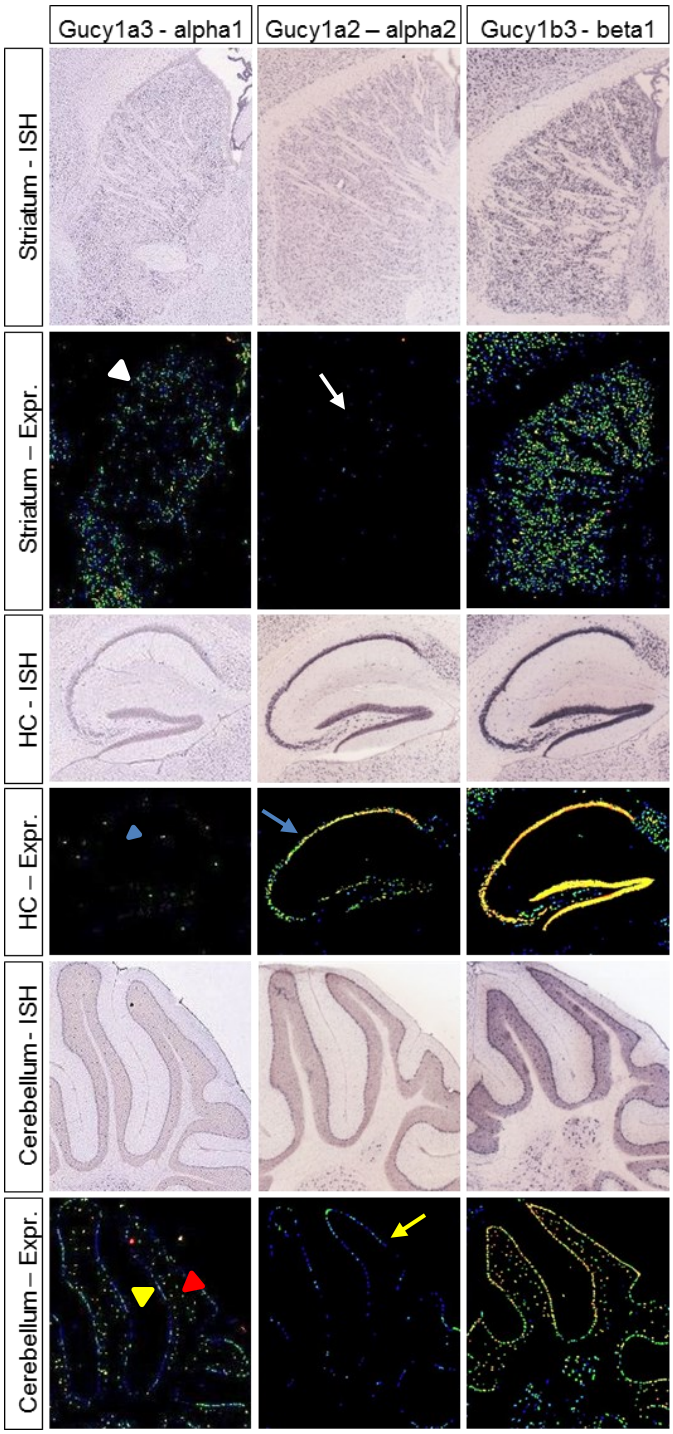

Figure 3-11: Expression of NO-GC1 mRNA is prominent in striatum and cerebellum, while NO-GC2 mRNA is strongly expressed in the hippocampus. Representative pictures of *in-situ* hybridization (ISH) experiments showing mRNA expression of NO-GC subunits in striatum, hippocampus (HC) and cerebellum of an adult C57BL/6 mouse. Pictures labelled with "ISH" represent the original ISH staining, while pictures labelled with "Expr." represent a heat map showing the relative amount of the respective mRNA (blue dots indicate low expression, yellow dots indicate high expression). NO-GC1 expression was detected in striatum (white arrowhead) and in the Purkinje cell layer (yellow arrowhead) and granule cell layer (red arrowhead) of the cerebellum. In the hippocampus, NO-GC1 expression was very low to undetectable (blue arrowhead), while NO-GC2 expression was high (blue arrow). Weak NO-GC2 expression was observed in the striatum (white arrow) and Purkinje cell layer of the cerebellum (yellow arrow). Data is taken from the Allen mouse brain atlas. Image credit: Allen Institute.[206]

As described in chapter 3.2.1, IWP-051 potentiates DEA/NO-induced cGMP levels in GCL and Purkinje cells of the cerebellum and in striatum but not in the hippocampal CA1 area. To investigate if this process is a mechanism specifically mediated by IWP-051, Bay 41-2272 was used to verify its potential to act as a NO-GC stimulator in murine striatum and hippocampus. Pilot experiments revealed that a concentration of 10 µM Bay 41-2272 was required to reliably detect a potentiating effect of this compound on DEA/NO-induced cGMP signals in brain slices. Thus, for comparative experiments IWP-051 and Bay 41-2272 were used in a concentration of 10 µM.

As shown in Figure 3-12 A (wildtype), 10 µM Bay 41-2272 (~ 2 fold) as well as 10 µM IWP-051 (~3.5 fold, see also Figure 3-12 C) potentiated DEA/NO-induced cGMP in murine striatum of wildtype mice expressing both isoforms – NO-GC1 and NO-GC2. On the contrary in hippocampal CA1 cells (Figure 3-12 B, wildtype), only Bay 41-2272 (10 µM) but not IWP-051 increased DEA/NO-induced cGMP production (see also Figure 3-12 D), indicating a brain area-specific role of IWP-051. Considering the mRNA expression pattern of NO-GC isoforms described in Figure 3-11, one could hypothesize that IWP-051 specifically acts on NO-GC1 but not on NO-GC2. To elucidate this hypothesis, mice that express the cGMP biosensor specifically in nestin-expressing cells [NesCre;R26-CAG-cGi500(L2)] and carried a total knockout for either NO-GC1 or NO-GC2 were bred. Interestingly, it was found that the knockout of NO-GC1 leads to a loss of function of IWP-051 in striatum (Figure 3-12 A and C, NO-GC1 KO). IWP-051 is not able to potentiate DEA/NO-induced cGMP while Bay 41-2272 does up to ~ 1.5 fold. It has to be mentioned that the cGMP signal induced by 5 µM DEA/NO alone was smaller in peak area and peak height than in wildtype striatum which is most likely due to the missing NO-GC1 isoform. In the hippocampal CA1 area of NO-GC1 KO mice, Bay 41-2272 significantly potentiated DEA/NO-induced cGMP while IWP-051 did not (Figure 3-12 B and D, NO-GC1 KO). These results are comparable with the data conducted in wildtype hippocampus where only a small proportion of hippocampal cells express NO-GC1.[24] In the striatum of NO-GC2 KO mice (Figure 3-12 A and C, NO-GC2 KO), Bay 41-2272 as well as IWP-051 (10 µM each) potentiated DEA/NO-induced cGMP levels. Thus, these results also support the hypothesis that IWP-051 acts NO-GC1-specific. In hippocampal CA1 cells of NO-GC2 mice (Figure 3-12 B and D), no DEA/NO-induced cGMP was detected. That is why no potential stimulating effect of IWP-051 and Bay 41-2272 was detected. Signal-to-noise ratio was too high to evaluate peak area values, hence this experiment was excluded from peak area evaluation.

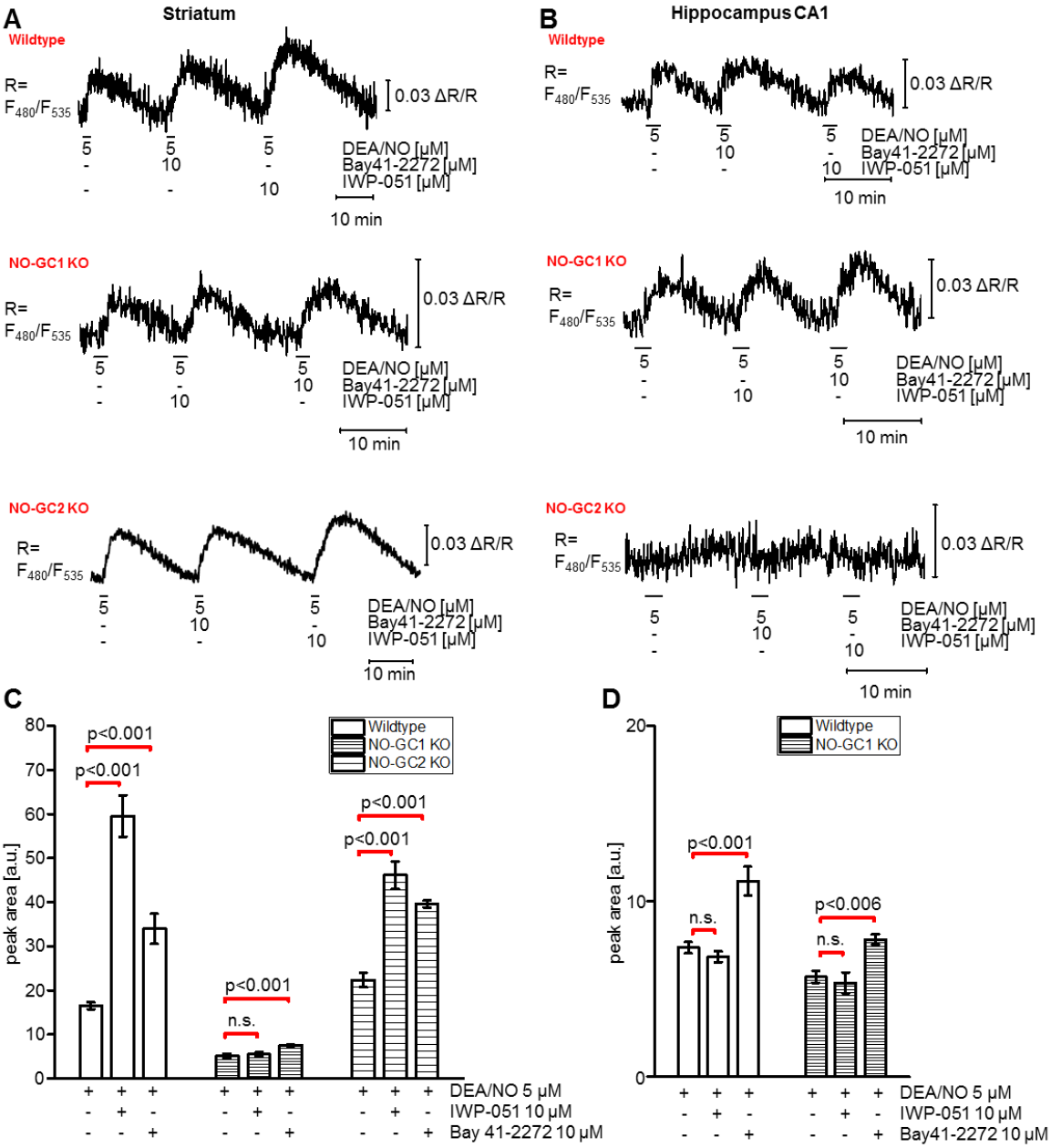

Figure 3-12: cGMP imaging in acute brain slices of NO-GC1 and NO-GC2 knockout mice reveals different activities of IWP-051 and Bay 41.2272 in (A,C) striatum and (B,D) hippocampus. Representative cGMP measurements (showing CFP/YFP ratios) performed in (A) the striatum and (B) hippocampus of wildtype, NO-GC1 KO and NO-GC2 KO mice that had been crossed to NesCre;R26-CAG-cGi500(L2) mice and, thus, expressed cGi500 in neurons and glia cells. DEA/NO, IWP-051, and Bay 41-2272 were applied in the indicated concentrations (black horizontal lines). Statistical analysis of respective cGMP signals in (C) striatum (wildtype, n = 22; NO-GC1 KO n = 16; NO-GC2 KO n = 16) and (D) hippocampus (wildtype, n = 22; NO-GC1 KO, n = 9) was performed with peak areas; data are shown as mean ± SEM (n-numbers represent number of evaluated ROIs from at least three brain slices per genotype); n.s. not significant. To avoid false-positive signals, only ROIs that were separated from surrounding blood vessels were analyzed. Note that the absence of detectable cGMP signals in the hippocampus of NO-GC2 KO precluded statistical analysis. For each genotype and brain region, similar results were obtained in independent experiments with brain slices from three mice.

Taken together, cGMP imaging in acute brain slices, in particular the comparative testing of IWP-051 and Bay 41-2272 in wildtype, NO-GC1 KO and NO-GC2 KO mice, and the expression profile of NO-GC isoforms, provided strong evidence for the notion that the brain-region-specific activity of IWP-051 was related to isoform-specific stimulation of NO-GC1 but not NO-GC2.

4 DISCUSSION

The recently developed cGMP sensor mice R26-CAG-cGi500(L1) and R26-CAG-mT/cGi500(L2) allow for the analysis of cGMP dynamics in a global or tissue-/cell type-specific manner, respectively. Using these sensor mice, the formation and degradation of cGMP was analyzed by performing FRET microscopy in different regions and cell types of the nervous system including DRGs, cerebellum, hippocampus and striatum.[197] In combination with the Ca^{2+}-sensitive dye Fura-2/AM, a possible interaction between the second messengers cGMP and Ca^{2+} was investigated in embryonic DRG neurons to unravel the molecular mechanisms behind DRG axon bifurcation. Furthermore, the recently developed NO-GC stimulator IWP-051 was tested for its potency to enhance NO-induced cGMP levels in murine cerebellum, hippocampus, and striatum. By using real-time imaging methods, the visualization of second messenger signals was possible in living cells and tissues, which might reflect the *in vivo* situation far better as compared to end-point measurements with dead cells and tissues.

4.1 Second messenger crosstalk in embryonic DRGs

Previously it was reported that the bifurcation – the splitting of an axon tip into two daughter branches – of murine DRG neurons during embryogenesis is dependent on a cGMP signaling cascade including CNP, GC-B and cGKIα.[43,65,66] The bifurcation process is not only restricted to developing DRG axons but was also found in murine cranial sensory ganglia of the hindbrain. Interestingly, the bifurcation process of these cells is dependent on the same signaling cascade.[209] The cGMP-FRET analysis of living E12.5 DRG neurons performed in this study clearly shows that among several endogenous cGMP-increasing agents only CNP is able to increase the cGMP level in somata and growth cones (for comparison, see Figure 3-1). Other cGMP elevating agents, such as the NO donor DEA/NO or the GC-A-activating peptides ANP and BNP, tested in somata of dissociated DRG neurons, did not elevate cGMP levels. These results demonstrate that CNP is exclusively responsible for the elevation of cGMP in murine E12.5 DRG neurons. Analysis of cGMP signaling in *ex vivo* preparations of the spinal cord with attached DRGs showed comparable results. Here, only CNP elevated cGMP in the dorsal root ganglia (see Figure 3-3). Both findings correlate well with data obtained from wildtype mice showing CNP expression in the dorsal part of murine spinal cord and GC-B and cGKIα expression in sensory neurons of murine DRGs, emphasizing the presence of this pathway

in the embryonic spinal cord including DRGs.[43,65,66] Furthermore, the *ex vivo* cGMP-FRET data shows that neither the NO/NO-GC nor the ANP/GC-A or BNP/GC-A pathway are present in E12.5 DRG neurons. That is in line with real-time PCR screens published by Schmidt et al. showing that GC-B is the major pGC expressed in E12 DRG neurons. Transcripts for NO-GCs and GC-A were not detected.[66] Furthermore, Schmidt et al. identified a physiological role of the CNP/GC-B/cGMP pathway in axon bifurcation of DRG neurons. In the absence of one of the signaling components, bifurcation is largely impaired. Axons grow either in caudal or rostral direction, while DRG axons of NO-GC KO mice bifurcate normally.[43,65,66]

Levels of cGMP and other cyclic nucleotides are not only regulated by their generators, but also by PDEs hydrolyzing them. However, it was not well understood which types of PDEs are responsible for the degradation of CNP-induced cGMP in murine E12.5 DRG neurons. With the use of R26-CAG-cGi500(L1) sensor mice and FRET-based cGMP imaging, PDE2A was identified to be responsible for the degradation of CNP-induced cGMP in these neurons (for comparison see Figure 3-2 D). Bay 60-7550 is a relatively specific inhibitor for PDE2A identified by Bayer with an EC_{50}=4.7 nM and was already shown to improve memory functions in mice.[210,211] These results correlate well with mRNA and protein expression data published by Schmidt et al. in 2016.[204] Among others they found PDE2A transcripts in E12.5 DRGs by performing real-time PCR screens and in situ hybridization assays. Additionally, PDE2A protein expression was identified in GC-B-expressing cells of E12.5 DRGs. Together with the FRET/cGMP measurements performed in the present work, these data strongly support the conclusion that PDE2A is the major enzyme responsible for cGMP degradation in murine E12.5 DRG neurons. Schmidt et al. also investigated the role of PDE2A on DRG axon bifurcation. Interestingly, a KO of PDE2A in mice, which should lead to high cGMP levels in the cells did not affect the bifurcation of DRG axons at embryonic stages. The authors conclude that DRG axon bifurcation tolerates presumably high concentrations of cGMP.[204] As mentioned before, Schmidt et al. identified further PDE transcripts in E12.5 DRGs by real-time PCR screens (PDE3A, PDE3B, PDE6D, PDE6G, PDE9A, PDE10A, PDE11A), while in our FRET-based cGMP study other PDE inhibitors did not affect cGMP levels.[204] Sildenafil is described as a selective PDE5 inhibitor, but to a certain extent it also blocks PDE6.[212, 213] Zaprinast is known to inhibit PDE5 and PDE6 as well as PDE9, PDE10 and PDE11 to a lower extent.[214,215,216,217] However, in the FRET study both inhibitors were without effect, demonstrating that these PDEs are not relevant for

cGMP degradation in sensory neurons of embryonic DRGs. The application of Milrinone (inhibits PDE3) or Vinpocetine (inhibits PDE1) were without effect on cGMP levels. Taken together, although several PDE transcripts were detected in real-time PCRs by Schmidt et al., the pharmacological FRET-based analysis revealed that PDE2A is the major enzyme responsible for degradation of CNP-induced cGMP in embryonic DRG neurons. It is well known that a present mRNA transcript does not have to be translated into the protein.[218] Since the real-time PCR data was obtained from whole DRGs including not only sensory neurons but also Schwann cells, fibroblasts an others, it might be possible that the other identified PDE transcripts were derived from these non-neuronal cell types.[219]

Central questions – how exactly cGMP mediates axon bifurcation and how exactly the bifurcation process occurs *in vivo* – are not completely answered yet. To address these questions, the outgrowth of sensory axons that enter the spinal cord should be observed *in vivo*. Imaging experiments in living mouse embryos which develop inside the mother are difficult for technical reasons. Since the chick embryo was reported to be a robust model to investigate vertebrate development, it was tested if it might be a suitable system to investigate cGMP signaling of DRG sensory neurons.[220] Kuleas et al. published time lapse recordings showing the migration of neural crest cells *in ovo*.[221,222] It was already published that in the chick, axons of DRG sensory neurons bifurcate during embryogenesis.[223] Our immunohistochemical staining for cGKI in the chick embryo transversal slices revealed the presence of cGKI in neurons residing inside the DRG as well as in their outgrowing axons (see Figure 3-4 A – D). To investigate cGMP signals, embryos were transfected with the CMV-cGi500 plasmid to induce cGi500 expression in DRG neurons. The strategy was to transfect neural crest cells at the dorsal site of the neural tube that will migrate and differentiate into DRG neurons during embryogenesis.[224] As can be seen in Figure 3-4 E, using the before mentioned strategy, cGi500 was successfully expressed in DRGs of the chick (yellow). Acute whole-mount preparations of embryos were used for FRET-based cGMP imaging. Signals were recorded in the DRGs. DEA/NO and CNP induced an increase in cGMP levels (Figure 3-4 F), indicating that cGMP can be generated via NO-GC as well as via GC-B in chick DRG neurons. The presence of a nNOS/NO/NO-GC/cGMP signaling cascade in embryonic chicken DRGs was reported previously by Tojima et al. in 2009 and was shown to be involved in chick DRG axon guidance.[225] But apparently there is nothing known about CNP/GC-B/cGMP signaling in chick DRGs. Taken together, by using FRET-based cGMP imaging in

embryonic chick DRGs, observations of cGMP generation and degradation might be possible *in ovo* while outgrowing DRG axons enter the spinal cord and bifurcate to understand the role of the cGMP signaling cascade in this process.

Another fundamental question is – what are the molecular mechanisms that interplay with cGMP to guide sensory axon bifurcation? The literature describes that there is an interplay of several factors that guide the bifurcation – the so called guidance cues. Cytoplasmic Ca^{2+} was shown to participate in transducing many guidance signals that regulate growth cone motility and steering.[77] In this study, we found that Ca^{2+} is increased in DRG neurons upon application of ACh and ATP. ACh-elevated Ca^{2+} might be regulated via nAChRs and was more prominent in the soma, while ATP-induced Ca^{2+} was possibly mediated via P_2X receptors and was more prominent in the growth cone versus the soma of a DRG neuron (Figure 3-5 A and Figure 3-6 A) but generally both agonists were able to induce Ca^{2+} influx to a certain extent (data not shown). The Ca^{2+} measurements in soma and growth cones were performed in different types of DRG neuron cultures (dissociated and explant culture), which might explain the different response patterns of ACh- *versus* ATP-induced Ca^{2+} influx. The expression of nAChRα7 and P_2X_3 receptors in embryonic DRGs were found in both axons and somata of the cells, which excludes a compartment-specific expression pattern of these receptors.[108,226] Figure 4-1 summarizes the CNP/cGMP/cGKIα signaling cascade in murine DRGs including PDE2 and the newly identified cGMP/Ca^{2+} crosstalk that can be induced by Ach or ATP at soma and growth cone, respectively.

An interesting novel finding was that cGMP interacts with Ca^{2+} in sensory neurons of murine DRGs. In the presence of CNP-induced cGMP, ACh- or ATP-induced Ca^{2+} levels are suppressed. This effect was observed in somata as well as in growth cones of E12.5 DRG sensory neurons (see Figure 3-5 A and B and Figure 3-6 A and B). In the absence of the cGMP downstream target cGKI, the suppressive effect of cGMP on Ca^{2+} was gone, indicating that the mechanism is mediated by cGKI in both compartments of the cell (Figure 3-5 and Figure 3-6). However, the physiological role of this newly identified cGMP/Ca^{2+} crosstalk is not yet clear. It is controversially discussed if an elevation of intracellular Ca^{2+} is related with growth cone attraction or repulsion. In *Xenopus* spinal neurons it was shown that ACh-induced Ca^{2+} influx from the extracellular space led to turning of the growth cone towards the neurotransmitter source indicating that an intracellular Ca^{2+} increase induces growth cone attraction in this model.[95] On the other

hand there is a hypothesis postulating that moderate Ca^{2+} signals promote and initiate growth cone motility and outgrowth while very high or very low Ca^{2+} levels inhibit the motility of a growth cone.[227] Almost 30 years ago, Silver et al. reported that in motile advancing growth cones of a neuroblastoma cell line, intracellular Ca^{2+} levels were low, while high Ca^{2+} levels where found in motile non-advancing growth cones.[228] These results indicate that increases of intracellular Ca^{2+} inhibits neurite outgrowth. Additionally, a further increase of intracellular Ca^{2+} in motile non-advancing growth cones seems to suppress the motility and even leads to retraction of the axon tip towards the cell body.[228]

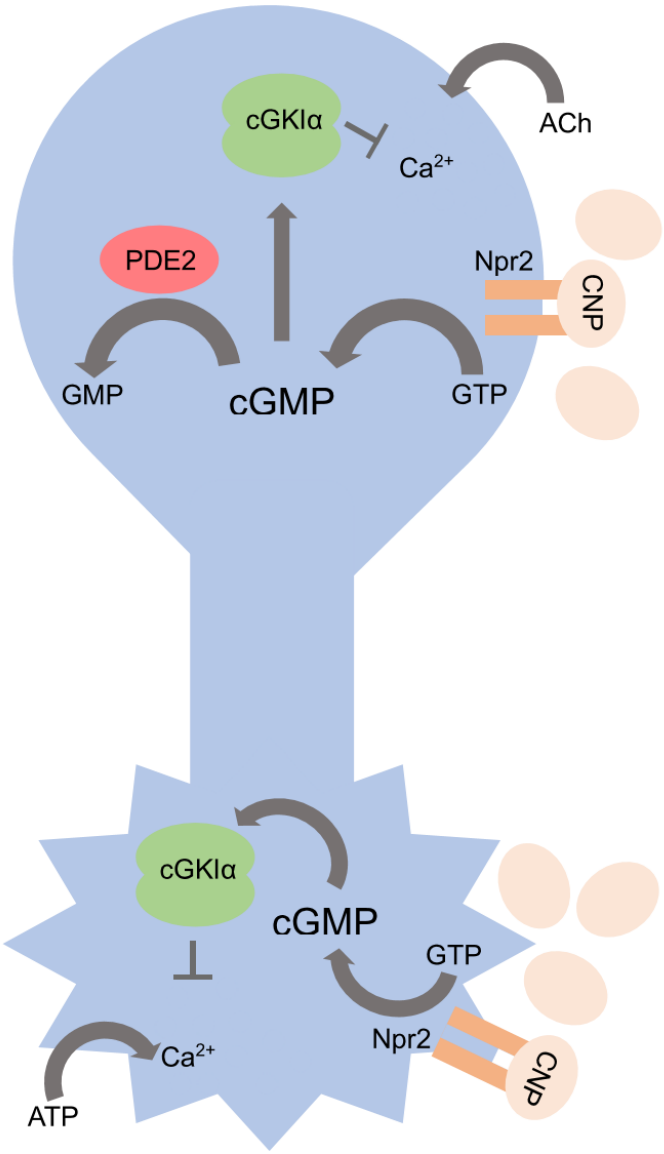

Figure 4-1: Summary of the newly discovered cGMP signaling cascade in DRGs. CNP-induced cGMP is degraded by PDE2. Ach- induced Ca^{2+} levels at the soma as well as ATP-induced Ca^{2+} levels at the growth cone are supressed by CNP-induced cGMP, respectively. This process is regulated by the protein kinase cGKIα.

Another functional role of the newly discovered cGMP/Ca^{2+} pathway might be related to Sema3a-induced growth cone collapse. It is well known that cGMP and its downstream effector cGKI counteract the Sema3a-induced growth cone collapse in murine DRG sensory neurons.[43] Additionally, Treinys and Kaselis et al. found that Sema3a elevates the intracellular Ca^{2+} levels in murine DRG neurons.[229] It might be possible that the molecular mechanism we discovered, connects the two above described signaling pathways. CNP-induced cGMP suppresses Ca^{2+} levels via activation of cGKI. That might mean that a high Ca^{2+} level in the cell during Sema3a-induced growth cone collapse is counteracted by cGMP/cGKI signaling pathway. Anyway, it is already known that the cGMP/cGKIα signaling cascade suppresses Ca^{2+} transients in vascular smooth muscle cells indicating a role in smooth muscle relaxation and vascular tone.[230] However, the above-described mechanisms were found *in vitro*, while the *in vivo* situation might be totally different. Nevertheless, Sema3a plays a very important role in axonal pathfinding in the nervous system, since it was shown that axonal pathfinding was impaired in Sema3a knockout mice.[231]

4.2 Brain region-specific action of IWP-051

The development of new therapeutic drugs or the re-purposing of clinically used drugs is important to treat diseases with poor prognoses. In the past decades, several drugs were developed that affect the cGMP signaling cascade, e.g. PDE inhibitors (Viagra®, Rolipram and others) and NO-GCs stimulators (YC-1, Bay 41-2272, IWP-051). However, the development of drugs to treat diseases of the nervous system is difficult, since drugs have to cross the blood-brain barrier. In this study, the NO-GC stimulator IWP-051 was tested to increase cGMP levels in three different murine brain regions, i.e. cerebellum, striatum, and hippocampus. For comparison, the NO-GC stimulator Bay 41-2272 was used as well. NO is a global messenger in the murine nervous system activating the NO/NO-GC/cGMP cascade. It was already shown by expression studies that the above-mentioned signaling cascade is present in Purkinje cells and granule cells of the cerebellum, as well as in striatal and hippocampal cells.[232-237] By performing FRET-based cGMP imaging, it was shown that the NO donor DEA/NO increased intracellular cGMP levels in Purkinje and granule cells of the cerebellum, as well as in the striatum and the hippocampal CA1 area. Surprisingly, the NO-GC stimulator IWP-051 potentiated NO-induced cGMP signals in the cerebellum and striatum but it failed to potentiate NO-induced cGMP in the hippocampal CA1 area (see Figure 3-7, Figure 3-8, Figure 3-9).

Since it was reported that NO-GC is expressed in the hippocampus and DEA/NO induced cGMP production in the hippocampal CA1 area, it was hypothesized that cGMP levels before application of IWP-051 might have been already too high to allow the potentiation of DEA/NO-induced cGMP by IWP-051. For that reason, the PDE inhibitor IBMX and the NO-GC inhibitor ODQ alone or in combination with DEA/NO were applied to the brain slices (Figure 3-9 D). IBMX alone did not affect the baseline cGMP level, but in combination with the NO-donor DEA/NO it enormously potentiated the DEA/NO-induced signal. These results clearly show that cGMP levels in the absence of IWP-051 were not too high and could be further potentiated. Additionally, ODQ did not lower the basal cGMP level in hippocampal cells indicating that basal cGMP levels were also not too high to be further increased. The functionality of ODQ was tested after it was applied as well as after the IBMX treatment, when DEA/NO was not able to increase cGMP any longer. Taken together, a potential high basal cGMP level in the hippocampus was not the reason for missing activity of IWP-051 in the hippocampus.

Consistent with brain slice imaging data, IWP-051 potentiated DEA/NO-induced cGMP signals in CGNs but not in HNs. In contrast, Bay 41-2272 enhanced DEA/NO-induced cGMP in both, hippocampal brain slices and primary neurons. Interestingly, mRNA expression date revealed that NO-GC2 is mainly expressed in hippocampal CA1 area, while both isoforms were found in cerebellar Purkinje cells and striatum. Based on these data, we hypothesized that IWP-051 preferentially stimulates NO-GC1 (Figure 4-2).

There might be different reasons for the differential ability of IWP-051 to induce cGMP in different brain regions, for example a differential penetration of the compound into different regions of our acute brain slices. This is, however, very unlikely since IWP-051 was not able to induce NO-induced cGMP signals in primary hippocampal neurons anyway. Thus, the easiest explanation for different ability of IWP-051 and Bay 41-2272 to potentiate cGMP in different brain regions would be a NO-GC1 preference of IWP-051, while Bay 41-2272 act on both isoforms. In addition to the stimulation of NO-GC, Bay 41-2272 might be attributable to inhibition of PDE5.[238,239] However, it is not known if IWP-051 significantly inhibits PDE5 or other PDEs.

It is not known if NO-GC isoform specificity of IWP-051 could be achieved at the molecular level, since NO-GC1 and NO-GC2 are structurally similar proteins.[240] Moreover, both stimulators were described to stimulate NO-GCs in a heme-dependent manner.[171,185] Isoform-specific NO-GC modulators have not been reported yet. But in

2022, Giesen et al. showed that NO-GC2 mainly generates NMDA- and AMPA-induced cGMP levels in hippocampus that are controlled by PDE1 and PDE2.[241]

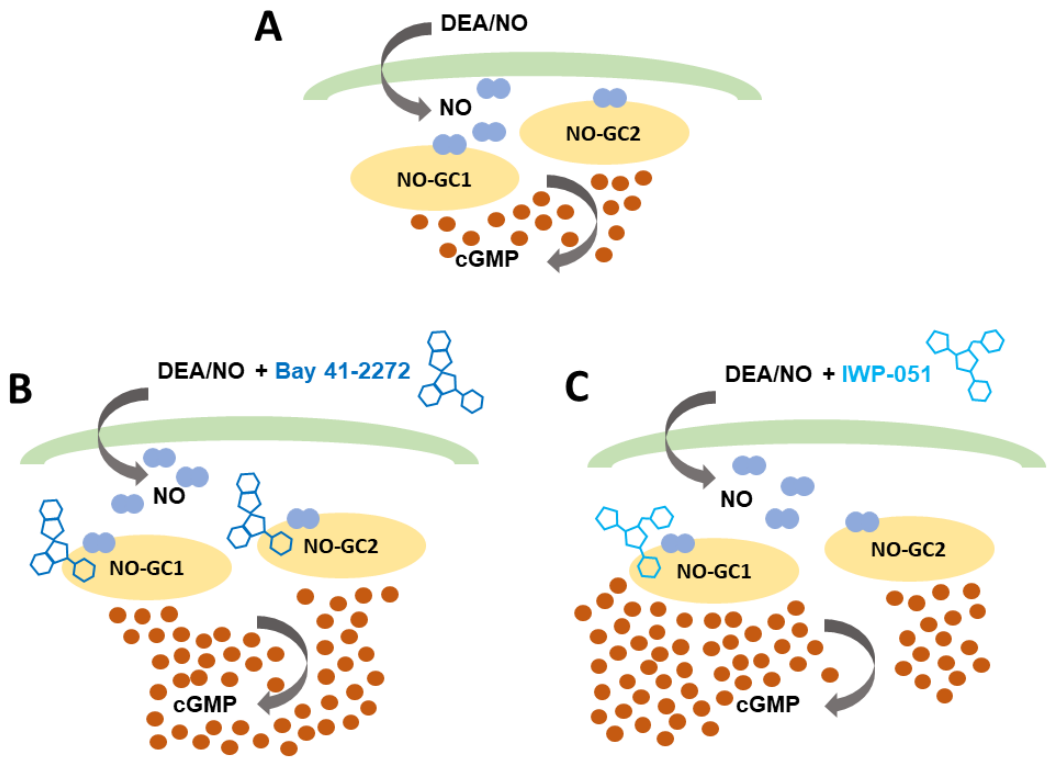

Figure 4-2: NO/NO-GC/cGMP pathway in the mouse brain. (A) NO-induced cGMP is generated by NO-GC1 and/ or NO-GC2, respectively. (B) The stimulator Bay 41-2272 stimulates both NO-GC isoforms synergistically with NO while (C) the stimulator IWP-051 stimulates NO-GC1 synergistically with NO or alone but not NO-GC2.

Strikingly, NO-GC1 is a cytosolic protein, whereas NO-GC2 is membrane-associated.[242] Thus, it could be that IWP-051- preferentially stimulates NO-GC1, while Bay 41-2272 stimulates NO-GC1 and NO-GC2, because of the different subcellular distribution of the compounds. In contrast to Bay 41-2272, IWP-051 might be less distributed to membrane compartments, where NO-GC2 is localized, thus showing a preference for NO-GC1 versus NO-GC2.

Interestingly, another experiment with whole brain homogenates did not show a preference of IWP-051 on NO-GC1. In these *in vitro* assays, [^{32}P] cGMP formation was determined in brain homogenates of wildtype, NO-GC1 and NO-GC2 homogenates after incubation with DEA/NO and both above mentioned stimulators, respectively. The results of the assays showed a similar activity profile of IWP-051 and Bay 41-2272 for both NO-GC isoforms without a NO-GC1-specific activity of IWP-051. But both methods, real time cGMP imaging with our sensor mice and the in vitro assays differ in their

experimental conditions. During FRET-based cGMP imaging, the formation of a specific intact brain area including a largely preserved tissue architecture or a specific intact cell culture, while the *in vitro* cGMP assay was performed with homogenates from the whole brain. Moreover, saturating concentrations of IWP-051 and Bay 41-2272 were used for [^{32}P] cGMP formation in the assay that are 5- to 20-fold higher than the concentration used during FRET-based cGMP imaging of acute brain slices. One could argue, that the isoform-specific activity of IWP-051 got lost at that high concentration. Another difference was that the cGMP measured in brain slices was derived from neuronal/glia cells while whole brain homogenates also contained cerebral blood vessels, which express both NO-GC isoforms.

Taken together, FRET-based cGMP imaging in acute brain slices revealed that the NO-GC stimulators Bay 41-2272 and IWP-051 potentiate NO-induces cGMP in different brain regions. In our study, IWP-051 had a preferential activity on NO-GC1 versus NO-GC2. IWP-051 might be the first NO-GC1-specific modulator acting in an isoform-specific manner, at least in acute brain slices. These results show that IWP-051 or CNS-penetrant derivatives might be interesting drugs to investigate brain functions and diseases. It would be interesting to compare the effect of IWP-051 on cerebellar and striatal functions (e.g. motor learning and reward systems) versus hippocampal functions (e.g. spatial learning). This might be a basis to develop novel brain region-specific drugs for disorders of the nervous system.

5 APPENDIX

5.1 PCR

Table 5-1: Primer sequences.

Primer	Sequence
BB01	CTCTGCTGCCTCCTGGCTTCT
BB02	CGAGGCGGATCACAAGCAATA
BB03	TCAATGGGCGGGGGTCGTT
BB12	ATGACAAATGAGCAGACG
BB13	TCCCGAGATGAAGTAGTTAGT
BB14	TGTAGAAGAGGGGATAGAAAGACC
BB15	TTTGAAATTACTTGGAGATAGA
BB16	AGGTGGGGCTGTCTCTGAA
BB17	AGGTGGGGCTGTCTCTGAA
BB18	GGGGGCCCTGACATTTGA
Cre800	GCTGCCACGACCAAGTGACAGCAATG
Cre1200	GTAGTTATTCGGATCATCAGCTACAC
RF53	CCTGGCTGTGATTTCACTCCA
RF118	AAATTATAACTTGTCAAATTCTTG
RF125	GTCAAGTGACCACTATG

Table 5-2: PCR conditions.

PCR	Primer	Conditions		
cGKI	RF53 RF118 RF125	95 °C	5 min	
		95 °C	10 sec	35x
		50 °C	30 sec	
		72 °C	30 sec	
		72 °C	5 min	
Cre	Cre800 Cre1200	95 °C	5 min	
		95 °C	10 sec	35x
		58 °C	30 sec	
		72 °C	30 sec	
		72 °C	5 min	
R26-cGi500(L1) and R26-mT/cGi500(L2)	BB01 BB02 BB03	95 °C	5 min	
		95 °C	10 sec	35x
		61 °C	30 sec	
		72 °C	30 sec	
		72 °C	5 min	
sGCα1	BB12 BB13	94 °C	3 min	
		94 °C	30 sec	

	BB14	58 °C	60 sec	30x
		72 °C	60 sec	
		72 °C	7 min	
sGCα2 wt allele	BB15 BB16	94 °C	3 min	
		94 °C	30 sec	30x
		55 °C	60 sec	
		72 °C	60 sec	
		72 °C	7 min	
sGCα2 KO allele	BB17 BB18	94 °C	3 min	
		94 °C	30 sec	30x
		61 °C	60 sec	
		72 °C	60 sec	
		72 °C	7 min	

5.2 Antibodies

Table 5-3: List of primary antibodies for immunohistochemistry.

Antibody	origin	Dilution	company	storage
βIII-tubulin (monoclonal, TUJ1)	Mouse	1:500	Covance	4 °C
cGKIc (DH) (polyclonal)	Rabbit	1:1000	Homemade by Feil lab	-20 °C
RMO	Mouse	1:500	Zymed/Invitrogen	-20 °C

Table 5-4: List of secondary antibodies for immunohistochemistry.

Antibody	origin	Dilution	company	storage
Anti-mouse Alexa488	Goat	1:500	Invitrogen	4 °C
Anti-mouse Alexa555	Goat	1:500	Invitrogen	4 °C
Anti-rabbit Alexa488	Goat	1:500	Invitrogen	4 °C
Anti-rabbit Alexa555	Goat	1:500	Invitrogen	4 °C

6 LITERATURE

1. Feil, R. & Kemp-Harper, B. cGMP signalling: from bench to bedside. *EMBO Rep.* **7**, 149–153 (2006).

2. Kemp-Harper, B. & Feil, R. cGMP matters. **1**, 1–7 (2008).

3. Friebe, A. & Koesling, D. The function of NO-sensitive guanylyl cyclase: What we can learn from genetic mouse models. *Nitric Oxide* **21**, 149–156 (2009).

4. Kuhn, M. Molecular Physiology of membrane guanylyl cyclase receptors. *Physiol. Rev.* **96**, 751–804 (2016).

5. Nathan, C. & Xie, Q. Nitric oxide synthases: Roles, tolls, and controls. *Cell* **78**, 915–918 (1994).

6. Krumenacker, J. S., Hanafy, K. A. & Murad, F. Regulation of nitric oxide and soluble guanylyl cyclase. *Brain Res. Bull.* **62**, 505–515 (2004).

7. Kone, B. C. Molecular biology of natriuretic peptides and nitric oxide synthases. *Cardiovasc. Res.* **51**, (2001).

8. Yuen, P. S. T., Potter, L. R. & Garbers, D. L. A new form of guanylyl cyclase is preferentially expressed in rat kidney. *Biochemistry* **29**, 10872–10878 (1990).

9. Budworth, J., Meillerais, S., Charles, I. & Powell, K. Tissue distribution of the human soluble guanylate cyclases. *Biochem. Biophys. Res. Commun.* **263**, 696–701 (1999).

10. Pyriochou, A. & Papapetropoulos, A. Soluble guanylyl cyclase: more secrets revealed. *Cell. Signal.* **17**, 407–413 (2005).

11. Schmidt, P. M., Schramm, M., Schröder, H., Wunder, F. & Stasch, J.-P. Identification of residues crucially involved in the binding of the heme moiety of soluble guanylate cyclase. *J. Biol. Chem.* **279**, 3025–32 (2004).

12. Kobiałka, M. & Gorczyca, W. A. Particulate guanylyl cyclases: multiple mechanisms of activation. *Acta Biochim. Pol.* **47**, 517–28 (2000).

13. Schulz, S., Green, C. K., Yuen, P. S. & Garbers, D. L. Guanylyl cyclase is a heat-

stable enterotoxin receptor. *Cell* **63**, 941–8 (1990).

14. Currie, M. G., Fok, K. F., Kato, J., Moore, R. J., Hamra, F. K., Duffin, K. L., Smith, C. E. Guanylin: an endogenous activator of intestinal guanylate cyclase. *Proc. Natl. Acad. Sci. U. S. A.* **89**, 947–51 (1992).

15. Hamra, F. K., Forte L. R., Eber, S. L., Pidhorodeckyj, N. V., Krause, W. J., Freeman, R. H., Chin, D. T., Tompkins, J. A., Fok, K. F., Smith, C. E. Uroguanylin: structure and activity of a second endogenous peptide that stimulates intestinal guanylate cyclase. *Proc. Natl. Acad. Sci. U. S. A.* **90**, 10464–8 (1993).

16. Paula M. B., Smirnov D., Smolenski A., Feil, S., Feil, R., Hofmann, F., Lohmann, S., Potter, L. R. A. A Sensitive method for determining the phosphorylation status of natriuretic peptide receptors: cGK-Iα does not regulate NPR-A. (2006).

17. Oliver, P. M., Fox, J. E., Kim, R., Rockman, H. A., Kin, H. S., Reddick, R. L., Pandey, K. N., Milgram, S. L., Smithies, O., Maeda, N. Hypertension, cardiac hypertrophy, and sudden death in mice lacking natriuretic peptide receptor A. *Proc. Natl. Acad. Sci. U. S. A.* **94**, 14730–5 (1997).

18. John, S. W., Krege, H. H., Oliver, P. M., Hagamaan, J. R., Hodgin, J. B., Pang, S. C., Flynn, T. G., Smithies, O. Genetic decreases in atrial natriuretic peptide and salt-sensitive hypertension. *Science (80-.).* **267**, (1995).

19. John, S. W., Veress, A. T., Honrath, U., Chong, C. K., Peng, L., Smithies, O., Sonnenberg, H., Blood pressure and fluid-electrolyte balance in mice with reduced or absent ANP. *Am. J. Physiol.* **271**, R109-14 (1996).

20. Tamura, N., Ogawa, Y., Chusho, H., Nakamura, K., Nakao, K., Suda, M., Kashara, M., Hashimoto, R., Katsuura, G., Mukoyama, M., Itoh, H., Saito, Y., Tanaka, I., Otani, H., Katsuki, M., Cardiac fibrosis in mice lacking brain natriuretic peptide. *Proc. Natl. Acad. Sci. U. S. A.* **97**, 4239–44 (2000).

21. Potter, L. R. Guanylyl cyclase structure, function and regulation. *Cell. Signal.* **23**, 1921–6 (2011).

22. Nagase, M., Katafuchi, T., Hirose, S., Fujita, T. Tissue distribution and

localization of natriuretic peptide receptor subtypes in stroke-prone spontaneously hypertensive rats. *J. Hypertens.* **15**, 1235–43 (1997).

23. Friebe, A., Sandner, P., Seifert, R. From bedside to bench—meeting report of the 7th International Conference on cGMP "cGMP: generators, effectors and therapeutic implications" in Trier, Germany, from June 19th to 21st 2015. *Naunyn. Schmiedebergs. Arch. Pharmacol.* **388**, 1237–1246 (2015).

24. Weber, I. T., Gilliland, G. L., Harman, J. G., Peterkofsky, A. Crystal structure of a cyclic AMP-independent mutant of catabolite gene activator protein. *J. Biol. Chem.* **262**, 5630–6 (1987).

25. Shabb, J. B. & Corbin, J. D. Cyclic nucleotide-binding domains in proteins having diverse functions. *J. Biol. Chem.* **267**, 5723–6 (1992).

26. Biel, M. & Michalakis, S. Cyclic nucleotide-gated channels. in cGMP: generators, effectors and therapeutic implication*s* 111–136 (Springer Berlin Heidelberg, (2009).

27. Yu, F. H., Yarov-Yarovoy, V., Gutman, G. A. & Catterall, W. A. Overview of molecular relationships in the voltage-gated ion channel superfamily. *Pharmacol. Rev.* **57**, 387–395 (2005).

28. Kaupp, U. B. & Seifert, R. Cyclic nucleotide-gated ion channels. *Physiol. Rev.* **82**, 769–824 (2002).

29. Brown, H. & Difrancesco, D. Voltage-clamp investigations of membrane currents underlying pace-maker activity in rabbit sino-atrial node. *J. Physiol.* **308**, 331–51 (1980).

30. Mistrík, P., Mader, R., Michalakis, S., Weidinger, M., Pfeifer, A., Biel, M. The murine HCN3 gene encodes a hyperpolarization-activated cation channel with slow kinetics and unique response to cyclic nucleotides. *J. Biol. Chem.* **280**, 27056–61 (2005).

31. Stieber, J., Stockl, G., Herrmann, S., Hassfurth, B. & Hofmann, F. Functional expression of the human HCN3 channel. *J. Biol. Chem.* **280**, 34635–34643 (2005).

32. Wahl-Schott, C., Fenske, S. & Biel, M. HCN channels: new roles in sinoatrial node function. *Curr. Opin. Pharmacol.* **15**, 83–90 (2014).

33. Fenske, S., Mader, R., Scharr, A.., Paparizos, C., Cao.Ehlker, X., Michalakis, S., Shaltiel, L., Weidinge, M., Stieber, J., Feil, S., Feil, R., Hofmann, F., Wahl-Schott, C., Biel, M. *et al.* HCN3 contributes to the ventricular action potential waveform in the murine heart. Novelty and significance. *Circ. Res.* **109**, (2011).

34. Combe CL, G. S. Ih from synapses to networks: HCN channel functions and modulation in neurons. *Prog Biophys Mol Biol.* **166**, 119–132 (2021).

35. He JT, Li XY, Zhao X, L. X. Hyperpolarization-activated and cyclic nucleotide-gated channel proteins as emerging new targets in neuropathic pain. *Rev Neurosci* **30**, 639–649 (2019).

36. Francis, S. H. & Corbin, J. D. Cyclic nucleotide-dependent protein kinases: intracellular receptors for cAMP and cGMP action. *Crit. Rev. Clin. Lab. Sci.* **36**, 275–328 (1999).

37. Pfeifer, A., Ruth, P., Dostmann, W., Sausbier, M., Klatt, P., Hofmann, F. Structure and function of cGMP-dependent protein kinases. in *Reviews of Physiology, Biochemistry and Pharmacology, Volume 135* 105–149 (Springer-Verlag, 1999). doi:10.1007/BFb0033671

38. Hofmann, F., Gensheimer, H.-P., Göbel, C. cGMP-dependent protein kinase. Autophosphorylation changes the characteristics of binding site 1. *Eur. J. Biochem.* **147**, 361–365 (1985).

39. Hofmann, F., Bernhard, D., Lukowski, R. & Weinmeister, P. cGMP regulated protein kinases (cGK). in *cGMP: Generators, Effectors and Therapeutic Implications* 137–162 (Springer Berlin Heidelberg, 2009). doi:10.1007/978-3-540-68964-5_8

40. Feil, S., Zimmermann, P., Norn, A., Brummer, S., Schlossmann, J., Hofmann, F., Feil, R. Distribution of cGMP-dependent protein kinase type I and its isoforms in the mouse brain and retina. *Neuroscience* **135**, 863–868 (2005).

41. Keilbach, A., Ruth, P. & Hofmann, F. Detection of cGMP dependent protein kinase isozymes by specific antibodies. *Eur. J. Biochem.* **208**, 467–73 (1992).

42. Weber, S., Bernhard, D., Lukowski, R., Weinmeister, P., Wörner, R., Wegener, J. W., Valtcheva, N., Feil, S., Schlossmann, J., Hofmann, F., Feil, R. Rescue of cGMP kinase I knockout mice by smooth muscle–specific expression of either isozyme. *Circ. Res.* **101**, (2007).

43. Schmidt, H., Werner, M., Heppenstall, P. A., Henning, M., More, M. I., Kühbandner, S., Lewin, G. R., Hofmann, F., Feil, R., Rathjen, F. G. cGMP-mediated signaling via cGKIalpha is required for the guidance and connectivity of sensory axons. *J. Cell Biol.* **159**, 489–98 (2002).

44. Lohmann, S. M., Vaandrager, A. B., Smolenski, A., Walter, U., De Jonge, H. R. Distinct and specific functions of cGMP-dependent protein kinases. *Trends Biochem. Sci.* **22**, 307–312 (1997).

45. De Vente, J., Asan, E., Gambaryan, S., Markerink-van Ittersum, M., Axer, H., Gallatz, K., Lohmann, S. M., Palkovits, M. Localization of cGMP-dependent protein kinase type II in rat brain. *Neuroscience* **108**, 27–49 (2001).

46. Koeppen, M. Feil, R., Siegl, D., Feil, S., Hofmann, F., Pohl, U., de Wit, C. cGMP-dependent protein kinase mediates NO- but not acetylcholine-induced dilations in resistance vessels in vivo. *Hypertension* **44**, (2004).

47. Pfeifer, A., Klatt, P., Massberg, S., Ny, L., Sausbier, M., Hirneiss, C., Wang, G. X., Korth, M., Aszodi, A., Andersson, K. E., Krombach, F., Mayerhofer, A., Ruth, P., Fässler, R., Hofmann, F. Defective smooth muscle regulation in cGMP kinase I-deficient mice. *EMBO J.* **17**, 3045–51 (1998).

48. Francis, S. H., Turko, I. V & Corbin, J. D. Cyclic nucleotide phosphodiesterases: relating structure and function. *Prog. Nucleic Acid Res. Mol. Biol.* **65**, 1–52 (2001).

49. Beavo, J. A. & Reifsnyder, D. H. Primary sequence of cyclic nucleotide phosphodiesterase isozymes and the design of selective inhibitors. *Trends Pharmacol. Sci.* **11**, 150–155 (1990).

50. Conti, M. & Beavo, J. Biochemistry and physiology of cyclic nucleotide phosphodiesterases: essential components in cyclic nucleotide signaling. *Annu. Rev. Biochem.* **76**, 481–511 (2007).

51. Francis, S. H., Corbin, J. D. & Bischoff, E. Cyclic GMP-hydrolyzing phosphodiesterases. in *cGMP: Generators, Effectors and Therapeutic Implications* 367–408 (Springer Berlin Heidelberg, 2009). doi:10.1007/978-3-540-68964-5_16

52. Rybalkin, S. D., Rybalkina, I. G., Feil, R., Hofmann, F. & Beavo, J. A. Regulation of cGMP-specific phosphodiesterase (PDE5) phosphorylation in smooth muscle cells. *J. Biol. Chem.* **277**, 3310–3317 (2002).

53. Shimizu-Albergine, M., Rybalkin, S. D., Rybalkina, I. G., Feil, R., Wolfsgruber, W., Hofmann, F., Beavo, J. A. Individual cerebellar Purkinje cells express different cGMP phosphodiesterases (PDEs): in vivo phosphorylation of cGMP-specific PDE (PDE5) as an indicator of cGMP-dependent protein kinase (PKG) activation. *J. Neurosci.* **23**, 6452–9 (2003).

54. Gross-Langenhoff, M., Hofbauer, K., Weber, J., Schultz, A. & Schultz, J. E. cAMP is a ligand for the tandem GAF domain of human phosphodiesterase 10 and cGMP for the tandem GAF domain of phosphodiesterase 11. *J. Biol. Chem.* **281**, 2841–2846 (2005).

55. Ahimsadasan N, Reddy V, Khan Suheb MZ, K. A. Neuroanatomy, dorsal root ganglion. *StatPearls Publ.* (2023).

56. Schmidt, H. & Rathjen, F. G. Signalling mechanisms regulating axonal branching in vivo. *Bioessays* **32**, 977–85 (2010).

57. Schmidt, H. & Rathjen, F. G. DiI-labeling of DRG neurons to study axonal branching in a whole mount preparation of mouse embryonic spinal cord. *J. Vis. Exp.* (2011). doi:10.3791/3667

58. McCormick, A. M., Jarmusik, N. A. & Leipzig, N. D. Co-immobilization of semaphorin3A and nerve growth factor to guide and pattern axons. *Acta Biomater.* **28**, 33–44 (2015).

59. Dickson, B. J. Molecular mechanisms of axon guidance. *Science (80-.).* **298**, (2002).

60. Acebes, A. & Ferrús, A. Cellular and molecular features of axon collaterals and dendrites. *Trends Neurosci.* **23**, 557–565 (2000).

61. Bastmeyer, M. & O'Leary, D. Dynamics of target recognition by interstitial axon branching along developing cortical axons. *J. Neurosci.* **16**, (1996).

62. Ozaki, S. & Snider, W. D. Initial trajectories of sensory axons toward laminar targets in the developing mouse spinal cord. *J. Comp. Neurol.* **380**, 215–29 (1997).

63. Mirnics, K. & Koerber, H. R. Prenatal development of rat primary afferent fibers: II. Central projections. *J. Comp. Neurol.* **355**, 601–14 (1995).

64. Gibson, D. A. & Ma, L. Developmental regulation of axon branching in the vertebrate nervous system. *Development* **138**, (2010).

65. Schmidt, H., Stonkute, A., Jüttner, R., Schäffer, S., Buttgereit, J., Feil, R., Hofmann, F., Rathjen, F. G. The receptor guanylyl cyclase Npr2 is essential for sensory axon bifurcation within the spinal cord. *J. Cell Biol.* **179**, 331–40 (2007).

66. Schmidt, H., Stonkute, A., Jüttner, R., Koesling, D., Friebe, A., Rathjen, F. G. C-type natriuretic peptide (CNP) is a bifurcation factor for sensory neurons. *Proc. Natl. Acad. Sci. U. S. A.* **106**, 16847–52 (2009).

67. Zhao, Z. & Ma, L. Regulation of axonal development by natriuretic peptide hormones. *Proc. Natl. Acad. Sci. U. S. A.* **106**, 18016–21 (2009).

68. Kennedy, T. E., Serafini, T., Ft de la forre, J., Lessier-Lavigne, M. Netrins are diffusible chemotropic factors for commissural axons in the embryonic spinal cord. *Cell* **79**, 425–435 (1994).

69. Masuda, T., Yaginuma, H., Sakuma, C. & Ono, K. Netrin-1 signaling for sensory axons: Involvement in sensory axonal development and regeneration. *Cell Adh. Migr.* **3**, 171–3 (2009).

70. Masuda, T., Sakuma, C., Ikenaka, K., Katsuhiko, O., Yaginuma, H. Netrin-1 acts as a repulsive guidance cue for sensory axonal projections toward the spinal cord. *J. Neurosci.* **28**, (2008).

71. Brose, K., Bland, K. S., Wang, K. H., Arnott, D., Henzel, W., Goodman, C. S., Tessier-Lavigne, M., Kidd, T. Slit proteins bind Robo receptors and have an evolutionarily conserved role in repulsive axon guidance. *Cell* **96**, 795–806

(1999).

72. Wang, K. H., Brose, K., Arnott, D., Kidd, T., Goodman, C. S., Henzel, W., Tessier-Lavigne, M. Biochemical purification of a mammalian slit protein as a positive regulator of sensory axon elongation and branching. *Cell* **96**, 771–784 (1999).

73. Luo, Y., Raible, D. & Raper, J. A. Collapsin: A protein in brain that induces the collapse and paralysis of neuronal growth cones. *Cell* **75**, 217–227 (1993).

74. Song, H., Ming, G., He, Z., Lehmann, M., McKerracher, L., Tessier-Lavigne, M., Poo, M. Conversion of neuronal growth cone responses from repulsion to attraction by cyclic nucleotides. *Science* **281**, 1515–8 (1998).

75. Brown, J. A., Wysolmerski, R. B. & Bridgman, P. C. Dorsal root ganglion neurons react to semaphorin 3A application through a biphasic response that requires multiple myosin II isoforms. *Mol. Biol. Cell* **20**, 1167–79 (2009).

76. Kennedy, T. E., Wang, H., Marshall, W. & Tessier-Lavigne, M. Axon guidance by diffusible chemoattractants: A gradient of netrin protein in the developing spinal cord. *J. Neurosci.* **26**, (2006).

77. Tojima, T., Hines, J. H., Henley, J. R. & Kamiguchi, H. Second messengers and membrane trafficking direct and organize growth cone steering. *Nat. Rev. Neurosci.* **12**, 191–203 (2011).

78. Hong, K., Nishiyama, M., Henley, J., Tessier-Lavigne, M., Poo, M. Calcium signalling in the guidance of nerve growth by netrin-1. *Nature* **403**, 93–98 (2000).

79. Akiyama, H., Matsu-ura, T., Mikoshiba, K. & Kamiguchi, H. Control of Neuronal growth cone navigation by asymmetric inositol 1,4,5-trisphosphate signals. *Sci. Signal.* **2**, (2009).

80. Henley, J. R., Huang, K., Wang, D., Poo, M. Calcium mediates bidirectional growth cone turning induced by myelin-associated glycoprotein. *Neuron* **44**, 909–916 (2004).

81. Ooashi, N., Futatsugi, A., Yoshihara, F., Mikoshiba, K., Kamiguchi, H. Cell

adhesion molecules regulate Ca2+-mediated steering of growth cones via cyclic AMP and ryanodine receptor type 3. *J. Cell Biol.* **170**, (2005).

82. Rukwied, R. & Heyer, G. Administration of acetylcholine and vasoactive intestinal polypeptide to atopic eczema patients. *Exp. Dermatol.* **8**, 39–45 (1999).

83. Bernardini, N., Sauer, S. K., Haberberger, R., Fischer, M. J. M. & Reeh, P. W. Excitatory nicotinic and desensitizing muscarinic (M2) effects on C-nociceptors in isolated rat skin. *J. Neurosci.* **21**, (2001).

84. Caulfield, M. P. & Birdsall, N. J. International Union of Pharmacology. XVII. Classification of muscarinic acetylcholine receptors. *Pharmacol. Rev.* **50**, 279–90 (1998).

85. Nandigama, R., Bonitz, M., Papadakis, T., Schwantes, U., Bschleipfer, T., Kummer, W. Muscarinic acetylcholine receptor subtypes expressed by mouse bladder afferent neurons. *Neuroscience* **168**, 842–850 (2010).

86. Chen, S.-R., Wess, J. & Pan, H.-L. Functional activity of the M2 and M4 receptor subtypes in the spinal cord studied with muscarinic acetylcholine receptor knockout mice. *J. Pharmacol. Exp. Ther.* **313**, 765–770 (2004).

87. Höglund, A. U. & Baghdoyan, H. A. M2, M3 and M4, but not M1, muscarinic receptor subtypes are present in rat spinal cord. *J. Pharmacol. Exp. Ther.* **281**, 470–7 (1997).

88. Cai, Y.-Q. *et al.* Role of M2, M3, and M4 muscarinic receptor subtypes in the spinal cholinergic control of nociception revealed using siRNA in rats. *J. Neurochem.* **111**, 1000–10 (2009).

89. Honda, K., Harada, A., Takano, Y. & Kamiya, H. Involvement of M3 muscarinic receptors of the spinal cord in formalin-induced nociception in mice. *Brain Res.* **859**, 38–44 (2000).

90. Iwamoto, E. T. & Marion, L. Characterization of the antinociception produced by intrathecally administered muscarinic agonists in rats. *J. Pharmacol. Exp. Ther.* **266**, 329–38 (1993).

91. Steen, K. H. & Reeh, P. W. Actions of cholinergic agonists and antagonists on

sensory nerve endings in rat skin, in vitro. *J. Neurophysiol.* **70**, (1993).

92. Rueter, L. E., Kohlhaas, K. L., Curzon, P., Surowy, C. S. & Meyer, M. D. Peripheral and central sites of action for A-85380 in the spinal nerve ligation model of neuropathic pain. *Pain* **103**, 269–276 (2003).

93. Lukas, R. J., Changeux, J. P., Le Novere, N., Albuquerque, E. X., Balfour, D. J., Berg, D. K., Bertrand, D., Chiappinelli, V. A., Clarke, P. B., Collins, A. C., Dani, J. A., Grady, S. R., Kellar, K. J., Lindstrom, J. M., Marks, M. J., Quik, M., Taylor, P. W., Wonnacott, S. International Union of Pharmacology. XX. Current status of the nomenclature for nicotinic acetylcholine receptors and their subunits. *Pharmacol. Rev.* **51**, (1999).

94. Genzen, J. R., Van Cleve, W., McGehee, D. S. Dorsal root ganglion neurons express multiple nicotinic acetylcholine receptor subtypes. *J. Neurophysiol.* **86**, (2001).

95. Zheng, J. Q., Felder, M., Connor, J. A. & Poo, M. Turning of nerve growth cones induced by neurotransmitters. *Nature* **368**, 140–144 (1994).

96. Zhong, L. R., Estes, S., Artinian, L. & Rehder, V. Acetylcholine elongates neuronal growth cone filopodia via activation of nicotinic acetylcholine receptors. *Dev. Neurobiol.* **73**, 487–501 (2013).

97. Hanson, M. G. & Landmesser, L. T. Characterization of the circuits that generate spontaneous episodes of activity in the early embryonic mouse spinal cord. *J. Neurosci.* **23**, (2003).

98. Burnstock, G. P2X receptors in sensory neurones. *Br. J. Anaesth.* **84**, 476–88 (2000).

99. Kobayashi, K., Yamanaka, H. & Noguchi, K. Expression of ATP receptors in the rat dorsal root ganglion and spinal cord. *Anat. Sci. Int.* **88**, 10–16 (2013).

100. Burnstock, G. Purine and pyrimidine receptors. *Cell. Mol. Life Sci.* **64**, 1471–1483 (2007).

101. Fischer, W. & Krügel, U. P2Y receptors: focus on structural, pharmacological and functional aspects in the brain. *Curr. Med. Chem.* **14**, 2429–55 (2007).

102. Torres, G. E., Egan, T. M. & Voigt, M. M. Hetero-oligomeric assembly of P2X receptor subunits. Specificities exist with regard to possible partners. *J. Biol. Chem.* **274**, 6653–9 (1999).

103. Collier, H. O., James, G. W. & Schneider, C. Antagonism by aspirin and fenamates of bronchoconstriction and nociception induced by adenosine-5'-triphosphate. *Nature* **212**, 411–2 (1966).

104. Jahr, C. E. & Jessell, T. M. ATP excites a subpopulation of rat dorsal horn neurones. *Nature* **304**, 730–3

105. Shieh, C.-C., Jarvis, M. F., Lee, C.-H. & Perner, R. J. P2X receptor ligands and pain. *Expert Opin. Ther. Pat.* **16**, 1113–1127 (2006).

106. Kobayashi, K., Fukuoka, T., Yamanaka, H., Dai, Y., Obata, K., Tokunaga, A., Noguchi, K. Differential expression patterns of mRNAs for P2X receptor subunits in neurochemically characterized dorsal root ganglion neurons in the rat. *J. Comp. Neurol.* **481**, 377–390 (2005).

107. Kobayashi, K., Fukuoka, T., Yamanaka, H., Dai, Y., Koichi, O., Tokunaga, A., Noguchi, K. Neurons and glial cells differentially express P2Y receptor mRNAs in the rat dorsal root ganglion and spinal cord. *J. Comp. Neurol.* **498**, 443–454 (2006).

108. Boldogköi, Z., Schütz, B., Sallach, J. & Zimmer, A. P2X3 receptor expression at early stage of mouse embryogenesis. *Mechanisms of Development* **118**, (2002).

109. Sanderson, T. M. & Sher, E. The role of phosphodiesterases in hippocampal synaptic plasticity. *Neuropharmacology* **74**, 86–95 (2013).

110. Kleppisch, T. & Feil, R. cGMP signalling in the mammalian brain: role in synaptic plasticity and behaviour. *Handb. Exp. Pharmacol.* 549–79 (2009).

111. Ito, M. Cerebellar long-term depression: characterization, signal transduction, and functional roles. *Physiol. Rev.* **81**, (2001).

112. Ito, M. Historical review of the significance of the cerebellum and the role of Purkinje cells in motor learning. *Ann. N. Y. Acad. Sci.* **978**, 273–288 (2002).

113. Manahan-Vaughan, D. & Braunewell, K. H. Novelty acquisition is associated

with induction of hippocampal long-term depression. *Proc. Natl. Acad. Sci. U. S. A.* **96**, 8739–44 (1999).

114. Shinnick-Gallagher, P. & McKernan, M. G. Fear conditioning induces a lasting potentiation of synaptic currents in vitro. *Nature* **390**, 607–611 (1997).

115. Sigurdsson, T., Doyère, V., Cain, C. K. & LeDoux, J. E. Long-term potentiation in the amygdala: A cellular mechanism of fear learning and memory. *Neuropharmacology* **52**, 215–227 (2007).

116. Rogan, M. T., Stäubli, U. V., LeDoux, J. E. Fear conditioning induces associative long-term potentiation in the amygdala. *Nature* **390**, 604–607 (1997).

117. Bird, C. M. & Burgess, N. The hippocampus and memory: insights from spatial processing. *Nat. Rev. Neurosci.* **9**, 182–194 (2008).

118. Amaral, D. G. & Witter, M. P. The three-dimensional organization of the hippocampal formation: A review of anatomical data. *Neuroscience* **31**, 571–591 (1989).

119. Lisman, J. & Raghavachari, S. A Unified model of the presynaptic and postsynaptic changes during LTP at CA1 synapses. *Sci. Signal.* **2006**, (2006).

120. Arancio, O., Kiebler, M., Lee, C. J., Lev-Ram, V., Tsien, R. Y., Kandel, E. R., Hawkins, R. D. Nitric oxide acts directly in the presynaptic neuron to produce long-term potentiationin cultured hippocampal neurons. *Cell* **87**, 1025–1035 (1996).

121. Arancio, O., Kandel, E. R. & Hawkins, R. D. Activity-dependent long-term enhancement of transmitter release by presynaptic 3′,5′-cyclic GMP in cultured hippocampal neurons. *Nature* **376**, 74–80 (1995).

122. Arancio, O., Antanova, I., Gambarayan, S., Lohmann, S. M., Wood, J. S., Lawrence, D. S., Hawkins, R. D. Presynaptic Role of cGMP-dependent protein kinase during long-lasting potentiation. *J. Neurosci.* **21**, (2001).

123. Zhuo, M., Hu, Y., Schultz, C., Kandel, E. R., Hawkins, R. D. Role of guanylyl cyclase and cGMP-dependent protein kinase in long-term potentiation. *Nature* **368**, 635–639 (1994).

124. Reyes-Harde, M., Empson, R., Potter, B. V, Galione, A., Stanton, P. K. Evidence of a role for cyclic ADP-ribose in long-term synaptic depression in hippocampus. *Proc. Natl. Acad. Sci. U. S. A.* **96**, 4061–6 (1999).

125. Reyes-Harde, M., Potter, B. V. L., Galione, A. & Stanton, P. K. Induction of hippocampal LTD requires nitric-oxide-stimulated PKG activity and Ca2+ release from cyclic ADP-ribose-sensitive stores. *J. Neurophysiol.* **82**, (1999).

126. Hashimoto, M. & Hibi, M. Development and evolution of cerebellar neural circuits. *Dev. Growth Differ.* **54**, 373–389 (2012).

127. Ito, M. Control of mental activities by internal models in the cerebellum. *Nat. Rev. Neurosci.* **9**, 304–313 (2008).

128. Lainé, J. & Axelrad, H. The candelabrum cell: A new interneuron in the cerebellar cortex. *J. Comp. Neurol.* **339**, 159–173 (1994).

129. Voogd, J. & Glickstein, M. The anatomy of the cerebellum. *Trends Neurosci.* **21**, 370–375 (1998).

130. Feil, R., Hartmann, J., Luo, C., Wolfsgruber, W., Schilling, K., Feil, S., Barski, J. J., Meyer, M., Konnerth, A., I De Zeeuw, C., Hofmann, F. Impairment of LTD and cerebellar learning by Purkinje cell-specific ablation of cGMP-dependent protein kinase I. *J. Cell Biol.* **163**, 295–302 (2003).

131. Lohmann, S. M., Walter, U., Miller, P. E., Greengard, P. & De Camilli, P. Immunohistochemical localization of cyclic GMP-dependent protein kinase in mammalian brain. *Proc. Natl. Acad. Sci. U. S. A.* **78**, 653–7 (1981).

132. Lev-Ram, V., Jiang, T., Wood, J., Lawrence, D. S., Tsien, R. Y. Synergies and coincidence requirements between NO, cGMP, and Ca2+ in the induction of cerebellar long-term depression. *Neuron* **18**, 1025–38 (1997).

133. Kawaguchi, Y., Wilson, C. J., Augood, S. J. & Emson, P. C. Striatal interneurones: chemical, physiological and morphological characterization. *Trends Neurosci.* **18**, 527–35 (1995).

134. Tepper, J. M. & Bolam, J. P. Functional diversity and specificity of neostriatal interneurons. *Curr. Opin. Neurobiol.* **14**, 685–692 (2004).

135. Zhou, F.-M., Wilson, C. J., Dani, J. A. Cholinergic interneuron characteristics and nicotinic properties in the striatum. *J. Neurobiol.* **53**, 590–605 (2002).

136. Kreitzer, A. C. & Malenka, R. C. Striatal plasticity and basal ganglia circuit function. *Neuron* **60**, 543–54 (2008).

137. Centonze, D., Picconi, B., Gubellini, P., Bernardi, G. & Calabresi, P. Dopaminergic control of synaptic plasticity in the dorsal striatum. *Eur. J. Neurosci.* **13**, 1071–1077 (2001).

138. Calabresi, P., Centonze, D., Gubellini, P., Marfia, G. A., Pisani, G., Sancesario, G., Bernardi, G. Synaptic transmission in the striatum: from plasticity to neurodegeneration. *Prog. Neurobiol.* **61**, 231–265 (2000).

139. Centonze, D., Gubellini, P., Pisani, A., Bernardi, G., Calabresi, P. Dopamine, acetylcholine and nitric oxide systems interact to induce corticostriatal synaptic plasticity. *Rev. Neurosci.* **14**, 207–16 (2003).

140. Chepkova, A. N., Schönfeld, S., Sergeeva, O. A. Age-related alterations in the expression of genes and synaptic plasticity associated with nitric oxide signaling in the mouse dorsal striatum. *Neural Plast.* **2015**, 458123 (2015).

141. Morello, M., Reiner, A., Sancesario, G., Karle, E. J. & Bernardi, G. Ultrastructural study of nitric oxide synthase-containing striatal neurons and their relationship with parvalbumin-containing neurons in rats. *Brain Res.* **776**, 30–39 (1997).

142. Schlossmann, J. & Schinner, E. cGMP becomes a drug target. *Naunyn. Schmiedebergs. Arch. Pharmacol.* **385**, 243–52 (2012).

143. Kouvelas, D., Goulas, A., Papazisis, G., Sardeli, C. & Pourzitaki, C. PDE5 Inhibitors: In vitro and In vivo pharmacological profile. *Curr. Pharm. Des.* **15**, 3464–3475 (2009).

144. Corbin, J. D. & Francis, S. H. Cyclic GMP phosphodiesterase-5: target of sildenafil. *J. Biol. Chem.* **274**, 13729–32 (1999).

145. Wood, A. J. J. & Lue, T. F. Erectile dysfunction. *N. Engl. J. Med.* **342**, 1802–1813 (2000).

146. Rossaint, R., Falke, K. J., Lopez, F., Slama, K., Pison, U., Zapol, W. M. Inhaled Nitric Oxide for the adult respiratory distress syndrome. *N. Engl. J. Med.* **328**, 399–405 (1993).

147. Zhao, L., Mason, N. A., Morrell, N. W., Kojonazarov, B., Sadykov, A., Maripov, A., Mirrakhimov, M. M., Aldashev, A., Wilkins, M. R. Sildenafil inhibits hypoxia-induced pulmonary hypertension. *Circulation* **104**, 424–8 (2001).

148. Galiè, N., Ghofrani, H. A., Torbicki, A., Barst, R. J., Rubin, L. J., Badesch, D., Fleming, T., Parpia, T., Burgess, G., Branzi, A., Grimminger, F., Kurzyna, M., Simoneau, G. Sildenafil citrate therapy for pulmonary arterial hypertension. *N. Engl. J. Med.* **353**, 2148–2157 (2005).

149. Lubamba, B., Lecourt, H., Lebacq, J., Lebecque, P., De Jonge, H., Wallemacq, P., Leal, T. Preclinical evidence that sildenafil and vardenafil activate chloride transport in cystic fibrosis. *Am. J. Respir. Crit. Care Med.* **177**, 506–515 (2008).

150. Nagayama, T., Hsu, S., Zhang, M., Koitabashi, N., Bedja, D., Gabrielson, K. L., Takimoto, E., Kass, D. A. Sildenafil stops progressive chamber, cellular, and molecular remodeling and improves calcium handling and function in hearts with pre-existing advanced hypertrophy caused by pressure overload. *J. Am. Coll. Cardiol.* **53**, 207–215 (2009).

151. Takimoto, E., Champion, H. C., Li, M., Belardi, D., Ren, S., Rodriguez, E. R., Bedja, D., Gabrielson, L., Wang, Y., Kass, D. A. Chronic inhibition of cyclic GMP phosphodiesterase 5A prevents and reverses cardiac hypertrophy. *Nat. Med.* **11**, 214–222 (2005).

152. García-Osta, A., Cuadrado-Tejedor, M., García-Barroso, C., Oyarzábal, J. & Franco, R. Phosphodiesterases as therapeutic targets for Alzheimer's disease. *ACS Chem. Neurosci.* **3**, 832–44 (2012).

153. Yu, J., Wolda, S. L., Frazier, A. L., Florio, V. A., Martins, T. J., Snyder, P. B., Harris, E. A., McCaw, K. N., Farrell, C. A., Steiner, B., Bentley, J. K., Beavo, J. A., Feruson, K., Gelinas, R. Identification and characterisation of a human calmodulin-stimulated phosphodiesterase PDE1B1. *Cell. Signal.* **9**, 519–29 (1997).

154. Lakics, V., Karran, E. H. & Boess, F. G. Quantitative comparison of phosphodiesterase mRNA distribution in human brain and peripheral tissues. *Neuropharmacology* **59**, 367–374 (2010).

155. Deshmukh, R., Sharma, V., Mehan, S., Sharma, N. & Bedi, K. L. Amelioration of intracerebroventricular streptozotocin induced cognitive dysfunction and oxidative stress by vinpocetine ? a PDE1 inhibitor. *Eur. J. Pharmacol.* **620**, 49–56 (2009).

156. Betolngar, D. B., Mota, E., Fabritius, A., Nielsen, J., Hougaard, C., Christoffersen, C. T., Yang, J., Kehler, J., Griesbeck, O., Castro, L. R. V., Vincent, P. Phosphodiesterase 1 bridges glutamate inputs with NO-and dopamine-induced cyclic nucleotide signals in the striatum. *Cereb. Cortex* **29**, 5022–5036 (2019).

157. Fieblinger T., Perez-Alvarez, A., Lamothe-Molina P.J., Gee, C.E., Oertner T.G. Presynaptic cGMP sets synaptic strength in the striatum and is important for motor learning. *EMBO Rep.*, **23**, e54361 (2022).

158. Boess, F. G., Hendrix, M., Van der Staay, F.-J., Erb, C., Schreiber, R., Van Staveren, W., De Vente, J., Prickaerts, J., Blokland, A., Koenig, G. Inhibition of phosphodiesterase 2 increases neuronal cGMP, synaptic plasticity and memory performance. *Neuropharmacology* **47**, 1081–1092 (2004).

159. Fujishige, K., Kotera, J., Omori, K. Striatum- and testis-specific phosphodiesterase PDE10A isolation and characterization of a rat PDE10A. *Eur. J. Biochem.* **266**, 1118–27 (1999).

160. Bender, A. T. & Beavo, J. A. Cyclic nucleotide phosphodiesterases: molecular regulation to clinical use. *Pharmacol. Rev.* **58**, 488–520 (2006).

161. Rodefer, J. S., Murphy, E. R., Baxter, M. G. PDE10A inhibition reverses subchronic PCP-induced deficits in attentional set-shifting in rats. *Eur. J. Neurosci.* **21**, 1070–1076 (2005).

162. Hebb, A. L. O., Robertson, H. A., Denovan-Wright, E. M. Striatal phosphodiesterase mRNA and protein levels are reduced in Huntington's disease transgenic mice prior to the onset of motor symptoms. *Neuroscience* **123**, 967–81

(2004).

163. Harada, A., Suzuki, K. & Kimura, H. TAK-063, a novel phosphodiesterase 10A inhibitor, protects from striatal neurodegeneration and ameliorates behavioral deficits in the R6/2 mouse model of huntingtons disease. *J. Pharmacol. Exp. Ther.* **360**, 75–83 (2016).

164. Dhayade, S., Kaesler, S., Sinnberg, T., Dobrowinski, H., Peters, S., Naumann, U., Liu, H., Hunger, R. E., Thunemann, M., Biedermann, T., Schittek, B., Simon, H.-U., Feil, S., Feil, R. Sildenafil potentiates a cGMP-dependent pathway to promote melanoma growth. *Cell Rep.* **14**, 2599–2610 (2016).

165. Li, W.-Q., Qureshi, A. A., Robinson, K. C., Han, J. Sildenafil use and increased risk of incident melanoma in US men: a prospective cohort study. *JAMA Intern. Med.* **174**, 964–70 (2014).

166. Chirkov, Y. Y. & Horowitz, J. D. Impaired tissue responsiveness to organic nitrates and nitric oxide: A new therapeutic frontier? *Pharmacol. Ther.* **116**, 287–305 (2007).

167. Stasch, J.-P., Pacher, P., Evgenov, O. V. Soluble guanylate cyclase as an emerging therapeutic target in cardiopulmonary disease. *Circulation* **123**, 2263–2273 (2011).

168. Stasch, J.-P. & Evgenov, O. V. Soluble guanylate cyclase stimulators in pulmonary hypertension. in *Handbook of experimental pharmacology* **218**, 279–313 (2013).

169. Evgenov, O. V., Pacher, P., Schmidt, P. M., Hasko, G., Schmidt, H. H. H. W., Stasch, J.-P. NO-independent stimulators and activators of soluble guanylate cyclase: discovery and therapeutic potential. *Nat. Rev. Drug Discov.* **5**, 755–768 (2006).

170. Stasch, J.-P. & Hobbs, A. J. NO-independent, haem-dependent soluble guanylate cyclase stimulators. in *cGMP: Generators, Effectors and Therapeutic Implications* 277–308 (Springer Berlin Heidelberg, 2009).

171. Stasch, J.-P., Becker, E. M., Alonso.Alija, C., Apeler, H., Dembowsky, K., Feurer, A., Gerzer, R., Minuth, T., Perzborn, E., Pleiss, U. Schröder, H.,

Schroeder, W., Stahl, E., Steinke, W., Straub, A., Schramm, M. NO-independent regulatory site on soluble guanylate cyclase. *Nature* **410**, 212–215 (2001).

172. Ko, F. N., Wu, C. C., Kuo, S. C., Lee, F. Y. & Teng, C. M. YC-1, a novel activator of platelet guanylate cyclase. *Blood* **84**, 4226–33 (1994).

173. Wu, C. C., Ko, F. N., Kuo, S. C., Lee, F. Y. & Teng, C. M. YC-1 inhibited human platelet aggregation through NO-independent activation of soluble guanylate cyclase. *Br. J. Pharmacol.* **116**, 1973–8 (1995).

174. Tsai, I.-F., Lin, C.-Y., Huang, C.-T., Lin, Y.-C., Yang, C.-M., Lin, Y.-C., Liao, C.-H. Modulation of human monocyte-derived dendritic cells maturation by a soluble guanylate cyclase activator, YC-1, in a cyclic nucleotide independent manner. *Int. Immunopharmacol.* **7**, 1299–1310 (2007).

175. Wang, J. P., Chang, L. C., Huang, L. J. & Kuo, S. C. Inhibition of extracellular Ca(2+) entry by YC-1, an activator of soluble guanylyl cyclase, through a cyclic GMP-independent pathway in rat neutrophils. *Biochem. Pharmacol.* **62**, 679–84 (2001).

176. Friebe, A., Müllershausen, F., Smolenski, A., Walter, U., Schultz, G., Koesling, D. YC-1 potentiates nitric oxide- and carbon monoxide-induced cyclic GMP effects in human platelets. *Mol. Pharmacol.* **54**, 962–7 (1998).

177. Mullershausen, F., Russwurm, M., Friebe, A. & Koesling, D. Inhibition of phosphodiesterase type 5 by the activator of nitric oxide-sensitive guanylyl cyclase BAY 41-2272. *Circulation* **109**, 1711–1713 (2004).

178. Schlaich, M. P., Parnell, M. M., Belinda, A. A., Finch, S., Marshall, T., Zhang, W.-Z., Kaye, D. M. Impaired L-arginine transport and endothelial function in hypertensive and genetically predisposed normotensive subjects. *Circulation* **110**, 3680–3686 (2004).

179. Taddei, S., Virdis, A., Mattei, P., Ghiadoni, L., Sudano, I., Salvetti, A. Defective L-arginine-nitric oxide pathway in offspring of essential hypertensive patients. *Circulation* **94**, 1298–303 (1996).

180. Rothermund, L., Friebe, A., Paul, M., Koesling, D. & Kreutz, R. Acute blood pressure effects of YC-1-induced activation of soluble guanylyl cyclase in

normotensive and hypertensive rats. *Br. J. Pharmacol.* **130**, 205–208 (2000).

181. Evgenov, O. V., Kohane, D. S., Bloch, K. D., Stasch, J.-P., Volpato, G. P., Bellas, E., Evgenov, N., V., Buys, E. S., Gnoth, M. J., Graveline, A. R., Liu, R., Hess, D. R., Langer, R., Zapol, W. M. Inhaled agonists of soluble guanylate cyclase induce selective pulmonary vasodilation. *Am. J. Respir. Crit. Care Med.* **176**, 1138–1145 (2007).

182. Mittendorf, J., Weigand, S., Alonso-Alija, C., Bischoff, E., Feurer, A., Gerisch, M., Kern, A., Knorr, A., Lang, D., Muenter, K., Radtke, M., Schirok, H., Schlemmer, K.-H., Stahl, E., Straub, A., Wunder, F., Stasch, J.-P. Discovery of Riociguat (BAY 63-2521): A potent, oral stimulator of soluble guanylate cyclase for the treatment of pulmonary hypertension. *ChemMedChem* **4**, 853–865 (2009).

183. Binder, C., Zotter-Tufaro, C. & Bonderman, D. Riociguat for the treatment of pulmonary hypertension: a safety evaluation. *Expert Opin. Drug Saf.* **15**, 1671–1677 (2016).

184. Shanmugam, E., Jena, A. & George, M. Riociguat: Something new in pulmonary hypertension therapeutics? *J. Pharmacol. Pharmacother.* **6**, 3–6 (2015).

185. Nakai, T., Perl, N. R., Barden, T. C., Carvalho, A., Fretzen, A., Germano, P., Im, G.-Y. J., Jin, H., Kim, C., Lee, T. W.-H., Long, K., Moore, J., Rohde, J. M., Sarno, R., Segal, C., Solberg, E. O., Tobin, J., Zimmer, D. P., Currie, M. G. Discovery of IWP-051, a novel orally bioavailable sGC stimulator with once-daily dosing potential in humans. *ACS Med. Chem. Lett.* **7**, 465–469 (2016).

186. Ettinger, A. & Wittmann, T. Fluorescence live cell imaging. *Methods Cell Biol.* **123**, 77–94 (2014).

187. Oldach, L. & Zhang, J. Genetically encoded fluorescent biosensors for live-cell visualization of protein phosphorylation. *Chem. Biol.* **21**, 186–97 (2014).

188. Williams, D. A., Fogarty, K. E., Tsien, R. Y. & Fay, F. S. Calcium gradients in single smooth muscle cells revealed by the digital imaging microscope using Fura-2. *Nature* **318**, 558–61

189. Grynkiewicz, G., Poenie, M. & Tsien, R. Y. A new generation of Ca2+ indicators with greatly improved fluorescence properties. *J. Biol. Chem.* **260**, 3440–50

(1985).

190. Paredes, R. M., Etzler, J. C., Watts, L. T., Zheng, W., Lechleiter, J. D. Chemical calcium indicators. *Methods* **46**, 143–51 (2008).

191. Spiering, D., Bravo-Cordero, J. J., Moshfegh, Y., Miskolci, V., Hodgson, L. Quantitative ratiometric imaging of FRET-biosensors in living cells. *Methods Cell Biol.* **114**, 593–609 (2013).

192. Feil, R., Lehners, M., Stehle, D. & Feil, S. Visualising and understanding cGMP signals in the cardiovascular system. *Br. J. Pharmacol.* **179**, 2394–2412 (2022).

193. Okumoto, S., Jones, A. & Frommer, W. B. Quantitative imaging with fluorescent biosensors. *Annu. Rev. Plant Biol.* **63**, 663–706 (2012).

194. Russwurm, M. *et al.* Design of fluorescence resonance energy transfer (FRET)-based cGMP indicators: a systematic approach. *Biochem. J.* **407**, 69–77 (2007).

195. Thunemann, M., Fomin, N., Krawutschke, C., Russwurm, M., Feil, R. Visualization of cGMP with cGi biosensors. *Methods Mol. Biol.* **1020**, 89–120 (2013).

196. Thunemann, M. *et al.* Correlative intravital imaging of cGMP signals and vasodilation in mice. *Front. Physiol.* **5**, 394 (2014).

197. Thunemann, M., Schmidt, K., De Wit, C., Han, X., Jain, R. K., Fukumura, D., Feil, R. Transgenic mice for cGMP imaging. *Circ. Res.* **113**, 365–71 (2013).

198. Muzumdar, M. D., Tasic, B., Miyamichi, K., Li, L. & Luo, L. A global double-fluorescent Cre reporter mouse. *genesis* **45**, 593–605 (2007).

199. Barski, J. J., Dethleffsen, K. & Meyer, M. Cre recombinase expression in cerebellar Purkinje cells. *Genesis* **28**, 93–8

200. Tronche, F., Kellendonk, C., Kretz, O., Gass, P., Anlag, K., Orban, P. C., Bock, R., Klein, R., Schütz, G. Disruption of the glucocorticoid receptor gene in the nervous system results in reduced anxiety. *Nat. Genet.* **23**, 99–103 (1999).

201. Mergia, E., Friebe, A., Dangel, O., Russwurm, M. & Koesling, D. Spare guanylyl cyclase NO receptors ensure high NO sensitivity in the vascular system. *J. Clin.*

Invest. **116**, 1731–1737 (2006).

202. Rasband, W. S. ImageJ. https://imagej.nih.gov/ij/,

203. Hamburger, V. & Hamilton, H. L. A series of normal stages in the development of the chick embryo. *J. Morphol.* **88**, 49–92 (1951).

204. Schmidt, H., Peters, S., Frank, K., Wen, L., Feil, R., Rathjen, F. G. Dorsal root ganglion axon bifurcation tolerates increased cyclic GMP levels: the role of phosphodiesterase 2A and scavenger receptor Npr3. *Eur. J. Neurosci.* **44**, 2991–3000 (2016).

205. Paolillo M., Peters S., Schramm A., Schlossmann J., F. R. Real-time imaging reveals augmentation of glutamate-induced Ca2+ transients by the NO-cGMP pathway in cerebellar granule neurons. *Int J Mol Sci* **19**, E2185 (2018).

206. Lein, E. S. *et al.* Genome-wide atlas of gene expression in the adult mouse brain. *Nature* **445**, 168–176 (2007).

207. Gibb, B. J. & Garthwaite, J. Subunits of the nitric oxide receptor, soluble guanylyl cyclase, expressed in rat brain. *Eur. J. Neurosci.* **13**, 539–44 (2001).

208. Mergia, E., Russwurm, M., Zoidl, G. & Koesling, D. Major occurrence of the new alpha2beta1 isoform of NO-sensitive guanylyl cyclase in brain. *Cell. Signal.* **15**, 189–95 (2003).

209. Ter-Avetisyan, G., Rathjen, F. G. & Schmidt, H. Bifurcation of axons from cranial sensory neurons is disabled in the absence of Npr2-induced cGMP signaling. *J. Neurosci.* **34**, 737–47 (2014).

210. Francis, S. H., Corbin, J. D. & Bischoff, E. Cyclic GMP-Hydrolyzing Phosphodiesterases. in *cGMP: Generators, Effectors and Therapeutic Implications* 367–408 (Springer Berlin Heidelberg, 2009). doi:10.1007/978-3-540-68964-5_16

211. Boess, F. G., Hendrix, M., Van der Staay, F.-J., Erb, C., Schreiber, R., Van Staveren, W., De Vente, J., Prickaerts, J., Blokland, A., Koenig, G. Inhibition of phosphodiesterase 2 increases neuronal cGMP, synaptic plasticity and memory performance. *Neuropharmacology* **47**, 1081–92 (2004).

212. Laties, A. & Zrenner, E. Viagra (sildenafil citrate) and ophthalmology. *Prog. Retin. Eye Res.* **21**, 485–506 (2002).

213. Zhang, X., Feng, Q., Cote, R. H. Efficacy and selectivity of phosphodiesterase-targeted drugs in inhibiting photoreceptor phosphodiesterase (PDE6) in retinal photoreceptors. *Invest. Ophthalmol. Vis. Sci.* **46**, 3060–6 (2005).

214. Gibson, A. Phosphodiesterase 5 inhibitors and nitrergic transmission-from zaprinast to sildenafil. *Eur. J. Pharmacol.* **411**, 1–10 (2001).

215. Turko, I. V, Ballard, S. A., Francis, S. H. & Corbin, J. D. Inhibition of cyclic GMP-binding cyclic GMP-specific phosphodiesterase (Type 5) by sildenafil and related compounds. *Mol. Pharmacol.* **56**, 124–30 (1999).

216. Gillespie, P. G. & Beavo, J. A. Inhibition and stimulation of photoreceptor phosphodiesterases by dipyridamole and M&B 22,948. *Mol. Pharmacol.* **36**, 773–81 (1989).

217. Nakamizo, T., Kawamata, J., Yoshida, K., Kawai, Y., Kanki, R., Sawada, H., Kihara, T., Yamashita, H., Shibasaki, H. Akaike, A., Shimohama, S. Phosphodiesterase inhibitors are neuroprotective to cultured spinal motor neurons. *J. Neurosci. Res.* **71**, 485–495 (2003).

218. Guo, Y., Xiao, P., Lei, S., Deng, F., Xiao, G. G., Liu, Y., Chen, X, Li, L., Wu, S., Chen, Y., Jiang, H., Tan, L., Xie, J., Zhu, X., Liang, S., Deng, H. How is mRNA expression predictive for protein expression? A correlation study on human circulating monocytes. *Acta Biochim. Biophys. Sin. (Shanghai).* **40**, 426–36 (2008).

219. Fields, K. L., Brockes, J. P., Mirsky, R., Wendon, L. M. Cell surface markers for distinguishing different types of rat dorsal root ganglion cells in culture. *Cell* **14**, 43–51 (1978).

220. Kulesa, P. M., Bailey, C. M., Cooper, C., Fraser, S. E. In ovo live imaging of avian embryos. *Cold Spring Harb. Protoc.* **2010**, pdb.prot5446 (2010).

221. Kulesa, P. M. & Fraser, S. E. In ovo time-lapse analysis of chick hindbrain neural crest cell migration shows cell interactions during migration to the branchial arches. *Development* **127**, 1161–72 (2000).

222. Kulesa, P., Bronner-Fraser, M., Fraser, S. In ovo time-lapse analysis after dorsal neural tube ablation shows rerouting of chick hindbrain neural crest. *Development* **127**, 2843–52 (2000).

223. Eide, A. L. & Glover, J. C. Developmental dynamics of functionally specific primary sensory afferent projections in the chicken embryo. *Anat. Embryol. (Berl).* **195**, 237–50 (1997).

224. Bronner-Fraser, M. Analysis of the early stages of trunk neural crest migration in avian embryos using monoclonal antibody HNK-1. *Dev. Biol.* **115**, 44–55 (1986).

225. Tojima, T., Itofusa, R. & Kamiguchi, H. The nitric oxide-cGMP pathway controls the directional polarity of growth cone guidance via modulating cytosolic Ca2+ signals. *J. Neurosci.* **29**, 7886–7897 (2009).

226. Hancock, M. L., Canetta, S. E., Role, L. W., Talmage, D. A. Presynaptic type III neuregulin1-ErbB signaling targets {alpha}7 nicotinic acetylcholine receptors to axons. *J. Cell Biol.* **181**, 511–21 (2008).

227. Henley, J. & Poo, M. Guiding neuronal growth cones using Ca2+ signals. *Trends Cell Biol.* **14**, 320–30 (2004).

228. Silver, R. A., Lamb, A. G., Bolsover, S. R. Elevated cytosolic calcium in the growth cone inhibits neurite elongation in neuroblastoma cells: correlation of behavioral states with cytosolic calcium concentration. *J. Neurosci.* **9**, 4007–20 (1989).

229. Treinys, R., Kaselis, A., Jover, E., Bagnard, D., Šatkauskas, S. R-type calcium channels are crucial for semaphorin 3A-induced DRG axon growth cone collapse. *PLoS One* **9**, e102357 (2014).

230. Feil, R., Gappa, N., Rutz, M., Schlossmann, J., Rose, C. R., Konnerth, A., Brummer, S., Kühbandner, S., Hofmann, F. Functional reconstitution of vascular smooth muscle cells with cGMP-dependent protein kinase I isoforms. *Circ. Res.* **90**, 1080–1086 (2002).

231. Taniguchi, M., Yuasa, S., Fujisawa, H., Naruse, I., Saga, S., Mishina, M., Yagi, T. Disruption of semaphorin III/D gene causes severe abnormality in peripheral nerve projection. *Neuron* **19**, 519–30 (1997).

232. Threlfell, S. & West, A. R. Modulation of striatal neuron activity by cyclic nucleotide signalling and phosphodiesterase inhibition. *Basal Ganglia* **3**, 137–146 (2013).

233. Feil, R., Hartmann, J., Luo, C., Wolfsgruber, W., Schilling, K., Feil, S., Barski, J. J., Meyer, M., Konnerth, A., De Zeeuw, C. I., Hofmann, F. Impairment of LTD and cerebellar learning by Purkinje cell-specific ablation of cGMP-dependent protein kinase I. *J. Cell Biol.* **163**, 295–302 (2003).

234. Wood, P. L., Emmett, M. R., Wood, J. A. Involvement of granule, basket and stellate neurons but not Purkinje or Golgi cells in cerebellar cGMP increases in vivo. *Life Sci.* **54**, 615–20 (1994).

235. Southam, E., Morris, R., Garthwaite, J. Sources and targets of nitric oxide in rat cerebellum. *Neurosci. Lett.* **137**, 241–4 (1992).

236. Kleppisch, T., Pfeifer, A., Klatt, P., Ruth, P., Montkowski, A., Fässler, R., Hofmann, F. Long-term potentiation in the hippocampal CA1 region of mice lacking cGMP-dependent kinases is normal and susceptible to inhibition of nitric oxide synthase. *J. Neurosci.* **19**, 48–55 (1999).

237. Kleppisch, T., Wolfsgruber, W., Feil, S., Allmann, R., Wotjak, C. T., Goebbels, S., Nave, K.-A., Hofman, F., Feil, R. Hippocampal cGMP-dependent protein kinase I supports an age- and protein synthesis-dependent component of long-term potentiation but is not essential for spatial reference and contextual memory. *J. Neurosci.* **23**, 6005–12 (2003).

238. Müllershausen, F., Russwurm, M., Friebe, A., Koesling, D. Inhibition of phosphodiesterase type 5 by the activator of nitric oxide-sensitive guanylyl cyclase BAY 41-2272. *Circulation* **109**, 1711–1713 (2004).

239. Bischoff, E. & Stasch, J. P. Effects of the sGC stimulator BAY 41-2272 are not mediated by phosphodiesterase 5 inhibition. *Circulation* **110**, (2004).

240. Mergia, E., Koesling, D., Friebe, A. Genetic mouse models of the NO receptor ‘soluble *lications* 33–46 (Springer Berlin Heidelberg). doi:10.1007/978-3-540-68964-5_3’ guanylyl cyclases. in *cGMP: Generators, Effectors and Therapeutic Imp*

241. Giesen, J., Mergia, E., Koesling, D., Russwurm M. Hippocampal AMPA- and NMDA-induced cGMP signals are mainly generated by NO-GC2 and are under tight control by PDEs 1 and 2. *Eur J Neurosci.*, **55**, 18-31, (2021).

242. Russwurm, M., Wittau, N., Koesling, D. Guanylyl cyclase/PSD-95 Interaction. *J. Biol. Chem.* **276**, 44647–44652 (2001).

7 DANKSAGUNG

An dieser Stelle möchte ich die Gelegenheit nutzen den Menschen zu danken, die mich bei der Fertigstellung meiner Doktorarbeit unterstützt haben.

Mein größter Dank gilt meinem Doktorvater Prof. Dr. Robert Feil für seine Unterstützung bei der Auswahl des Themas und dessen Bearbeitung, für die Diskussion und Ausarbeitung der verschiedenen Fragestellungen, für die Möglichkeit mit vielen nationalen und internationalen Kollaborationspartnern zusammenzuarbeiten und an verschiedenen Tagungen und Retreats teilnehmen bzw. sogar mitwirken zu können. In den vier Jahren, die ich im Feil Lab in Tübingen verbringen durfte, habe ich mich fachlich aber vor allem auch persönlich weiterentwickelt. Dafür möchte ich mich auch ganz besonders bei Dir bedanken, Robert. Und natürlich auch meinen allerherzlichsten Dank für Dein Vertrauen und deine Geduld – bis zum Schluss! Ich bin sehr dankbar, Mitglied der cGMP-Familie gewesen zu sein.

Mein Dank gilt außerdem Prof. Dr. Peter Ruth, der die Zweitbetreuung und die Erstellung des Zweitgutachtens übernommen hat und mir ebenfalls mit seiner fachlichen Expertise und regelmäßigem Austausch stets zur Seite stand.

Vielen Dank an Dr. Susanne Feil, die mir alles über das „Mouse handling“ beigebracht hat. Vielen Dank auch an alle anderen Lab members – Angelos, Jacek, Michael P., Barbara, Moritz, Martin, Lai, Markus, Hannes, Michael K., Daniel und unseren Praktikantinnen Selin, Lina und Hannah – für die Unterstützung, Diskussionsrunden, gute Stimmung und Freundschaft innerhalb und außerhalb des Labors. Ein ganz großer Dank gilt all den Kooperationspartnern dieser Arbeit: Dr Andrea Wizenmann, für die Unterstützung bei den Hühnerembryoversuchen, dem Team von Ironwood Pharmaceuticals aus Boston für die Möglichkeit die Wirkung von IWP-051 im Mausgehirn zu untersuchen. Ebenfalls einen großen Dank an Lea Kennel und Prof. Dr. Achim Schmidtko für die Unterstützung bei den mRNA-Experimenten und an das Team von Prof. Dr. Doris Kösling für die *in vitro* assays.

Außerdem möchte ich meiner Familie und meinen Freunden von Herzen danken – allen voran meinen Eltern. Ihr zeigt mir jeden Tag, dass immer alles möglich ist, unterstützt mich bei all meinen Projekten und Ideen und lenkt mich wieder auf den richtigen Weg, sollte ich mal kurz abgewichen sein. Dafür danke ich euch sehr!